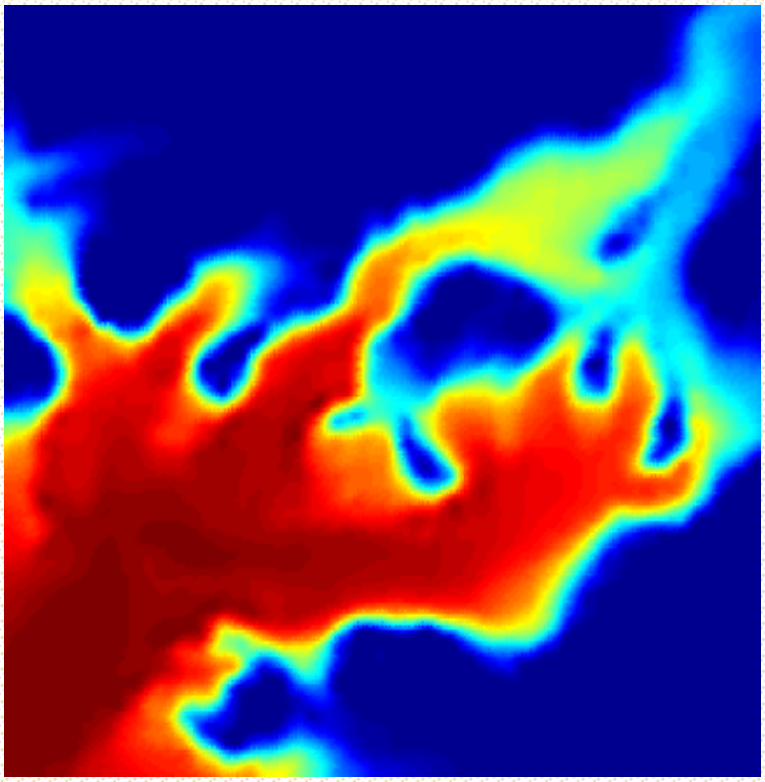

Luís Miguel Dias Pinto

Parabolic Partial Integro-Differential Equations: Superconvergence Estimates and Applications

2013

· U C ·

Universidade de Coimbra

Parabolic Partial Integro-Differential Equations: Superconvergence Estimates and Applications

· U  C ·

Luís Pinto

Department of Mathematics

University of Coimbra

A thesis submitted in partial fulfilment
of the requirements for the degree of

Doctor of Mathematics

August 2013

The work presented in this thesis is a part of the UTAustin/MAT/0066/2008 "Reaction-Diffusion in Porous Media" project funded by FCT (Fundação Portuguesa para a Ciência e a Tecnologia) and FEDER (Fundo Europeu de Desenvolvimento Regional) within the POFC (Programa Operacional Factores de Competitividade) - COMPETE program of QREN (Quadro de Referência Estratégico Nacional).

Abstract

Partial integro-differential equations of parabolic type arise naturally in the modeling of many phenomena in various fields of physics, engineering, and economics. The main aim of this thesis is to study finite element methods with numerical quadrature for this class of equations. Both one- and two-dimensional problems are considered. We investigate the stability and convergence properties of the schemes and obtain superconvergence error estimates. It is important to note that these superconvergence results hold also for the equivalent finite difference methods and, in this context, they stand without restrictions on the spatial mesh. In the derivation of these results, we introduce an approach to error analysis that deviates from the traditional one. The significant advantage of this modified strategy is that less regularity for the solution of the continuous problem is needed. The discretization in time using an implicit-explicit method is also addressed, and stability and convergence estimates are derived.

The mathematical modeling and numerical simulation of non-reactive solute transport in porous media is also in the scope of this thesis. Among many other applications, this fluid dynamic problem plays a major role in hydrology, medical science, and the petroleum industry. Fick's law is the underlying principle for obtaining the traditional partial differential equation that describes the solute concentration profile; however, several deviations from this law have been reported. With foundations in the non-Fickian dispersion theory, an integro-differential model is proposed in this thesis. The accuracy of the model is tested in one dimension, and the results indicate that the model is much improved over the conventional one. In fact, even in laboratory-scale homogeneous porous media, these transport processes may exhibit anomalous non-Fickian behavior that only the alternative model correctly reproduces. A robust numerical discretization is also presented and some numerical experiments are conducted. These experiments illustrate the applicability and computational feasibility of the proposed model to simulate two-dimensional problems.

A natural extension of our model would allow concentration-dependent viscosity. In this thesis, we also study finite element methods with numerical quadrature for coupled problems that include a simplified version of such a model as a particular case. Again, our numerical method allows the derivation of superconvergence approximations for the variables involved.

Resumo

Equações parciais integro-diferenciais do tipo parabólico surgem na modelação de vários fenómenos em diversas áreas da física, engenharia e economia. O objectivo principal desta dissertação é o estudo, uni e bidimensional, de métodos de elementos finitos com quadratura numérica para esta classe de equações. A estabilidade e a convergência de aproximações semi-discretas assim definidas são analisadas e estimativas de erro superconvergentes são estabelecidas. Estes resultados de superconvergência são igualmente válidos para métodos de diferenças finitas equivalentes, sendo que, neste contexto, vigoram sem qualquer tipo de restrição sobre a malha espacial. Na derivação destes resultados é introduzida uma forma de análise do erro que difere daquela normalmente utilizada. Esta abordagem permite reduzir a regularidade exigida à solução do problema contínuo. A estabilidade e a convergência de um método de discretização completa do tipo implícito-explícito são também analisadas.

Nesta dissertação discutimos ainda a modelação e simulação numérica do transporte de solutos não-reactivos em meios porosos. Entre outras aplicações, este problema de dinâmica de fluidos desempenha um papel de relevo na hidrologia, ciência médica e industria petrolífera. Subjacente à tradicional equação de derivadas parciais que descreve a evolução da concentração do soluto encontra-se a lei de Fick, um princípio físico que tem sido amplamente questionado. Com base na teoria de dispersão não-Fickiana propomos nesta dissertação um modelo do tipo integro-diferencial. A acuidade da versão unidimensional do modelo é analisada recorrendo a um conjunto de dados laboratoriais. Os resultados obtidos indicam que o modelo representa uma melhoria significativa em relação ao modelo tradicional. Mesmo em laboratório, verificamos que os processos de transporte em meios porosos podem exibir um comportamento anómalo não-Fickiano que apenas o modelo alternativo consegue reproduzir. Com o intuito de ilustrar a viabilidade computacional do modelo para simular problemas bidimensionais é ainda apresentada uma discretização numérica eficiente e são realizadas algumas experiências numéricas.

Uma extensão natural do modelo proposto passa por considerar a viscosidade dependente da concentração. Nesta dissertação analisamos também métodos de elementos finitos com quadratura numérica para sistemas de equações diferenciais que incluem como caso particular uma versão simplificada de tal modelo. Os métodos introduzidos permitem a derivação de aproximações superconvergentes para as variáveis envolvidas.

Acknowledgements

I would like to express gratitude to my advisor, Professor Doctor José Augusto Ferreira, for his guidance and support. Without him, this thesis would not be possible. Thanks are also due to FCT (Fundação Portuguesa para a Ciência e a Tecnologia) and FSE (Fundo Social Europeu) for the financial support within the scope of the QCA III (Quadro Comunitário de Apoio III) and under grant reference SFRH/BD/33101/2007. Last, but not least, I would like to thank my parents.

Contents

Abstract **vii**

Acknowledgements **xi**

1 Introduction **1**

1.1 Parabolic PIDEs 3

1.1.1 Error Estimates 4

1.1.2 Contributions of this Work 8

1.2 Non-Fickian Tracer Transport in Porous Media 9

1.2.1 An Integro-Differential Model 9

1.2.2 Contributions of this Work 13

1.3 A Parabolic-Elliptic Coupled Problem 13

1.3.1 Contributions of this Work 15

2 A FEM for Parabolic PIDEs in One Dimension **17**

2.1 A Semi-Discrete Galerkin Method 18

2.1.1 Stability Analysis 20

2.1.2 Error Estimates 24

2.1.3 Equivalence with a Finite Difference Method 29

2.2 Numerical Experiments 30

3 A FEM for Parabolic PIDEs in Two Dimensions **33**

3.1 A Semi-Discrete Galerkin Method 34

3.1.1 Error Estimates 40

3.2 A Fully Discrete Method 45

3.2.1 Stability and Convergence Analysis 46

3.3 Numerical Experiments 52

4 A Parabolic-Elliptic Coupled Problem **55**
4.1 A Semi-Discrete Galerkin Method 56
4.1.1 Stability Analysis 57
4.1.2 Error Estimates 59
4.2 A Fully Discrete Method 69
4.2.1 Convergence Analysis 70
4.3 Numerical Experiments 73

5 Applications: Non-Fickian Tracer Transport in Porous Media **75**
5.1 Model Validation: Breakthrough curve analysis 75
5.1.1 Data Set 1 78
5.1.2 Data Set 2 79
5.1.3 Data Set 3 81
5.1.4 Scale-Dependent Prediction 84
5.2 Numerical Experiments in Two Dimensions 85
5.2.1 The Numerical Scheme 85
5.2.2 Code Validation 94
5.2.3 Numerical Simulation 99

6 Conclusions and Future Work **103**

Bibliography **106**

Chapter 1

Introduction

Numerical simulation is a valuable tool for solving challenging scientific and industrial problems. Nowadays, more and more companies from a broad range of industries are looking to computer simulation to improve their productivity. It can offer reliable solutions to complex problems and is flexible and inexpensive. In order to enhance this statement, we quote a report [146] from the NASA integrated technology roadmap.

"Modeling, simulation and decision-making are closely coupled and have become core technologies in science and engineering. In the simplest sense, a model represents the characteristics of something, while a simulation represents its behavior. Through the combination of the two, we can make better decisions and communicate those decisions early enough in the design and development process that changes are easy and quick, as opposed to during production when they are extremely costly and practically impossible."

A key aspect of the simulation process is the formulation of proper mathematical models. The model must be able to emulate the physical phenomena under investigation. Traditionally, partial differential equations (PDEs) play a major role in the modeling of many processes. However, in many evolutionary problems, the history of the phenomena under investigation is of relevance and must be incorporated in the mathematical model. Classical PDEs models cannot reproduce this property, and it is a well-known fact that they fail to provide a reliable description of such processes. As a solution to overcome this drawback, PDEs have been replaced by partial integro-differential equations (PIDEs). The theoretical and experimental research that has been conducted in recent years shows that mathematical models based on PIDEs, which take into account this memory effect, are more accurate than the traditional PDE models.

As an example, consider the important problem of non-reactive solute (tracer) transport in porous media. In classical Fickian dispersion theory, these processes are

described by the equation

$$\partial_t c + \nabla \cdot (vc) = \nabla \cdot (D \nabla c) \quad \text{in } \Omega \times (0, T], \tag{1.1}$$

where c denotes the concentration of the tracer, v the velocity, and D a dispersion tensor. This equation may give accurate results in a laboratory environment for perfectly homogeneous media; however, the same cannot be said for real-life situations, where heterogeneities are expected. When the porous medium is heterogeneous, it is believed that a memory effect is present in these processes. Therefore, this kind of problem, the so-called non-Fickian transport, can be better understood if it is modeled by PIDEs [52,57,68,93,155]. Here, in particular, we propose a PIDE of type

$$\partial_t c + \nabla \cdot (vc) + \nabla \cdot (D \nabla c) = \int_0^t B(s,t) c(s)\, ds \quad \text{in } \Omega \times (0, T],$$

where $B(s,t)$ is a memory operator to be specified. Beyond tracer transport, PIDEs arise also, for instance, in the modeling of immunology [24], financial processes [119], and viscoelastic polymers [139].

Naturally, solving the equations involved is necessary to extract information from the mathematical models. However, an analytical solution generally is unavailable and a numerical approximation must be introduced. The numerical treatment of these problems is a demanding mathematical and computational task. In fact, for most problems of interest, the complexity and dimension of the models are such that very efficient numerical methods are essential. Over the last few decades, advances in numerical analysis and computer capabilities have led to the development of powerful numerical tools. Nonetheless, solving the current problems can easily become problematic. For this reason, the development of accurate, stable, and computationally effective numerical methods for advanced mathematical models remains a high priority.

As we mentioned before, PIDEs can be more effective than standard PDEs for the modeling of some processes, and hence have attracted widespread attention of scientists and engineers. Despite very active research in this field, the numerical and analytical treatment of such equations present some serious difficulties and many unresolved problems still remain.

Before proceeding, a short comment about notation must be made: the letter C, with our without subscripts, will be used to denote a positive constant, independent of mesh parameters, that may take different values in different places. Additionally, we represent by ∇ the spatial derivative or the gradient operator, as appropriate;

by $\nabla\cdot$, the divergence operator; by Δ, the Laplacian; and by ∂_t^n, the derivatives in time of order n. Throughout this thesis, we use standard notation from the theory of Sobolev spaces as can be found in [66] and many others.

1.1 Parabolic PIDEs

In this thesis, we are mainly concerned with parabolic PIDEs of the form

$$\partial_t c + Ac = \int_0^t B(s,t)c(s)\,ds + f \quad \text{in } \Omega \times (0,T], \tag{1.2}$$

where A is a differential operator with coefficients independent of t,

$$Ac = -\nabla\cdot(A_2\nabla c) + \nabla\cdot(A_1 c) + a_0 c, \tag{1.3}$$

while $B(s,t)$ is a similar operator, but with time dependent coefficients,

$$B(s,t)c = -\nabla\cdot(B_2(s,t)\nabla c) + \nabla\cdot(B_1(s,t)c) + b_0(s,t)c. \tag{1.4}$$

Equation (1.2) must be complemented with an initial condition,

$$c(0) = c_0 \quad \text{in } \Omega \tag{1.5}$$

and proper boundary conditions. Here we consider primarily Dirichlet homogeneous boundary conditions,

$$c(t) = 0 \quad \text{on } \partial\Omega \times (0,T]. \tag{1.6}$$

Assume for now that the coefficients of A and $B(s,t)$ are smooth functions and that Ω is a regular domain. For a discussion regarding the well-posedness of the problem (1.2)-(1.6) we refer to [46, 116, 163, 169]. The aim of this thesis is to study numerical methods for such a problem.

A large number of schemes are available in the literature for solving this kind of PIDE. The most common solutions are based on approximations in space by finite element methods (FEMs) or finite difference methods (FDMs) followed by finite differences and quadrature rules in time [39, 61, 131, 133]. Other spatial discretization methods include orthogonal spline collocation methods [130], mixed finite element methods [76], finite volume methods [71], and discontinuous Galerkin methods [140]. Time integration methods based on Laplace transform [122], Runge-Kutta methods [166], and multistep methods [167, 168] have also been subject of study. A common difficulty in solving PIDEs is that the evaluation of the time integral term by traditional quadrature rules requires a huge amount of storage, since all time step solutions must be retained. In [133, 149, 169], special quadrature rules with less memory demands were proposed.

1.1.1 Error Estimates

Finite differences and quadrature rules were used in [61] to conduct the first numerical analysis of parabolic PIDEs. In that work, a convergence study was performed and error estimates in discrete Sobolev norms for a uniform partition in space and time were provided. The approximation by finite elements was considered for the first time in [163], and optimal-order error estimates in the L^2-norm were obtained for an equation similar to (1.2), in which $B(s,t)$ is a non-linear operator that depends, at most, on first-order derivatives in space of the function c.

Optimal error estimates for the problem (1.2)-(1.6) are presented in [38,39,112,154] for the L^2- and H^1-norms and in [111] for the maximum L^∞-norm. For instance, in [112], the so-called Ritz-Volterra projection, introduced in [39], is used to show that the results known for the equivalent parabolic PDE, i.e., when $B(s,t) = 0$, can be extended to this case. Namely, it is established that if

$$\|c_0 - c_{h,0}\|_{L^2} \leq Ch^2 \|c_0\|_{H^2},$$

then the piecewise linear finite element approximations are second-order convergent with respect to the L^2-norm,

$$\|c(t) - c_h(t)\|_{L^2} \leq Ch^2 \Big(\|c_0\|_{H^2} + \int_0^t \|\partial_t c(s)\|_{H^2}\, ds \Big)$$

and they are first-order convergent with respect to the H^1-norm,

$$\|c(t) - c_h(t)\|_{H^1} \leq Ch, \tag{1.7}$$

where h is a mesh parameter, c_h is the finite element approximation to c, and $c_{h,0}$ is a suitable approximation to c_0.

Piecewise linear finite elements with quadrature were analyzed in [131, 132] and optimal-order error estimates were established in discrete L^2- and H^1-norms. In particular, for an appropriate approximation $c_{h,0}$, it was proved that,

$$\|c(t) - c_h(t)\|_h \leq Ch^2 \Big(\|c(t)\|_{H^2} + \Big(\int_0^t \|c(s)\|_{H^2}^2 + \|\partial_t c(s)\|_{H^2}^2\, ds \Big)^{1/2} \Big).$$

where $\|\cdot\|_h$ denotes a discrete L^2-norm.

Finite volume methods (FVMs) based on piecewise linear functions have been analyzed in [70, 71, 148]. The one-dimensional case was considered in [70], and in [71], the analysis was carried over to the two-dimensional case. In [70, 71], optimal-order estimates with respect to the L^2- and H^1-norms were shown, provided that $c_0 \in H^3(\Omega)$

and $c \in H^1(0,T;H^3(\Omega))$. These smoothness assumptions were weakened in [148] for the homogeneous case. Here, the authors established second-order convergence in the L^2-norm, assuming that $c_0 \in H^2(\Omega)$ and that

$$\|c(t)\|_{H^2} \quad \text{and} \quad \int_0^t \|c(s)\|_{H^2}^2 + s^2 \|\partial_t c(s)\|_{H^2}^2 \, ds \tag{1.8}$$

are finite. These FVMs, which can be seen as Petrov-Galerkin FEMs, have been applied also to elliptic [74] and parabolic PDE problems [41, 42].

Integro-differential equations nearly identical to (1.2) can be rewritten equivalently in the form

$$\partial_t c = \nabla \cdot z - a_0 c + f \quad \text{in } \Omega \times (0,T], \tag{1.9}$$

$$z = \tilde{A}c + \int_0^t \tilde{B}(s,t)c(s)\, ds \quad \text{in } \Omega \times (0,T], \tag{1.10}$$

where $\tilde{A}c = A_2 \nabla c - A_1 c$ and $\tilde{B}(s,t)c = -B_2(s,t)\nabla c + B_1(s,t)c$. This approach was used, for instance, in [75–77,129], where mixed finite element methods (MFEMs) were studied. The results reported there are equivalent to those described in [43, 104, 128], where MFEMs for parabolic PDE problems were discussed. In particular, for the two-dimensional case, it was proved in [76] that the approximation of c and z by the lowest-order Raviart-Thomas (RT_0) elements satisfies

$$\|c(t) - c_h(t)\|_{L^2}^2 + \|z(t) - z_h(t)\|_{L^2}^2 \le Ch^2 \Big(\|c_0\|_{H^1}^2 + \|z_0\|_{H^1}^2 + \int_0^t \|c(s)\|_{H^2}^2 + \|\partial_t c(s)\|_{H^1}^2 \, ds \Big) \tag{1.11}$$

for convenient approximations of the initial functions c_0 and z_0.

The issue of time discretization is also addressed in many of the above cited papers. For example, optimal second-order error estimates for the Crank-Nicolson method and optimal first-order estimates for the implicit Euler method were established in [133, 169]. In these works, the discretization in space was performed using FEMs. More precisely, for piecewise linear finite elements in space and the implicit Euler method combined with the rectangular rule in time holds the following [169]:

$$\|c(t_n) - c_h^n\|_{L^2} \le Ch^2 \Big(\|c_0\|_{H^2} + \int_0^{t_n} \|\partial_t c(s)\|_{H^2} \, ds \Big) + C\Delta t \Big(\|c_0\|_{L^2} + \int_0^{t_n} \|\partial_t c(s)\|_{L^2} + \|\partial_t^2 c(s)\|_{L^2} \, ds \Big).$$

Here, we represent by Δt the uniform time step, $\Delta t = t_n - t_{n-1}$, for $n = 1, \ldots, N$, with $t_0 = 0$ and $t_N = T$, and by c_h^n the approximation of $c(t_n)$.

An interesting subject in the study of the convergence of numerical methods is the so-called superconvergence phenomena. The term superconvergence is widely used in the literature and does not always carry the same meaning. Before proceeding, we present some definitions and clarify our terminology. Let g be some function and denote by g_h an approximation of g computed by some numerical method. Assume also that the convergence analysis reveals the following optimal error estimate,

$$\|g - g_h\| \leq Ch^r,$$

where $\|\cdot\|$ represents some norm. We say that there is superconvergence if the error measured in some discrete norm $\|\cdot\|_h$ satisfies

$$\|g - g_h\|_h \leq Ch^s \quad \text{for } s > r. \tag{1.12}$$

That is, the convergence rate of the approximation at some points or regions is greater than the optimal global convergence rate of the approximation. We also say that we have superconvergence when

$$\|P_h g - g_h\| \leq Ch^s \quad \text{for } s > r,$$

and we will call it supercloseness. Here, $P_h : G \longrightarrow G_h$ is some interpolation operator being G_h, the finite-dimensional space where g_h resides, and G, the space of the function g. Note that in the FDM context, (1.12) is known as supraconvergence [107]. Note also that we do not consider as superconvergence the results obtained after post-processing of g_h. From an application point of view, superconvergence can be used in the construction of a posteriori error estimators, which is directly related to adaptive methods, an important tool in numerical modeling. For more details about this subject, see [6, 13, 14, 31, 32, 44].

Superconvergence has been the subject of intensive study since the first report of this phenomena in [126], and by now the literature on this field is very extensive. For an overview of some results on superconvergence in FEMs, we refer to [108, 157] and the references therein. However, while there are many papers about superconvergence, most of them are on numerical methods for PDEs, and it seems that only a few deal with parabolic PIDEs of type (1.2); some exceptions are [110] for FEMs, [75, 77] for MFEMs, and [70, 71] for FVMs. Next, we review these studies.

Consider the mixed formulation (1.9)-(1.10) and the mixed method that leads to estimate (1.11). For rectangular elements and convenient initial approximations, the

following error bound was established in [75]

$$\|c(t)-c_h(t)\|_h+\|z(t)-z_h(t)\|_{h^*}\leq Ch^2\Big(\|c(t)\|_{H^2}+\|z(t)\|_{H^2}+\Big(\int_0^t\|c(s)\|_{H^1}+\|z(s)\|_{H^2}+\|\partial_t c(s)\|_{H^1}+\|\partial_t z(s)\|_{H^2}\,ds\Big)^{1/2}\Big), \tag{1.13}$$

where $\|\cdot\|_h$ and $\|\cdot\|_{h^*}$ are discrete L^2-norms. When we compare this result with the optimal estimate (1.11), we see that (1.13) is a superconvergence result. In [77], the authors studied this same problem and obtained superconvergence L^∞-error estimates. The superconvergence of mixed methods on rectangular elements is a well-known fact for elliptic [9, 78] and parabolic PDEs [69].

Now we refer to the FVMs that were introduced in the discussion of the estimate (1.8). Assuming an adequate approximation $c_{h,0}$, it was proved in [70, 71] that

$$\|c(t)-c_h(t)\|_{1,h}\leq Ch^2\Big(\|c_0\|_{H^3}+\|c(t)\|_{H^3}+\int_0^t\|c(s)\|_{H^3}+\|\partial_t c(s)\|_{H^3}\,ds\Big). \tag{1.14}$$

Since $\|\cdot\|_{1,h}$ is a discrete H^1-norm, this estimate can be seen as a superconvergence result for the gradient ∇c.

As the inequality (1.7) illustrates, the finite element approximation of the problem (1.2)-(1.6) has an optimal convergence rate of order one in the H^1-norm, when piecewise linear functions are used. In [110], for this method, the authors derived the following supercloseness result

$$\|P_h c(t)-c_h(t)\|_{H^1}\leq Ch^2\Big(\int_0^t\Big(\|\partial_t c(s)\|_{H^2}+\|c(s)\|_{H^4}+\int_0^s\|c(\mu)\|_{H^4}\,d\mu\Big)^2 ds\Big)^{1/2}, \tag{1.15}$$

where P_h is the usual interpolation operator in $H^1(\Omega)$.

We observe that, as usual, the superconvergence results (1.13)-(1.15) require regularity assumptions on data that are higher than the ones necessary for the correspondent optimal estimates. To obtain superconvergence results under less demanding conditions, not only on data but also on the discretization of the domain, is a challenging problem. Note also that, for the one-dimensional case, the superconvergence result (1.14) is in fact identical to the one we present in Chapter 2. It seems, however, that the result of [70] is valid only for a simplified version of (1.2).

We finish this section with a comment: in the great majority of the above mentioned papers, the error estimates were obtained following the strategy introduced by

Wheeler for the study of parabolic PDEs [160]. The idea is to write the error as

$$\begin{aligned} e_h(t) &= c(t) - \Pi_h c(t) + \Pi_h c(t) - c_h(t) \\ &= \rho_h(t) + \theta_h(t), \end{aligned} \tag{1.16}$$

with Π_h being a suitable projection operator. After that split, each part is estimated separately.

1.1.2 Contributions of this Work

In Chapters 2 and 3 of this thesis, we deal with the numerical solution of the PIDE problem (1.2)-(1.6). To this end, piecewise linear FEMs with special quadrature rules are proposed. We study stability and convergence properties of the schemes and obtain superconvergence error estimates.

In particular, the one-dimensional case is treated in Chapter 2, and assuming that

$$\|P_h c_0 - c_{h,0}\|_h \leq Ch^2,$$

we prove the following supercloseness estimate for the gradient

$$\int_0^t \|P_h c(s) - c_h(s)\|_{H^1}^2 \, ds \leq Ch^4 \Big(\int_0^t \|c(s)\|_{H^3}^2 \, ds + \|c(t)\|_{H^3}^2 + \|\partial_t c(t)\|_{H^3}^2 \Big). \tag{1.17}$$

In order to establish the inequality (1.17), we require that

$$\begin{gathered} c \in L^\infty(0,T; H^3(\Omega) \cap H_0^1(\Omega)), \\ \partial_t c \in L^\infty(0,T; H^3(\Omega)), \quad \text{and} \quad \partial_t^2 c \in L^\infty(0,T; L^1(\Omega)). \end{gathered} \tag{1.18}$$

In Chapter 3, we consider the two-dimensional version of the same problem. A supercloseness result similar to (1.17) is deduced for the semi-discrete approximation. In the process, we introduce an approach to error analysis that deviates from the traditional splitting strategy (1.16). The advantage is that less regularity for the solution of the continuous problem is needed. The restriction (1.18) can be relaxed to the weaker condition

$$c \in L^\infty(0,T; H^3(\Omega) \cap H_0^1(\Omega)) \quad \text{and} \quad \partial_t c \in L^\infty(0,T; H^2(\Omega)). \tag{1.19}$$

By using the same strategy, we can derive condition (1.19) for the one-dimensional case. The proof is straightforward and is not reported here.

It is important to notice that our supercloseness results can be seen as supra-convergence results of equivalent FDMs. This is valid for both the one- and the

two-dimensional problems. Moreover, these results hold with no mesh restrictions at all. Note that in the two-dimensional case, this is only true for the FDM. These theoretical results are the main achievement of this thesis and have been published in [17, 86]. Note also that similar superconvergence results have been obtained for elliptic [16, 82] and parabolic PDEs [15]. Therefore, our work can be considered an extension of these studies.

1.2 Non-Fickian Tracer Transport in Porous Media

Real-world applications are also in the scope of this thesis. The application that we explore here is transport in porous media. Among many other applications, the numerical modeling of transport problems in porous media plays a major role in hydrology, medical science, and the petroleum industry. The specific problem that we address is tracer transport. As mentioned in Section 1, the classical model for this problem relies on the PDE (1.1). However, tracer transport that is not adequately described by this model has been observed both in field and laboratory experiments [90, 109, 150]. The heterogeneity of the medium seems to be a common factor in this so-called anomalous or non-Fickian behavior. Nevertheless, such phenomena can also be found in homogeneous media [49]. In order to overcome this limitation, different models have been proposed in the literature. An in-exhaustive list includes the continuous time random walk model, the mobile/immobile model, and the spatial fractional advection-dispersion equation. A detailed discussion of these and other models, as well as non-Fickian transport in general, can be found in [29, 88, 92, 123, 125] and the references therein.

1.2.1 An Integro-Differential Model

In this thesis, we present a non-Fickian model for tracer transport that is based on the delayed dispersion theory [57]. To specify the problem considered, let Ω be a bounded domain of $\mathbb{R}^2$ representing the porous medium, and let $[0, T]$ be the time interval, for some $T > 0$. The classical PDE governing this fluid problem in porous media can be written as

$$\phi \partial_t c + \nabla \cdot (vc) = \nabla \cdot (D \nabla c) + q c^* \quad \text{in } \Omega \times (0, T], \tag{1.20}$$

where ϕ represents the porosity of the medium, q sources and sinks terms, and c^* a prescribed concentration at sources or c at sinks. The dispersion tensor D is given

by [23]

$$D = d_m I + d_t \|v\| I + \frac{d_l - d_t}{\|v\|} v v^{\mathrm{T}}, \tag{1.21}$$

with $\|v\|^2 = v^{\mathrm{T}} v$ and where I denotes the two by two identity matrix, d_m the molecular diffusion coefficient, and d_l and d_t the longitudinal and transverse dispersion coefficients, respectively. Let us summarize the main steps in the construction of this model. Express the total mass flux as

$$J = J_{adv} + J_{dis}, \tag{1.22}$$

where

$$J_{adv} = vc, \tag{1.23}$$

which represents the advection mass due to the fluid velocity, and assume that the dispersive mass flux J_{dis} satisfies the Fick's law

$$J_{dis} = -D\nabla c. \tag{1.24}$$

Then, we can obtain equation (1.20) from (1.22)-(1.24) with the aid of the mass conservation equation,

$$\phi \partial_t c + \nabla \cdot J = q c^*. \tag{1.25}$$

Now we derive the PIDE model. The underlying assumption behind this model is that the history of the transport must be considered. One possible way to incorporate this concept into the mathematical model is to introduce a memory dispersive flux. In the words of Thompson [155]: *"...dispersive flux... is influenced by weighted contributions from all previous mass fraction gradients through a convolution or memory integral"*. In this perspective, we split (1.24) in two components

$$J_{dis} = J_{dis}^f + J_{dis}^{nf}, \tag{1.26}$$

where J_{dis}^f accounts for Fickian dispersion and naturally obeys the Fickian law

$$J_{dis}^f = -D_f \nabla c, \tag{1.27}$$

and J_{dis}^{nf}, which accounts for deviations from ideal Fickian behavior and satisfies the non-Fickian relation

$$J_{dis}^{nf}(t+\tau) = -D_{nf} \nabla c(t), \tag{1.28}$$

where $\tau > 0$ is a time delay parameter [57]. That is, the non-Fickian flux J_{dis}^{nf}, at time t depends, in some fashion, on the history up to time t of the flux. As has been stressed repeatedly, one key drawback of equation (1.24) is that it imposes a instantaneous relation between the cause, concentration gradient, and the effect, mass flux. This non-physical infinite speed of propagation is removed in (1.28), assuming the existence of a time interval between the cause and the effect.

Expanding the left term of (1.28) into a Taylor's series of order one, and integrating the resulting equality with respect to t, we obtain the approximation

$$J_{dis}^{nf}(t) = -\int_0^t K(t-s)\nabla \cdot (D_{nf}\nabla c(s))\, ds, \tag{1.29}$$

with the memory term

$$K(t) = \frac{1}{\tau}\exp(-t/\tau),$$

and assuming for simplicity that $J_{dis}(0) = 0$. Then, substituting (1.22), (1.23), (1.26), (1.27) and (1.29) into (1.25) results in the following integro-differential equation for the concentration

$$\phi\partial_t c + Ac = \int_0^t K(t-s)Bc(s)\, ds + qc^* \quad \text{in } \Omega \times (0,T], \tag{1.30}$$

with A and B given by

$$Ac = \nabla \cdot (vc) - \nabla \cdot (D_f \nabla c) \quad \text{and} \quad Bc(s) = \nabla \cdot (D_{nf}\nabla c(s)).$$

Here, D_f and D_{nf} denote a Fickian and non-Fickian dispersion tensor, respectively. We notice that if q is null, this equation is a particular case of the integro-differential equation (1.2). Following a different approach, Thompson [155] has proposed a very similar, but non-identical model. Equations similar to (1.30) were also obtained by Cattaneo [40] and by Joseph and Preziosi [105] to model heat conduction. In this context, one can view equation (1.30) as a type of Jeffrey's equation with advection.

If the velocity field v is unknown, an additional equation is needed. For this, we assume that v satisfies the incompressibility condition

$$\nabla \cdot v = q \quad \text{in } \Omega \tag{1.31}$$

and obeys Darcy's law, while depending only on the porous medium,

$$v = -\bar{K}\nabla p \quad \text{in } \Omega. \tag{1.32}$$

Here p is the pressure of the fluid mixture and $\bar{K}$ is the permeability tensor of the medium, which is a measure of the medium's ability to transmit the fluid. As usual, we assume that $\bar{K}$ is symmetric positive definite.

Therefore, the proposed mathematical model for describing flow and non-Fickian transport in porous media is described by the uncoupled system (1.30)-(1.32). This system also needs to be closed by an initial condition for the concentration,

$$c(0) = c_0 \quad \text{in } \Omega, \tag{1.33}$$

and the boundary conditions

$$p = p_D \quad \text{on } \partial\Omega_D, \tag{1.34}$$

$$\bar{K}\nabla p \cdot \eta = v \cdot \eta = g \quad \text{on } \partial\Omega_N, \tag{1.35}$$

$$c = c_D \quad \text{on } \partial\Omega_D \times (0,T], \tag{1.36}$$

$$\Big(vc - D_f\nabla c - \int_0^t K(t-s)D_{nf}\nabla c(s)\,ds\Big)\cdot\eta = f \quad \text{on } \partial\Omega_N \times (0,T], \tag{1.37}$$

where η is the unit outward normal vector to $\partial\Omega$, and $\partial\Omega_D$ and $\partial\Omega_N$ are the Dirichlet and Neumann parts of the boundary, respectively.

In these problems, where advection is the dominant process and the medium is highly heterogeneous, we expect the equations (1.30)-(1.32) to have complex solutions with moving steep fronts and rough velocity fields. Therefore, standard methods such as finite differences and finite elements are not appropriate [67].

To conclude this section, we would like to mention that for many porous media problems, Darcy's law (1.32) depends also on the concentration through the expression

$$v = -\frac{\bar{K}}{\mu(c)}\nabla p, \tag{1.38}$$

where $\mu(c)$ is the viscosity of the fluid mixture. In this case, our mathematical model would consist of a coupled integro-differential elliptic system.

This and other possible modifications create new challenging theoretical and numerical issues that will certainly be topics of future work. In fact, coupled systems resulting from the use of equation (1.38) are the subject of ongoing studies. At this point, we are dealing with a simplified problem; however, we think that the preliminary theoretical results are quite interesting and novel. For this reason, we decided to present them in this thesis. In Section 1.3, we specify the problem in more detail.

1.2.2 Contributions of this Work

In this thesis, we introduce a PIDE model to describe non-Fickian tracer transport in porous media. In Chapter 5, we test the accuracy of the one-dimensional model and how it compares against the classical PDE model. A small set of experiments are analyzed, and we can conclude that even in laboratory-scale homogeneous porous media, transport processes may exhibit anomalous non-Fickian behavior that the PIDE model can reproduce and that the classical PDE model fails to capture. Overall, the results indicate that the PIDE model provides a substantial improvement over the standard PDE model. However, further work is needed to test the proposed model using much more experimental data. A more profound physical and mathematical analysis of the model should also be carried out.

Also in Chapter 5, we propose an accurate and stable numerical method for the discretization in two dimensions. In space, it is based on the combination of mixed finite element and finite volume methods over an unstructured triangular mesh. For the time integration, we use a multistep method combined with a numerical quadrature rule for the integral term. As we will demonstrate, this time procedure can be implement in a memory-efficient way as a three-time-level scheme. Therefore, we overcome one of the intrinsic drawbacks usually associated with PIDE models, namely, the memory requirements need to evaluate the time integral term. Some results regarding this integro-differential model were published in [83].

1.3 A Parabolic-Elliptic Coupled Problem

Following the discussion at the end of Section 1.2.1, we introduce now a coupled system formed by the elliptic equation

$$-\nabla \cdot (a(c)\nabla p) = q_1 \quad \text{in } \Omega \times (0,T] \tag{1.39}$$

and by the parabolic equation

$$\partial_t c + \nabla(b(c,\nabla p)c) - \nabla(d(c,\nabla p)\nabla c) = q_2 \quad \text{in } \Omega \times (0,T], \tag{1.40}$$

complemented with homogeneous Dirichlet boundary conditions

$$p = c = 0 \quad \text{on } \partial\Omega \times (0,T], \tag{1.41}$$

and the initial conditions

$$p(0) = p_0, \quad c(0) = c_0 \quad \text{in } \Omega. \tag{1.42}$$

Here the domain Ω is one-dimensional and $a : \mathbb{R} \to \mathbb{R}$ and $b, d : \mathbb{R}^2 \to \mathbb{R}$ are given functions.

In the absence of sources and sinks, and with a suitable choice of functions a, b and d, it is easy to observe that the equations (1.39)-(1.42) can yield a classical one-dimensional PDE model for the tracer transport problem. Note, however, that here we allow a relation like (1.38) for the velocity, and therefore the resulting system is coupled. This is more complex than we have assumed before for the PIDE model (see equation (1.32)). With some modifications to account for sources and sinks, the two-dimensional version of such a system with Dirichlet, Neumann, or mixed Dirichlet-Neumann boundary conditions has been extensively analyzed in the literature. Without being exhaustive, we refer to [67, 73] for the numerical treatment and to [45] for the question of existence and uniqueness of the solution. Convergence studies and error estimates are available for some numerical methods. For instance, in [81] the sub-optimal bound

$$\|p(t) - p_h(t)\|_{H^1} + \|c(t) - c_h(t)\|_{L^2} \leq Ch,$$

was obtained for piecewise linear FEMs. Assuming that the dispersion tensor D does not depend on ∇p, the following optimal bound was also proved,

$$\|c(t) - c_h(t)\|_{L^2} \leq Ch^2.$$

As mentioned before, traditional FEMs are ineffective to solve these kind of problems; therefore other approaches were investigated. For example, in [117], FEMs were used to calculate the pressure, but a proper post-processing technique was employed to approximate the velocity, and a stabilized FEM was applied to the concentration equation. The error of the semi-discrete approximation was analyzed, and a near optimal rate of convergence for the piecewise case was obtained:

$$\|c(t) - c_h(t)\|_{L^2} \leq Ch^{1.5}.$$

Mixed finite elements are highly regarded methods to approximate p and v. The combination of RT_0 elements with piecewise linear FEMs for the concentration equation was proved [60, 79] to yield the estimate

$$\|c(t) - c_h(t)\|_{L^2} + \|v(t) - v_h(t)\|_{H(div)} + \|p(t) - p_h(t)\|_{L^2} \leq Ch,$$

which can be improved to h^2 if first-order Raviart-Thomas mixed elements are employed or the Darcy's velocity is post-processed [59, 80]. On the other hand, optimal convergence for the concentration of the form

$$\|c(t) - c_h(t)\|_{H^1} + \|v(t) - v_h(t)\|_{L^2} \leq Ch,$$

was demonstrated in [151], by coupling RT_0 elements with discontinuous FEMs.

1.3.1 Contributions of this Work

In this thesis, we develop a non-standard piecewise linear FEM to numerically solve the problem (1.39)-(1.42). Our major contribution appears in Chapter 4, where we prove supercloseness to the gradients ∇c and ∇p. The estimate is of the form

$$\begin{aligned}\|P_h p(t) - p_h(t)\|_{H^1}^2 + \int_0^t \|P_h c(s) - c_h(s)\|_{H^1}^2 \, ds \\ \leq Ch^4 \int_0^t \|c(s)\|_{H^3}^2 + \|p(s)\|_{H^3}^2 + \|\partial_t c(s)\|_{H^2}^2 \, ds,\end{aligned}$$

with h associated with an arbitrary non-uniform mesh. To our knowledge, supercloseness of the gradient ∇c has not been established before for this kind of problem. However, we note that our problem is one-dimensional and a somewhat simplified version of the usual one. We are assuming Dirichlet boundary conditions and that there are no source or sink terms. The main contents of this chapter have been published in [85]. Some additional results were published in [84].

Chapter 2

A FEM for Parabolic PIDEs in One Dimension

In this chapter, we consider the one-dimensional version of our main equation

$$\partial_t c + Ac = \int_0^t B(s,t)c(s)\,ds + f \quad \text{in } \Omega \times (0,T], \tag{2.1}$$

subject to homogeneous Dirichlet boundary conditions

$$c = 0 \quad \text{on } \partial\Omega \times (0,T], \tag{2.2}$$

and with the initial condition

$$c(0) = c_0 \quad \text{in } \Omega. \tag{2.3}$$

The differential operators A and $B(s,t)$ are defined as follows:

$$Ac = -\nabla(a_2\nabla c) + \nabla(a_1 c) + a_0 c$$

and

$$B(s,t)c = -\nabla(b_2(s,t)\nabla c) + \nabla(b_1(s,t)c) + b_0(s,t)c.$$

For the coefficient functions, we assume that a_2 and $b_2(s,t)$ are in $C(\bar{\Omega})$ and a_0, a_1, $b_0(s,t)$, and $b_1(s,t)$ belong to $W^{2,\infty}(\Omega)$, for $s,t \in (0,T]$. We also assume that c_0 and f are smooth enough and set, without loss of generality, $\Omega = (0,1)$.

In the next sections, we study the numerical approximation in space of problem (2.1)-(2.3) using piecewise linear finite elements with special quadrature rules. The stability and convergence of the semi-discrete method is discussed and supercloseness in the H^1-norm is proved without any smoothness assumptions on the mesh.

2.1 A Semi-Discrete Galerkin Method

Let us denote by $(\cdot,\cdot)$ the standard inner product in $L^2(\Omega)$. A variational formulation of our problem is: find $c:[0,T]\to H_0^1(\Omega)$ such that, for all $v\in H_0^1(\Omega)$,

$$\begin{cases} (\partial_t c, v) + a(c,v) = \displaystyle\int_0^t b(s,t,c(s),v)\,ds + (f,v) \quad \text{for } t\in(0,T], \\ \\ c(0) = c_0, \end{cases} \tag{2.4}$$

where for $w, v\in H_0^1(\Omega)$,

$$a(w,v) = (a_2\nabla w, \nabla v) - (a_1 w, \nabla v) + (a_0 w, v)$$

and

$$b(s,t,w,v) = (b_2(s,t)\nabla w, \nabla v) - (b_1(s,t)w, \nabla v) + (b_0(s,t)w, v).$$

Next, we present the standard semi-discrete Galerkin FEM for (2.4) using piecewise linear functions. First, we introduce some useful notation. For a positive integer N, let

$$\Omega_h = \{x_i : 0 = x_0 < x_1 < \ldots < x_N = 1\}$$

be an arbitrary spatial grid, and set $h_i = x_i - x_{i-1}$ and $x_{i-1/2} = x_i - h_i/2$, for $i = 1,\ldots,N$. Denote by h the vector $(h_1,\ldots,h_N)$ and define $h_{max} = \max h$, then, represent by H a sequence of grid vectors $h^{(k)}$ with $h_{max}^{(k)}\to 0$, if $k\to\infty$. At last, we denote by $S_h\subset H_0^1(\Omega)$ the space of continuous piecewise linear functions over the grid Ω_h that vanish at the end points.

Let $c_{h,0}\in S_h$ be an appropriate approximation of c_0. A standard semi-discrete FEM consists in finding $c_h:[0,T]\to S_h$ such that, for all $v_h\in S_h$,

$$\begin{cases} (\partial_t c_h, v_h) + a(c_h,v_h) = \displaystyle\int_0^t b(s,t,c_h(s),v_h)\,ds + (f,v_h) \quad \text{for } t\in(0,T], \\ \\ c_h(0) = c_{h,0}, \end{cases} \tag{2.5}$$

with

$$a(w_h,v_h) = (a_2\nabla w_h, \nabla v_h) - (a_1 w_h, \nabla v_h) + (a_0 w_h, v_h) \tag{2.6}$$

and

$$b(s,t,w_h,v_h) = (b_2(s,t)\nabla w_h, \nabla v_h) - (b_1(s,t)w_h, \nabla v_h) + (b_0(s,t)w_h, v_h), \tag{2.7}$$

for $w_h, v_h \in S_h$.

The semi-discrete FEM that we propose is obtained by using numerical quadrature to evaluate the inner products appearing in (2.5)-(2.7). Before describing our method, we need to introduce some definitions and notations. Let ϕ_i, for $i = 1, \ldots, N-1$, be the standard hat functions associated with the nodes x_i. Since this set of functions is a basis for the space S_h, we write any function v_h in S_h as

$$v_h(x) = \sum_{i=1}^{N-1} v_h(x_i)\phi_i(x) \quad \text{for } x \in \Omega.$$

Next, we define the inner product

$$(w_h, v_h)_h = \sum_{i=1}^{N-1} h_{i+1/2} w_h(x_i) v_h(x_i) \quad \text{for } w_h, v_h \in S_h, \tag{2.8}$$

where $h_{i+1/2} = (h_i + h_{i+1})/2$. Observe that (2.8) corresponds to an approximation of the L^2-inner product in S_h by the composite trapezoidal rule. The norm associated with the inner product (2.8) is denoted by $\|\cdot\|_h$. It can be proved that this norm is equivalent to the L^2-norm on S_h. Finally, for a sufficiently smooth function g, we set

$$M(g(x)) = g(x_{i-1/2}) \quad \text{and} \quad M^*(g(x)) = (g(x_{i-1}) + g(x_i))/2,$$

for $x \in (x_{i-1}, x_i]$, and where $i = 1, \ldots, N$, we define the grid approximation

$$(g(x_i))_h = \begin{cases} \dfrac{1}{h_{i+1/2}} \displaystyle\int_{x_{i-1/2}}^{x_{i+1/2}} g(x)\, dx & \text{for } i = 1, \ldots, N-1, \\ \\ 0 & \text{for } i = 0, N, \end{cases}$$

and, with the additional condition that g is null on $\partial\Omega$, we also define its interpolant $P_h g$ in S_h by

$$P_h g(x) = \sum_{i=1}^{N-1} g(x_i)\phi_i(x) \quad \text{for } x \in \Omega.$$

Then, our semi-discrete FEM reads as follows: find $c_h : [0, T] \to S_h$ such that, for all $v_h \in S_h$,

$$\begin{cases} (\partial_t c_h, v_h)_h + a_h(c_h, v_h) = \displaystyle\int_0^t b_h(s, t, c_h(s), v_h)\, ds + ((f)_h, v_h)_h \ \text{ for } t \in (0, T], \\ \\ c_h(0) = c_{h,0}, \end{cases} \tag{2.9}$$

with

$$a_h(w_h, v_h) = (M(a_2)\nabla w_h, \nabla v_h) - (M^*(a_1 w_h), \nabla v_h) + (a_0 w_h, v_h)_h \tag{2.10}$$

and

$$\begin{aligned} b_h(s,t,w_h,v_h) = (M(b_2(s,t))\nabla w_h, \nabla v_h) \\ - (M^*(b_1(s,t)w_h), \nabla v_h) + (b_0(s,t)w_h, v_h)_h, \end{aligned} \tag{2.11}$$

for $w_h, v_h \in S_h$. Observe that a solution c_h can be expanded in the form

$$c_h(x,t) = \sum_{i=1}^{N-1} c_h(x_i,t)\phi_i(x) \quad \text{for } x \in \Omega,\ t \in [0,T].$$

We point out that the first two terms arising on the right-hand side of (2.10) and (2.11) are approximations by the composite midpoint and trapezoidal rule, respectively, of the equivalent terms in (2.6) and (2.7). For later convenience, we assume that $a_h(\cdot,\cdot)$ is continuous

$$|a_h(w_h, v_h)| \le C_{a,c}\|w_h\|_{H^1}\|v_h\|_{H^1} \quad \text{for all } w_h, v_h \in S_h \tag{2.12}$$

and elliptic, in the sense that

$$a_h(v_h, v_h) \ge C_{a,e}\|v_h\|_{H^1}^2 \quad \text{for all } v_h \in S_h. \tag{2.13}$$

We also suppose that $b_h(s,t,\cdot,\cdot)$ is bounded uniformly with respect to s and t, i.e.,

$$|b_h(s,t,w_h,v_h)| \le C_{b,c}\|w_h\|_{H^1}\|v_h\|_{H^1} \quad \text{for all } w_h, v_h \in S_h,\ s,t \in [0,T]. \tag{2.14}$$

We close this section with some remarks. First, if $f(t)$ is at least in $H^2(\Omega)$, the approximation $(f(t))_h$ in (2.9) can be replaced by $R_h f(t)$, with R_h being the restriction operator to the grid Ω_h (see Remark 3.4 in [16]). Additionally, in the following we write $h \in \mathrm{H}$ to indicate the convergence with respect to h running through the sequence H.

2.1.1 Stability Analysis

We say that a function v_h belongs to $C^1([0,T]; S_h)$ if v_h and $\partial_t v_h$ are continuous functions from $[0,T]$ to S_h endowed with the norm $\|\cdot\|_h$. The main result of this section is given in Theorem 2.1, where we prove a stability result for a solution c_h of (2.9). From there, assuming that $f = 0$, the stability of c_h, with respect to perturbations of the initial condition $c_{h,0}$ in the norm $\|\cdot\|_{H^1}$, can easily be derived.

Theorem 2.1 *Let us suppose that $a_h(\cdot,\cdot)$ and $b_h(s,t,\cdot,\cdot)$ satisfy (2.13) and (2.14), respectively. If a solution c_h of (2.9) is in $C^1([0,T];S_h)$, then*

$$\|c_h(t)\|_h^2 + \int_0^t \|c_h(s)\|_{H^1}^2\, ds \le Ce^{Ct}\Big(\|c_{h,0}\|_h^2 + \int_0^t \|(f(s))_h\|_h^2\, ds\Big), \tag{2.15}$$

for $t \in [0,T]$, with

$$C = \frac{max\{1, C_{b,c}^2 T/2\epsilon^2\}}{min\{1, 2(C_{a,e} - \epsilon^2)\}} \tag{2.16}$$

and for all $\epsilon \neq 0$, such that

$$C_{a,e} - \epsilon^2 > 0. \tag{2.17}$$

Proof: Taking in (2.9) $v_h = c_h(t)$, we establish

$$\frac{1}{2}\partial_t\|c_h(t)\|_h^2 + C_{a,e}\|c_h(t)\|_{H^1}^2 \le C_{b,c}\int_0^t \|c_h(s)\|_{H^1}\|c_h(t)\|_{H^1}\, ds + \frac{1}{2}\Big(\|(f(t))_h\|_h^2 + \|c_h(t)\|_h^2\Big).$$

Since we have

$$\int_0^t \|c_h(s)\|_{H^1}\|c_h(t)\|_{H^1}\, ds \le \frac{1}{4\epsilon^2}\Big(\int_0^t \|c_h(s)\|_{H^1}\, ds\Big)^2 + \epsilon^2\|c_h(t)\|_{H^1}^2,$$

for all $\epsilon \neq 0$, we deduce

$$\partial_t\|c_h(t)\|_h^2 + 2(C_{a,e} - \epsilon^2)\|c_h(t)\|_{H^1}^2 \le \frac{C_{b,c}^2}{2\epsilon^2}\Big(\int_0^t \|c_h(s)\|_{H^1}\, ds\Big)^2 + \|(f(t))_h\|_h^2 + \|c_h(t)\|_h^2. \tag{2.18}$$

Using the inequality

$$\Big(\int_0^t \|c_h(s)\|_{H^1}\, ds\Big)^2 \le T\int_0^t \|c_h(s)\|_{H^1}^2\, ds$$

in (2.18) and integrating from 0 to t, we obtain

$$\|c_h(t)\|_h^2 + 2(C_{a,e} - \epsilon^2)\int_0^t \|c_h(s)\|_{H^1}^2\, ds \le \int_0^t \|(f(s))_h\|_h^2\, ds + \|c_{h,0}\|_h^2 + \frac{C_{b,c}^2 T}{2\epsilon^2}\int_0^t\int_0^s \|c_h(\mu)\|_{H^1}^2\, d\mu\, ds + \int_0^t \|c_h(s)\|_h^2\, ds.$$

Choosing ϵ satisfying (2.17), we obtain

$$\|c_h(t)\|_h^2 + \int_0^t \|c_h(s)\|_{H^1}^2\, ds \le C\Big(\int_0^t \|(f(s))_h\|_h^2\, ds + \|c_{h,0}\|_h^2\Big) + C\int_0^t\Big(\int_0^s \|c_h(\mu)\|_{H^1}^2\, d\mu + \|c_h(s)\|_h^2\Big)\, ds$$

with C defined by (2.16). Finally, applying the Gronwall's lemma (see Lemma 2.1 in [46]), we get (2.15).

■

In the next theorem, we state a stability result for the temporal derivative of c_h.

Theorem 2.2 *Let us suppose that the inequalities (2.13) and (2.14) hold. Moreover, assume that*

$$b_h(t,t,v_h,v_h) \geq C_{b,e}\|v_h\|_{H^1}^2 \quad \textit{for all } v_h \in S_h \tag{2.19}$$

and

$$|\partial_t b_h(s,t,w_h,v_h)| \leq C_{b,d}\|w_h\|_{H^1}\|v_h\|_{H^1} \quad \textit{for all } w_h, v_h \in S_h,\ s,t \in [0,T]. \tag{2.20}$$

If a solution c_h of (2.9) is in $C^1([0,T];S_h)$, then

$$\int_0^t \|\partial_s c_h(s)\|_h^2\, ds + \|c_h(t)\|_{H^1}^2 + \int_0^t \|c_h(s)\|_{H^1}^2\, ds \leq C_1 e^{C_2 t}\Big(C_{a,c}\|c_{h,0}\|_{H^1}^2 + \int_0^t \|(f(s))_h\|_h^2\, ds\Big) \tag{2.21}$$

for $t \in [0,T]$, with ϵ and η such that

$$C_{a,e} - \eta^2 > 0 \quad \textit{and} \quad C_{b,e} - \epsilon^2 > 0, \tag{2.22}$$

and where

$$C_1 = \frac{1}{min\{1, C_{a,e}-\eta^2, 2(C_{b,e}-\epsilon^2)\}}, \quad C_2 = C_1 max\{C_{b,c}^2 T/\eta^2, C_{b,d}^2 T/2\epsilon^2\}. \tag{2.23}$$

Proof: Placing $v_h = \partial_t c_h(t)$ in (2.9), we get

$$\|\partial_t c_h(t)\|_h^2 + a_h(c_h(t), \partial_t c_h(t)) = \int_0^t b_h(s,t,c_h(s),\partial_t c_h(t))\, ds + ((f(t))_h, \partial_t c_h(t))_h. \tag{2.24}$$

Since

$$\partial_t a_h(c_h(t), c_h(t)) = 2a_h(c_h(t), \partial_t c_h(t))$$

and

$$\partial_t \int_0^t b_h(s,t,c_h(s),c_h(t))\, ds = b_h(t,t,c_h(t),c_h(t)) + \int_0^t b_h(s,t,c_h(s),\partial_t c_h(t))\, ds + \int_0^t \partial_t b_h(s,t,c_h(s),c_h(t))\, ds,$$

from (2.24), we estimate

$$\frac{1}{2}\|\partial_t c_h(t)\|_h^2 + \frac{1}{2}\partial_t a_h(c_h(t), c_h(t)) \le \partial_t \int_0^t b_h(s,t,c_h(s),c_h(t))\,ds$$
$$- \int_0^t \partial_t b_h(s,t,c_h(s),c_h(t))\,ds - b_h(t,t,c_h(t),c_h(t)) + \frac{1}{2}\|(f(t))_h\|_h^2. \tag{2.25}$$

Using the inequalities (2.19) and (2.20) in (2.25), we find

$$\frac{1}{2}\|\partial_t c_h(t)\|_h^2 + \frac{1}{2}\partial_t a_h(c_h(t), c_h(t)) + C_{b,e}\|c_h(t)\|_{H^1}^2 \le \partial_t \int_0^t b_h(s,t,c_h(s),c_h(t))\,ds$$
$$+ C_{b,d}\int_0^t \|c_h(s)\|_{H^1}\,ds \|c_h(t)\|_{H^1} + \frac{1}{2}\|(f(t))_h\|_h^2.$$

Consequently, as

$$C_{b,d}\int_0^t \|c_h(s)\|_{H^1}\,ds\|c_h(t)\|_{H^1} \le \frac{C_{b,d}^2 T}{4\epsilon^2}\int_0^t \|c_h(s)\|_{H^1}^2\,ds + \epsilon^2\|c_h(t)\|_{H^1}^2$$

holds for any $\epsilon \neq 0$, we have

$$\|\partial_t c_h(t)\|_h^2 + \partial_t a_h(c_h(t), c_h(t)) + 2(C_{b,e} - \epsilon^2)\|c_h(t)\|_{H^1}^2$$
$$\le 2\partial_t \int_0^t b_h(s,t,c_h(s),c_h(t))\,ds + \frac{C_{b,d}^2 T}{2\epsilon^2}\int_0^t \|c_h(s)\|_{H^1}^2\,ds + \|(f(t))_h\|_h^2,$$

and performing the integration from 0 to t leads to

$$\int_0^t \|\partial_s c_h(s)\|_h^2\,ds + a_h(c_h(t), c_h(t)) + 2(C_{b,e} - \epsilon^2)\int_0^t \|c_h(s)\|_{H^1}^2\,ds$$
$$\le 2\int_0^t b_h(s,t,c_h(s),c_h(t))\,ds + \frac{C_{b,d}^2 T}{2\epsilon^2}\int_0^t\int_0^s \|c_h(\mu)\|_{H^1}^2\,d\mu\,ds$$
$$+ a_h(c_{h,0}, c_{h,0}) + \int_0^t \|(f(s))_h\|_h^2\,ds.$$

According to (2.13) and (2.14), there follows

$$\int_0^t \|\partial_s c_h(s)\|_h^2\,ds + (C_{a,e} - \eta^2)\|c_h(t)\|_{H^1}^2 + 2(C_{b,e} - \epsilon^2)\int_0^t \|c_h(s)\|_{H^1}^2\,ds$$
$$\le \frac{C_{b,c}^2 T}{\eta^2}\int_0^t \|c_h(s)\|_{H^1}^2\,ds + \frac{C_{b,d}^2 T}{2\epsilon^2}\int_0^t\int_0^s \|c_h(\mu)\|_{H^1}^2\,d\mu\,ds$$
$$+ C_{a,c}\|c_{h,0}\|_{H^1}^2 + \int_0^t \|(f(s))_h\|_h^2\,ds,$$

and so

$$\int_0^t \|\partial_s c_h(s)\|_h^2\,ds + \|c_h(t)\|_{H^1}^2 + \int_0^t \|c_h(s)\|_{H^1}\,ds \le C_2\int_0^t \Big(\int_0^s \|c_h(\mu)\|_{H^1}^2\,d\mu$$
$$+ \|c_h(s)\|_{H^1}^2\Big)\,ds + C_1\Big(C_{a,c}\|c_{h,0}\|_{H^1}^2 + \int_0^t \|(f(s))_h\|_h^2\,ds\Big),$$

for ϵ and η satisfying (2.22), and with C defined by (2.23).

Applying Gronwall's lemma to the previous inequality, we conclude (2.21).

2.1.2 Error Estimates

In this section, the convergence properties of our semi-discrete method are discussed and a supercloseness estimate for the error

$$e_h(t) = P_h c(t) - c_h(t) \tag{2.26}$$

is provided. In the analysis, we follow the classical approach presented in [160] for parabolic equations. First, we split the error (2.26) into two terms:

$$\begin{aligned} e_h(t) &= P_h c(t) - \tilde{c}_h(t) + \tilde{c}_h(t) - c_h(t) \\ &= \rho_h(t) + \theta_h(t), \end{aligned} \tag{2.27}$$

where $\tilde{c}_h(t)$ is a solution of the auxiliary variational problem

$$a_h(\tilde{c}_h(t), v_h) = (g_h(t), v_h)_h \quad \text{for all } v_h \in S_h, \tag{2.28}$$

with

$$g_h(t) = \int_0^t (B(s,t)c(s))_h \, ds - (\partial_t c(t))_h + (f(t))_h.$$

Now, we proceed by estimating the terms $\rho_h(t)$ and $\theta_h(t)$. We begin with the term $\rho_h(t)$. We successively have

$$\begin{aligned} C_{a,e}\|\rho_h(t)\|_{H^1}^2 &\le a_h(\rho_h(t), \rho_h(t)) \\ &= a_h(P_h c(t), \rho_h(t)) - (g_h(t), \rho_h(t))_h \\ &= a_h(P_h c(t), \rho_h(t)) - ((Ac(t))_h, \rho_h(t))_h \\ &= a_h(P_h c(t), \rho_h(t)) - \sum_{i=1}^{N-1} \int_{x_{i-1/2}}^{x_{i+1/2}} Ac(x,t)\, dx \rho_h(x_i, t) \\ &= \tau_h^{(a)}(\rho_h(t)), \end{aligned}$$

from which we can conclude

$$\|\rho_h(t))\|_{H^1}^2 \le \frac{1}{C_{a,e}} \tau_h^{(a)}(\rho_h(t)). \tag{2.29}$$

A bound for $\rho_h(t)$ is obtained using Lemma 2.1 and (2.29). The proof of this lemma, as well as the proofs of Lemmas 2.2, 2.3, and 2.4, is essentially identical to the proof of Theorem 3.1 in [16].

Lemma 2.1 *Assume that $a_h(\cdot,\cdot)$ satisfies the inequalities (2.12) and (2.13). If $c(t) \in H^{1+r}(\Omega) \cap H_0^1(\Omega)$, for $r \in \{1,2\}$, and $\partial_t c(t) \in L^2(\Omega)$, then, for the functional $\tau_h^{(a)}$, the following is held:*

$$|\tau_h^{(a)}(v_h)| \le C\Big(\sum_{i=1}^{N} h_i^{2r} \|c(t)\|^2_{H^{1+r}(x_{i-1},x_i)}\Big)^{1/2} \|v_h\|_{H^1} \quad \text{for } v_h \in S_h,\ h \in \mathrm{H}.$$

Proposition 2.1 *Under the assumptions of Lemma 2.1, the term $\rho_h(t)$ satisfies the estimate*

$$\|\rho_h(t)\|_{H^1} \le C\Big(\sum_{i=1}^{N} h_i^{2r} \|c(t)\|^2_{H^{1+r}(x_{i-1},x_i)}\Big)^{1/2} \quad \text{for } r \in \{1,2\}.$$

For later use, we need to bound the quantity $\|\partial_t \rho_h(t)\|_{H^1}$. Proceeding as in the estimation of $\|\rho_h(t)\|_{H^1}$, we get

$$\begin{aligned}
C_{a,e}\|\partial_t \rho_h(t)\|^2_{H^1} &\le a_h(\partial_t P_h c(t) - \partial_t \tilde{c}_h(t), \partial_t \rho_h(t)) \\
&= a_h(\partial_t P_h c(t), \partial_t \rho_h(t)) - (\int_0^t (\partial_t B(s,t)c(s))_h \, ds, \partial_t \rho_h(t))_h \\
&\quad - ((B(t,t)c(t))_h, \partial_t \rho_h(t))_h + ((\partial_t^2 c(t) + \partial_t f(t))_h, \partial_t \rho_h(t))_h \\
&= a_h(\partial_t P_h c(t), \partial_t \rho_h(t)) - ((A\partial_t c(t))_h, \partial_t \rho_h(t))_h \\
&= a_h(\partial_t P_h c(t), \partial_t \rho_h(t)) - \sum_{i=1}^{N-1} \int_{x_{i-1/2}}^{x_{i+1/2}} A\partial_t c(x,t)\, dx \partial_t \rho_h(x_i,t) \\
&= \tau_h^{(d)}(\partial_t \rho_h(t)),
\end{aligned}$$

that is:

$$C_{a,e}\|\partial_t \rho_h(t)\|^2_{H^1} \le \tau_h^{(d)}(\partial_t \rho_h(t)). \tag{2.30}$$

Here, it is important to remark that, in the above derivation, we need to impose some regularity conditions on $\partial_t^2 c(t)$. This is made clear in the next lemma.

Lemma 2.2 *Assume that $a_h(\cdot,\cdot)$ satisfies the inequalities (2.12) and (2.13). If $\partial_t^2 c(t) \in L^1(\Omega)$ and $\partial_t c(t) \in H^{1+r}(\Omega)$, for $r \in \{1,2\}$, then, for the functional $\tau_h^{(d)}$, the following is held:*

$$|\tau_h^{(d)}(v_h)| \le C\Big(\sum_{i=1}^{N} h_i^{2r} \|\partial_t c(t)\|^2_{H^{1+r}(x_{i-1},x_i)}\Big)^{1/2} \|v_h\|_{H^1} \quad \text{for } v_h \in S_h,\ h \in \mathrm{H}.$$

From Lemma 2.2 and the inequality (2.30) we obtain the next proposition.

Proposition 2.2 *Under the assumptions of Lemma 2.2, the term $\partial_t \rho_h(t)$ satisfies the estimate*

$$\|\partial_t \rho_h(t)\|_{H^1} \le C\Big(\sum_{i=1}^{N} h_i^{2r} \|\partial_t c(t)\|^2_{H^{1+r}(x_{i-1},x_i)}\Big)^{1/2} \quad \text{for } r \in \{1,2\}.$$

Lemma 2.3 *The functional $\tau_h^{(b)}$ defined by*

$$\tau_h^{(b)}(t, v_h) = \int_0^t b_h(s,t,P_h c(s), v_h) - (B(s,t)c(s), v_h)_h \, ds \quad \text{for } v_h \in S_h,$$

satisfies

$$|\tau_h^{(b)}(t, v_h)| \le C \int_0^t \Big(\sum_{i=1}^{N} h_i^{2r} \|c(s)\|^2_{H^{1+r}(x_{i-1},x_i)}\Big)^{1/2} ds \|v_h\|_{H^1} \quad \text{for } r \in \{1,2\},\ h \in \mathrm{H},$$

provided that $c \in L^\infty(0,T; H^{1+r}(\Omega) \cap H_0^1(\Omega))$.

Lemma 2.4 *If $\partial_t c(t) \in H^{1+r}(\Omega)$, for $r \in \{1,2\}$, then, for*

$$\tau_h^{(c)}(t, v_h) = (\partial_t P_h c(t), v_h)_h - ((\partial_t c(t))_h, v_h)_h,$$

with $v_h \in S_h$, we have

$$|\tau_h^{(c)}(t, v_h)| \le C\Big(\sum_{i=1}^{N} h_i^{2r} \|\partial_t c(t)\|^2_{H^{1+r}(x_{i-1},x_i)}\Big)^{1/2} \|v_h\|_{H^1} \quad \text{for } h \in \mathrm{H}.$$

Now, we deal with the term $\theta_h(t)$. We define

$$\tau_{h,r}^{(b)}(t) = C \int_0^t \Big(\sum_{i=1}^{N} h_i^{2r} \|c(s)\|^2_{H^{1+r}(x_{i-1},x_i)}\Big)^{1/2} ds$$

and

$$\tau_{h,r}^{(c)}(t) = C\Big(\sum_{i=1}^{N} h_i^{2r} \|\partial_t c(t)\|^2_{H^{1+r}(x_{i-1},x_i)}\Big)^{1/2}.$$

The following lemma plays a central role in the proof of the main theorem.

Lemma 2.5 *Let us suppose that $a_h(\cdot,\cdot)$ and $b_h(s,t,\cdot,\cdot)$ satisfy (2.13) and (2.14), respectively. If $c \in L^\infty(0,T; H^{1+r}(\Omega) \cap H_0^1(\Omega))$, $\partial_t c \in L^\infty(0,T; H^{1+r}(\Omega))$, for $r \in \{1,2\}$, and $\partial_t^2 c \in L^\infty(0,T; L^1(\Omega))$, then the following holds*

$$\begin{aligned}\|\theta_h(t)\|_h^2 + 2(C_{a,e} - 3\epsilon^2) \int_0^t \|\theta_h(s)\|^2_{H^1} \, ds &\le \frac{C_{b,c}^2 T}{2\epsilon^2} \int_0^t \int_0^s \|e_h(\mu)\|^2_{H^1} \, d\mu \, ds \\ &+ \|\theta(0)\|_h^2 + \frac{1}{2\epsilon^2} \int_0^t \|\partial_s \rho_h(s)\|_h^2 + \tau_{h,r}(s)^2 \, ds, \end{aligned} \tag{2.31}$$

for $t \in [0,T]$, with $\tau_{h,r}(s) = \tau_{h,r}^{(b)}(s) + \tau_{h,r}^{(c)}(s)$ and for any $\epsilon \neq 0$.

Proof: It is easy to show that $\partial_t\theta_h(t)$ is a solution of the variational problem

$$(\partial_t\theta_h(t), v_h)_h = (\partial_t\tilde{c}_h(t), v_h)_h + a_h(c_h(t), v_h) - \int_0^t b_h(s,t,c_h(s),v_h)\,ds - ((f(t))_h, v_h)_h,$$

for all $v_h \in S_h$ and $t \in (0,T]$. According to this, and by the definition (2.27) of $\theta_h(t)$ and (2.28), we obtain

$$\begin{aligned}(\partial_t\theta_h(t), v_h)_h = (\partial_t\tilde{c}_h(t), v_h)_h - a_h(\theta_h(t), v_h) - \int_0^t b_h(s,t,c_h(s),v_h)\,ds \\ - ((\partial_t c(t))_h, v_h)_h + (\int_0^t (B(s,t)c(s))_h\,ds, v_h)_h,\end{aligned}$$

which is equivalent to

$$(\partial_t\theta_h(t), v_h)_h + a_h(\theta_h(t), v_h) = \int_0^t b_h(s,t,e_h(s),v_h)\,ds - (\partial_t\rho_h(t), v_h)_h + \tau_h(t, v_h),$$

for $v_h \in S_h$ and with $\tau_h(t,v_h) = \tau_h^{(c)}(t,v_h) - \tau_h^{(b)}(t,v_h)$.

Setting $v_h = \theta_h(t)$, since $\tau_h(t,\theta_h) \le \tau_{h,r}(t)\|\theta_h(t)\|_{H^1}$, using the same type of arguments as in the stability analysis, we find

$$\begin{aligned}\frac{1}{2}\partial_t\|\theta_h(t)\|_h^2 + C_{a,e}\|\theta_h(t)\|_{H^1}^2 \le \frac{C_{b,c}^2 T}{4\eta^2}\int_0^t \|e_h(s)\|_{H^1}^2\,ds + \eta^2\|\theta_h(t)\|_{H^1}^2 \\ + \frac{1}{4\epsilon^2}\|\partial_t\rho_h(t)\|_h^2 + \epsilon^2\|\theta_h(t)\|_{H^1}^2 + \frac{1}{4\sigma^2}\tau_{h,r}(t)^2 + \sigma^2\|\theta_h(t)\|_{H^1}^2,\end{aligned}$$

for $\epsilon \neq 0$, $\sigma \neq 0$ and for $t \in [0,T]$. Hence, setting $\epsilon = \eta = \sigma$ we arrive at

$$\begin{aligned}\partial_t\|\theta_h(t)\|_h^2 + 2(C_{a,e} - 3\epsilon^2)\|\theta_h(t)\|_{H^1}^2 \le \frac{C_{b,c}^2 T}{2\epsilon^2}\int_0^t \|e_h(s)\|_{H^1}^2\,ds \\ + \frac{1}{2\epsilon^2}\Big(\|\partial_t\rho_h(t)\|_h^2 + \tau_{h,r}(t)^2\Big). \qquad (2.32)\end{aligned}$$

We conclude the proof by integrating (2.32).

■

Now, we are able to establish the main result of this chapter.

Theorem 2.3 *Let c be a solution of the variational problem (2.4) and c_h its approximation defined by (2.9). Then, under the assumptions of Lemma 2.5, the error $e_h(t)$, for $t \in [0,T]$, satisfies the estimate*

$$\begin{aligned}\|e_h(t)\|_h^2 + \int_0^t \|e_h(s)\|_{H^1}^2\,ds \le e^{C_2 t}\Big(\int_0^t 2\|\rho_h(s)\|_{H^1}^2\,ds + 2\|\rho_h(t)\|_h^2 \\ + C_1\Big(\|\theta(0)\|_h^2 + \frac{1}{2\epsilon^2}\int_0^t \|\partial_s\rho_h(s)\|_h^2 + \tau_{h,r}(s)^2\,ds\Big)\end{aligned}$$

for $r \in \{1,2\}$, where C_1 and C_2 are defined by

$$C_1 = \frac{2}{min\{1, 2(C_{a,e} - 3\epsilon^2)\}}, \quad C_2 = C_1 \frac{C_{b,c}^2 T}{2\epsilon^2}$$

and ϵ is non-zero, such that

$$C_{a,e} - 3\epsilon^2 > 0. \tag{2.33}$$

Proof: Since

$$\|e_h(t)\|_h^2 + \int_0^t \|e_h(s)\|_{H^1}^2 \, ds \leq 2\Big(\|\rho_h(t)\|_h^2 + \int_0^t \|\rho_h(s)\|_{H^1}^2 \, ds + \|\theta_h(t)\|_h^2 + \int_0^t \|\theta_h(s)\|_{H^1}^2 \, ds\Big),$$

from (2.31) and with $\epsilon \neq 0$ under the condition (2.33), it follows that

$$\|e_h(t)\|_h^2 + \int_0^t \|e_h(s)\|_{H^1}^2 \, ds \leq C_2 \int_0^t \int_0^s \|e_h(\mu)\|_{H^1}^2 \, d\mu \, ds + \int_0^t 2\|\rho_h(s)\|_{H^1}^2 \, ds + 2\|\rho_h(t)\|_h^2 + C_1\Big(\|\theta(0)\|_h^2 + \frac{1}{2\epsilon^2} \int_0^t \|\partial_s \rho_h(s)\|_h^2 + \tau_{h,r}(s)^2 \, ds\Big).$$

An application of Gronwall's lemma completes the proof.

■

Combining Theorem 2.3 with Propositions 2.1 and 2.2, and by the definitions of $\tau_h^{(b)}(t)$ and $\tau_h^{(c)}(t)$, we conclude the following result.

Corollary 2.1 *Let c be a solution of the variational problem (2.4) and c_h its approximation defined by (2.9). If $a_h(\cdot,\cdot)$ and $b_h(s,t,\cdot,\cdot)$ satisfy (2.13) and (2.14), respectively, then, for $r \in \{1,2\}$,*

$$\|e_h(t)\|_h^2 + \int_0^t \|e_h(s)\|_{H^1}^2 \leq C\Big(\sum_{i=1}^N h_i^{2r}\Big(\int_0^t \|c(s)\|_{H^{1+r}(x_{i-1},x_i)}^2 \, ds + \|c(t)\|_{H^{1+r}(x_{i-1},x_i)}^2 + \|\partial_t c(t)\|_{H^{1+r}(x_{i-1},x_i)}^2\Big) + \|P_h c_0 - c_{h,0}\|_h^2\Big),$$

for $t \in [0,T]$ and $h \in \mathrm{H}$, provided that $c \in L^\infty(0,T; H^{1+r}(\Omega) \cap H_0^1(\Omega))$, $\partial_t c \in L^\infty(0,T; H^{1+r}(\Omega))$, $\partial_t^2 c \in L^\infty(0,T; L^1(\Omega))$, and $\|\theta(0)\|_h^2 \leq C h_{max}^{2r}$.

Thus, our supercloseness result follows as a particular case of Corollary 2.1, by taking $r = 2$ and defining $c_{h,0}$, such that

$$\|P_h c_0 - c_{h,0}\|_h \leq C h_{max}^2. \tag{2.34}$$

We state this in the corollary below.

Corollary 2.2 *Assume that (2.34) and the assumptions of Corollary 2.1 hold. Then,*

$$\int_0^t \|P_h c(s) - c_h(s)\|_{H^1}^2 \, ds \leq C h_{max}^4 \Big(\int_0^t \|c(s)\|_{H^3}^2 \, ds + \|c(t)\|_{H^3}^2 + \|\partial_t c(t)\|_{H^3}^2 \Big),$$

for $t \in [0,T]$, provided that $c \in L^\infty(0,T;H^3(\Omega) \cap H_0^1(\Omega))$, $\partial_t c \in L^\infty(0,T;H^3(\Omega))$, and $\partial_t^2 c \in L^\infty(0,T;L^1(\Omega))$.

In the following section, we establish the equivalence between the semi-discrete FEM (2.9) and a finite difference semi-discretization of (2.1)-(2.3).

2.1.3 Equivalence with a Finite Difference Method

Let W_h be the space of grid functions v_h^F defined on Ω_h that are null on $\partial\Omega$. In W_h we introduce the following finite difference operators

$$D_c v_h^F(x_i) = \frac{v_h^F(x_{i+1}) - v_h^F(x_{i-1})}{h_{i+1} + h_i}, \quad Dv_h^F(x_i) = \frac{v_h^F(x_{i+1/2}) - v_h^F(x_{i-1/2})}{h_{i+1/2}}$$

and

$$Dv_h^F(x_{i+1/2}) = \frac{v_h^F(x_{i+1}) - v_h^F(x_i)}{h_{i+1}},$$

where $v_h^F(x_{i+1/2})$ is used as appropriate.

Now, we successively replace v_h in (2.9) by the basis functions ϕ_j, for $j = 1, \ldots, N-1$. After a straightforward calculation, we obtain for $c_h^F : [0,T] \to W_h$ the following ordinary differential problem

$$\begin{cases} \partial_t c_h^F + A_h c_h^F = \displaystyle\int_0^t B_h(s,t) c_h^F(s) \, ds + (f)_h \quad \text{for } t \in (0,T], \\ \\ c_h^F(0) = c_{h,0}^F, \end{cases} \tag{2.35}$$

where, for $v_h^F \in W_h$,

$$A_h v_h^F = -D(a_2 D v_h^F) + D_c(a_1 v_h^F) + a_0 v_h^F$$

and

$$B_h(s,t) v_h^F = -D(b_2(s,t) D v_h^F) + D_c(b_1(s,t) v_h^F) + b_0(s,t) v_h^F.$$

We remark that c_h, defined by

$$c_h(x,t) = \sum_{i=1}^{N-1} c_h^F(x_i,t) \phi_i(x) \quad \text{for } x \in \Omega, \ t \in [0,T],$$

furnishes a solution to the problem (2.9) whenever c_h^F is a solution of the problem (2.35). From this relation, and from observing that the discrete norm

$$\|v_h^F\|_{1,h}^2 = \|v_h^F\|_h^2 + \|v_h^F\|_{h^*}^2,$$

with

$$\|v_h^F\|_{h^*}^2 = \sum_{i=1}^{N} h_i D v_h^F(x_{i-1/2})^2,$$

is equivalent to the H^1-norm on S_h, we can see our supercloseness result as a supraconvergence result for the FDM (2.35). In fact, the estimate

$$\int_0^t \|c(s) - c_h^F(s)\|_{1,h}^2 \, ds \leq C h_{max}^4 \Big(\int_0^t \|c(s)\|_{H^3}^2 \, ds + \|c(t)\|_{H^3}^2 + \|\partial_t c(t)\|_{H^3}^2 \Big),$$

holds under the assumptions of Corollary 2.2.

2.2 Numerical Experiments

In this section, we illustrate the convergence result of Corollary 2.1 by applying the proposed method to one simple problem with a known exact solution.

In the temporal domain $[0, T]$, let us introduce the uniform time grid $t_n = n\Delta t$, for $n = 0, \ldots, N$, with $t_N = T$, and where Δt is a fixed time step. We define the error as

$$\text{Error} = \Big(\|c(t_N) - c_h^N\|_h^2 + \Delta t \sum_{n=1}^{N} \|c(t_n) - c_h^n\|_{1,h}^2 \Big)^{1/2}$$

where c_h^n is a numerical solution at time level t_n, and where the summation is an approximation to the integral appearing on the left-hand side of Corollary 2.1.

Example 2.1 *Consider the integro-differential problem (2.1)-(2.3) with* $T = 0.1$ *and the coefficient functions*

$$a_2(x) = a_1(x) = x + 1, \quad a_0 = b_0(s,t) = b_1(s,t) = 0, \quad \textit{and} \quad b_2(s,t) = e^{-t+s}.$$

Choose f *and* c_0*, such that the problem has the solution*

$$c(x,t) = tx(x-1)|x - 0.5|^\alpha \quad \textit{for } \alpha \in \mathbb{R}.$$

Starting with a random spatial grid, we repeatedly solve Example 2.1, each time doubling the size of the grid vector h by taking $h_i = h_i/2$. We repeat this procedure twice, first by considering $\alpha = 2.1$, and then by considering $\alpha = 3.1$. Observe that

h_{max}	N_x	Error	Rate
9.6988×10^{-2}	19	1.5092×10^{-4}	1.0337
4.8494×10^{-2}	39	7.3717×10^{-5}	1.1120
2.4247×10^{-2}	79	3.4106×10^{-5}	1.0688
1.2124×10^{-2}	159	1.6259×10^{-5}	1.0876
6.0618×10^{-3}	319	7.6503×10^{-6}	1.0924
3.0309×10^{-3}	639	3.5880×10^{-6}	1.0924
1.5154×10^{-3}	1279	1.6827×10^{-6}	-

Table 2.1: Discrete norm error and convergence rate for Example 2.1, with $\alpha = 2.1$.

the solution of the Example 2.1 belongs to $H_0^2(\Omega)$ if $\alpha > 2$ and to $H_0^3(\Omega)$ if $\alpha > 3$. Therefore, according to Corollary 2.1, we expect convergence rates of order one and order two for each case, respectively. The numerical results presented in Tables 2.1 and 2.2 confirm this expectation. Here we denote by N_x the number of interior nodes.

h_{max}	N_x	Error	Rate
9.4732×10^{-2}	19	5.7534×10^{-5}	1.6960
4.7366×10^{-2}	39	1.7758×10^{-5}	1.9413
2.3683×10^{-2}	79	4.6237×10^{-6}	2.0876
1.1841×10^{-2}	159	1.0878×10^{-6}	2.0579
5.9207×10^{-3}	319	2.6126×10^{-7}	2.0270
2.9604×10^{-3}	639	6.4103×10^{-8}	2.0071
1.4802×10^{-3}	1279	1.5947×10^{-8}	-

Table 2.2: Discrete norm error and convergence rate for Example 2.1, with $\alpha = 3.1$.

In the numerical computations of this section, we have applied the implicit Euler method for the time discretization and the rectangular rule to compute the integral term. The time step used, $\Delta t = 10^{-6}$, is lower than the minimum of all values h_{max}^2. This is small enough to avoid significant errors due to time discretization.

Chapter 3

A FEM for Parabolic PIDEs in Two Dimensions

In this chapter, we deal with the two-dimensional version of the integro-differential problem that we are discussing. Unless otherwise stated, the notation used here should be interpreted as previously defined.

Let Ω be a simple polygonal domain of $\mathbb{R}^2$, i.e., an open connected set with piecewise linear boundary. We consider discretizations of the integro-differential problem

$$\begin{cases} \partial_t c + Ac = \displaystyle\int_0^t B(s,t)c(s)\,ds + f \quad \text{in } \Omega \times (0,T], \\ \\ c(0) = c_0 \quad \text{in } \Omega, \end{cases} \tag{3.1}$$

completed with homogeneous Dirichlet boundary conditions. The differential operators A and $B(s,t)$ are given by

$$Ac = -\nabla \cdot (A_2 \nabla c) + \nabla \cdot (A_1 c) + a_0 c \tag{3.2}$$

and

$$B(s,t)c = -\nabla \cdot (B_2(s,t)\nabla c) + \nabla \cdot (B_1(s,t)c) + b_0(s,t)c, \tag{3.3}$$

where $A_2 = [a_{ij}]$ and $B_2(s,t) = [b_{ij}(s,t)]$ for $i,j = 1,2$ are symmetric matrices, and where $A_1 = [a_i]$ and $B_1(s,t) = [b_i(s,t)]$ for $i = 1,2$ are vectors. Moreover, we assume that the coefficient functions of A and $B(s,t)$ are in $W^{2,\infty}(\Omega)$, for $s,t \in (0,T]$, and that c_0 and f are regular enough.

In the following sections, we propose and analyze a semi-discrete FEM that can be seen as a natural extension of the one-dimensional scheme presented in the previous chapter. As before, we are able to prove supercloseness in the H^1-norm. However,

here we introduce an error analysis framework that allows us to reduce the smoothness assumptions on the analytical solution. The discretization in time using an implicit-explicit (IMEX) method is also considered, and stability and convergence results are derived.

3.1 A Semi-Discrete Galerkin Method

We start this section with the variational formulation of the problem. This is followed by the presentation of our semi-discrete method, first in the absence of mixed derivatives, and then for the full problem. As we will see, the presence of mixed derivatives requires extra effort. Here, we skip the derivation of a standard FEM, since it is essentially identical to that appearing in Section 2.1.

A variational formulation of problem (3.1)-(3.3) is: find $c : [0,T] \to H_0^1(\Omega)$ such that, for all $v \in H_0^1(\Omega)$,

$$\begin{cases} (\partial_t c, v) + a(c,v) = \displaystyle\int_0^t b(s,t,c(s),v)\,ds + (f,v) \quad \text{for } t \in (0,T], \\ \\ c(0) = c_0, \end{cases} \tag{3.4}$$

where for $w, v \in H_0^1(\Omega)$,

$$a(w,v) = (A_2 \nabla w, \nabla v) - (A_1 w, \nabla v) + (a_0 w, v) \tag{3.5}$$

and

$$b(s,t,w,v) = (B_2(s,t)\nabla w, \nabla v) - (B_1(s,t)w, \nabla v) + (b_0(s,t)w, v). \tag{3.6}$$

To formulate our finite element approximation in space, some notations and definitions are required. Let $\mathcal{T}_h = \{T_i : i = 1, \ldots, N_T\}$ be an admissible triangulation (see Definition 8.3.7 in [91]) of the domain Ω with rectangular triangles. Denote the nodes of the triangulation by z_{jl}, for $j, l \in \mathbb{Z}$, and index them in such a way that the grid of points is obtained:

$$\bar{\Omega}_h = \big\{(x_j, y_l) : x_j = x_{j-1} + h_j^x,\ y_l = y_{l-1} + h_l^y,\ \text{for } j,l \in \mathbb{Z}\big\},$$

where (x_j, y_l) are the coordinates of the node z_{jl}. In addition, we introduce

$$h_{max} = \max h \quad \text{with} \quad h = \big\{h_j^x, h_l^y : j, l \in \mathbb{Z}\big\},$$

and the set $\Omega_h = \bar{\Omega}_h \cap \Omega$ of all the interior points of $\bar{\Omega}_h$. For every triangle $T \in \mathcal{T}_h$, we define h_T as the diameter of T and, as shown in Figure 3.1, we denote the rectangular vertex of T by v_T^1, the vertex having the same x-coordinate as the rectangular vertex by v_T^2, and the remaining vertex of the triangle by v_T^3. Take also m_T^{12} as the midpoint of the edge between v_T^1 and v_T^2, and define m_T^{13} analogously.

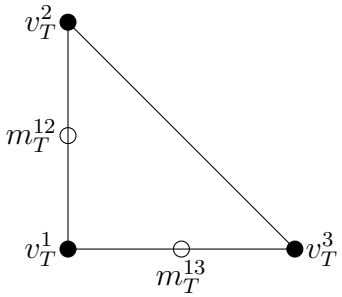

Figure 3.1: A generic triangle T and the notation.

Let the space S_h consist of the continuous piecewise linear functions over the triangulation $\mathcal{T}_h$ that vanish on $\partial\Omega$. Representing by ϕ_{jl} the usual basis functions of S_h, we have, for every function $v_h \in S_h$,

$$v_h(x,y) = \sum_{z_{jl} \in \Omega_h} v(x_j, y_l)\phi_{jl}(x,y) \quad \text{for } (x,y) \in \Omega.$$

In the space S_h, we define the inner product

$$(w_h, v_h)_h = \sum_{z_{jl} \in \Omega_h} h^x_{j+1/2} h^y_{l+1/2} w_h(x_j, y_l) v_h(x_j, y_l) \quad \text{for } w_h, v_h \in S_h, \tag{3.7}$$

which may be looked upon as an approximation to the L^2-inner product on S_h. By $\|\cdot\|_h$, we denote the norm determined by (3.7). At last, for a sufficiently smooth function g, we set

$$M_T^{1j}(g(x,y)) = (g(v_T^1) + g(v_T^j))/2 \quad \text{for } j = 2, 3,$$

and the grid approximation

$$(g(x_j, y_l))_h = \begin{cases} \dfrac{1}{|R_{jl}|} \displaystyle\int_{R_{jl}} g(x,y)\, dxdy & \text{for } z_{jl} \in \Omega_h, \\ \\ 0 & \text{for } z_{jl} \in \partial\Omega, \end{cases}$$

where $|R_{jl}|$ is the measure of the rectangle

$$R_{jl} = [x_{j-1/2}, x_{j+1/2}] \times [y_{l-1/2}, y_{l+1/2}].$$

Suppose for now that the problem (3.4)-(3.6) contains no mixed derivatives. Therefore, with $c_{h,0} \in S_h$, a suitable approximation of c_0, our semi-discrete FEM is formulated as follows: find $c_h : [0,T] \to S_h$ such that, for all $v_h \in S_h$,

$$\begin{cases} (\partial_t c_h, v_h)_h + a_h(c_h, v_h) = \displaystyle\int_0^t b_h(s,t,c_h(s),v_h)\,ds + ((f)_h, v_h)_h \quad \text{for } t \in (0,T], \\ \\ c_h(0) = c_{h,0}, \end{cases}$$

with

$$a_h(w_h, v_h) = \sum_{i=1}^{2} a_h^{ii}(w_h, v_h) - \sum_{i=1}^{2} a_h^{i}(w_h, v_h) + a_h^{0}(w_h, v_h),$$

and

$$b_h(s,t,w_h, v_h) = \sum_{i=1}^{2} b_h^{ii}(s,t,w_h, v_h) - \sum_{i=1}^{2} b_h^{i}(s,t,w_h, v_h) + b_h^{0}(s,t,w_h, v_h),$$

for $w_h, v_h \in S_h$, and where $a_h^{ii}(\cdot,\cdot)$, $a_h^{i}(\cdot,\cdot)$, and $a_h^{0}(\cdot,\cdot)$ represent the discrete bilinear forms associated with the coefficient functions a_{ii}, a_i, and a_0, respectively. In particular, we have

$$a_h^0(w_h, v_h) = (a_0 w_h, v_h)_h, \tag{3.8}$$

$$a_h^1(w_h, v_h) = \sum_{T \in \mathcal{T}_h} M_T^{13}(a_1 w_h) \int_T \nabla^x v_h \, dxdy, \tag{3.9}$$

$$a_h^2(w_h, v_h) = \sum_{T \in \mathcal{T}_h} M_T^{12}(a_2 w_h) \int_T \nabla^y v_h \, dxdy, \tag{3.10}$$

with ∇^x and ∇^y the partial derivatives in x and y, respectively, as well as

$$a_h^{11}(w_h, v_h) = \sum_{T \in \mathcal{T}_h} a_{11}(m_T^{13}) \int_T \nabla^x w_h \nabla^x v_h \, dxdy, \tag{3.11}$$

$$a_h^{22}(w_h, v_h) = \sum_{T \in \mathcal{T}_h} a_{22}(m_T^{12}) \int_T \nabla^y w_h \nabla^y v_h \, dxdy. \tag{3.12}$$

In an analogous way, we define $b_h(s,t,\cdot,\cdot)$.

Next, we discuss our FEM for the case of mixed derivatives. The definition of the bilinear forms associated with those derivatives is more technical and complex. In fact, two special rectangular triangulations that we call $\mathcal{T}_h^1$ and $\mathcal{T}_h^2$ must be designed. We proceed as follows: take a non-uniform grid $\bar{\Omega}_h$, defined as before, and consider the disjoint decomposition

$$\bar{\Omega}_h = \Omega_h^1 \,\dot\cup\, \Omega_h^2,$$

where the sum $j+l$ of the indices of the points (x_j, y_l) in Ω_h^1 and in Ω_h^2 is even and odd, respectively. In order to simplify the following definitions, we introduce also $\Omega_h^3 = \Omega_h^1$. To each point $(x_j, y_l) \in \bar{\Omega}_h$, we associate the four rectangular triangles T_{jl}^i, $i = 1, 2, 3, 4$, which have the angle $\pi/2$ at (x_j, y_l), and two of the four horizontal/vertical neighbor grid points of (x_j, y_l) as further vertices. We then define the triangulations

$$\mathcal{T}_h^k = \mathcal{T}_{h,1}^k \cup \mathcal{T}_{h,2}^k \quad \text{for } k = 1, 2,$$

with

$$\mathcal{T}_{h,1}^k = \left\{ T_{jl}^i \subset \Omega : (x_j, y_l) \in \Omega_h^k, i = 1, 2, 3, 4 \right\},$$

and

$$\mathcal{T}_{h,2}^k = \left\{ T_{jl}^i \subset (\Omega \setminus \cup \{T : T \in \mathcal{T}_{h,1}^k\}) : (x_j, y_l) \in \Omega_h^{k+1}, i = 1, 2, 3, 4 \right\}.$$

For better understanding, an example of such triangulations is displayed in Figure 3.2.

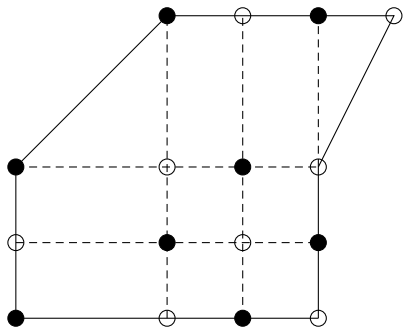

(a) Grid $\bar{\Omega}_h = \Omega_h^1 \dot{\cup} \Omega_h^2$.

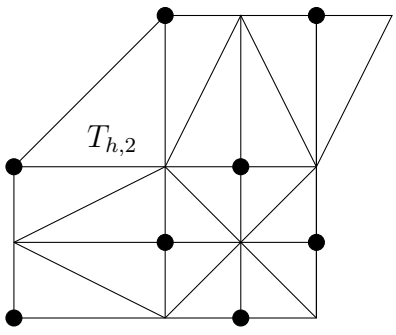

(b) Triangulation $\mathcal{T}_h^1$.

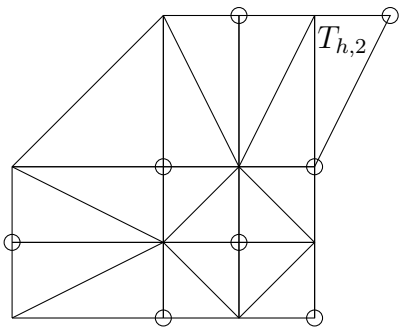

(c) Triangulation $\mathcal{T}_h^2$.

Figure 3.2: In (a) • represents a node of Ω_h^1 and ∘ represents a node of Ω_h^2. In (b) and (c) $T_{h,2}$ indicates a triangle of $\mathcal{T}_{h,2}^k$, for $k = 1, 2$.

On each triangulation $\mathcal{T}_h^k$, we define, in a natural way, the space S_h^k, and for every element $v_h \in S_h$, we associate $v_h^1 \in S_h^1$ and $v_h^2 \in S_h^2$, as defined by

$$v_h^k(x,y) = \sum_{z_{jl} \in \Omega_h} v(x_j, y_l)\phi_{jl}^k(x,y) \quad \text{for } (x,y) \in \Omega,\ k = 1,2, \tag{3.13}$$

with ϕ_{jl}^k the standard basis of S_h^k and $v(x_j, y_l)$ the coordinates of v_h in the space S_h.

Assume that $c_{h,0} \in S_h$ is an adequate approximation for c_0. Hence, our spatially discrete FEM for the full problem is: find $c_h : [0,T] \to S_h$ such that for all $v_h \in S_h$,

$$\begin{cases} (\partial_t c_h, v_h)_h + a_h(c_h, v_h) = \displaystyle\int_0^t b_h(s,t,c_h(s),v_h)\,ds + ((f)_h, v_h)_h \ \text{ for } t \in (0,T], \\ \\ c_h(0) = c_{h,0}, \end{cases} \tag{3.14}$$

where for $w_h, v_h \in S_h$,

$$a_h(w_h, v_h) = \sum_{i,j=1}^{2} a_h^{ij}(w_h, v_h) - \sum_{i=1}^{2} a_h^i(w_h, v_h) + a_h^0(w_h, v_h), \tag{3.15}$$

and

$$b_h(s,t,w_h,v_h) = \sum_{i,j=1}^{2} b_h^{ij}(s,t,w_h,v_h) - \sum_{i=1}^{2} b_h^i(s,t,w_h,v_h) + b_h^0(s,t,w_h,v_h). \tag{3.16}$$

The discrete bilinear forms $a_h^0(\cdot,\cdot)$, $a_h^i(\cdot,\cdot)$ and $a_h^{ii}(\cdot,\cdot)$, for $i = 1,2$, are as given in (3.8)-(3.12), so only those associated with the mixed derivatives, $a_h^{12}(\cdot,\cdot)$ and $a_h^{21}(\cdot,\cdot)$, require definition.

Remember that $a_{12} = a_{21}$, and use a_{mix} to represent both functions. With the notation of Figure 3.1, we define

$$V^{\triangle}(a_{mix}) = \begin{cases} a_{mix}(v_T^1) & \text{if } T \in \mathcal{T}_{h,1}^k, \\ \\ a_{mix}(v_T^2) & \text{if } T \in \mathcal{T}_{h,2}^k, \end{cases} \qquad V^{\triangleright}(a_{mix}) = \begin{cases} a_{mix}(v_T^1) & \text{if } T \in \mathcal{T}_{h,1}^k, \\ \\ a_{mix}(v_T^3) & \text{if } T \in \mathcal{T}_{h,2}^k. \end{cases}$$

Then, using the notation of (3.13), we write

$$a_h^{12}(w_h, v_h) = \frac{1}{2}\sum_{k=1}^{2}\sum_{T \in \mathcal{T}_h^k} \int_T V^{\triangleright}(a_{mix})\nabla^x w_h^k \nabla^y v_h^k\,dxdy$$

and

$$a_h^{21}(w_h, v_h) = \frac{1}{2}\sum_{k=1}^{2}\sum_{T \in \mathcal{T}_h^k} \int_T V^{\triangle}(a_{mix})\nabla^y w_h^k \nabla^x v_h^k\,dxdy.$$

Analogously, we can easily determine the expression of the discrete bilinear form $b_h(s,t,\cdot,\cdot)$ given by (3.16).

For later purposes, we assume that $a_h(\cdot,\cdot)$ is S_h-coercive, i.e., positive constants $C_{a,c}$, $C_{a,e}$, and $C_{a,\lambda} \in \mathbb{R}$ exist such that

$$|a_h(w_h, v_h)| \leq C_{a,c}\|w_h\|_{H^1}\|v_h\|_{H^1} \quad \text{for all } w_h, v_h \in S_h$$

and

$$a_h(v_h, v_h) \geq C_{a,e}\|v_h\|_{H^1}^2 - C_{a,\lambda}\|v_h\|_h^2 \quad \text{for all } v_h \in S_h. \tag{3.17}$$

We also assume that $b_h(s,t,\cdot,\cdot)$ is bounded uniformly with respect to s and t, i.e., a positive constant $C_{b,c}$ exists such that

$$|b_h(s,t,w_h,v_h)| \leq C_{b,c}\|w_h\|_{H^1}\|v_h\|_{H^1} \quad \text{for all } w_h, v_h \in S_h,\ s,t \in [0,T]. \tag{3.18}$$

Now, it is important to observe that this FEM can be numerically implemented as a simple FDM. The formulation given by (3.14)-(3.16) was introduced mainly for theoretical reasons, since the convergence theorems investigated in the next sections are based on this finite element approach. In the remainder of this section, we present the equivalent finite difference scheme.

Let Ω_h be the non-uniform grid previously defined over the domain Ω. Note that this grid does not require any special construction. Denote by W_h the space of grid functions vanishing on the boundary. For $v_h^F \in W_h$, take

$$\begin{aligned}
D_c^x v_h^F(x_j, y_l) &= \frac{v_h^F(x_{j+1}, y_l) - v_h^F(x_{j-1}, y_l)}{h_{j+1}^x + h_j^x}, \\
D^x v_h^F(x_j, y_l) &= \frac{v_h^F(x_{j+1/2}, y_l) - v_h^F(x_{j-1/2}, y_l)}{h_{j+1/2}^x}, \\
D^x v_h^F(x_{j+1/2}, y_l) &= \frac{v_h^F(x_{j+1}, y_l) - v_h^F(x_j, y_l)}{h_{j+1}^x},
\end{aligned}$$

and define similar operators in the y-direction. Observe that when the domain is not rectangular, the operators D_c^x and D_c^y may refer to values of grid functions on nodes outside the grid Ω_h. As in [82], we make a kind of antisymmetric extension, taking the negative value of the function evaluated at the closest interior node.

We equip the space W_h with the discrete norm

$$\|v_h^F\|_{1,h}^2 = \|v_h^F\|_h^2 + \|v_h^F\|_{h^*}^2, \tag{3.19}$$

with $\|\cdot\|_h$ given by (3.7) and where

$$\|v_h^F\|_{h^*}^2 = \sum_{z_{j_*l}\in\Omega_h} h^y_{l+1/2} h^x_j D^x v_h^F(x_{j-1/2}, y_l)^2 + \sum_{z_{jl_*}\in\Omega_h} h^x_{j+1/2} h^y_l D^y v_h^F(x_j, y_{l-1/2})^2.$$

Here, we have used the subscript to indicate that the index abuts the boundary nodes. It can be shown that the norm (3.19) is equivalent to the H^1-norm restricted to S_h.

Set $c_{h,0}^F \in W_h$ as an approximation of c_0. The FDM is then to find $c_h^F : [0,T] \to W_h$, such that

$$\begin{cases} \partial_t c_h^F + A_h c_h^F = \displaystyle\int_0^t B_h(s,t) c_h^F(s)\, ds + (f)_h \quad \text{for } t \in (0,T], \\ \\ c_h^F(0) = c_{h,0}^F, \end{cases} \tag{3.20}$$

where, for $v_h^F \in W_h$,

$$A_h v_h^F = -D^x(a_{11} D^x v_h^F) - D^y(a_{22} D^y v_h^F) - D_c^x(a_{12} D_c^y v_h^F) - D_c^y(a_{21} D_c^x v_h^F) + D^x(a_1 v_h^F) + D^y(a_2 v_h^F) + a_0 v_h^F,$$

and $B_h(s,t)v_h^F$ as $A_h v_h^F$, with the obvious adjustments. Suppose now that c_h^F is a solution of problem (3.20); hence, it can be proved that

$$c_h(x,y,t) = \sum_{z_{jl}\in\Omega_h} c_h^F(x_j, y_l, t)\phi_{jl}(x,y) \quad \text{for } (x,y) \in \Omega,\ t \in [0,T]$$

is a solution of the finite element formulation (3.14)-(3.16).

We finish this section with a comment on the stability of the FEM (3.14)-(3.16), or equivalently, of the FDM (3.20). The same kind of study as given for the one-dimensional method can be carried out for the present case. It will yield results that are identical to those given by Theorems 2.1 and 2.2 of Section 2.1.1. We note that to prove the equivalent to Theorem 2.2, we require that the bilinear form $a_h(\cdot,\cdot)$ satisfies (3.17) with $C_{a,\lambda} = 0$, i.e., it must be elliptic.

3.1.1 Error Estimates

Let c be a solution of the variational problem (3.4)-(3.6) and let c_h be the numerical approximation obtained by the FEM (3.14)-(3.16). We define the error of the method by

$$e_h(t) = P_h c(t) - c_h(t). \tag{3.21}$$

Assume for now that the domain Ω is rectangular and $a_h(\cdot,\cdot)$ is elliptic. Following the standard splitting approach [160] and proceeding just as described in the one-dimensional case, we find out that, if

$$\begin{aligned} c &\in L^\infty(0,T;H^3(\Omega)\cap H_0^1(\Omega)),\\ \partial_t c \in L^\infty(0,T;H^3(\Omega)),\quad &\text{and}\quad \partial_t^2 c \in L^\infty(0,T;L^1(\Omega)), \end{aligned} \tag{3.22}$$

then

$$\int_0^t \|e_h(s)\|_{H^1}^2\,ds \le Ch_{max}^4\Big(\int_0^t \|c(s)\|_{H^3}^2\,ds + \|c(t)\|_{H^3}^3 + \|\partial_t c(t)\|_{H^3}^2\Big), \tag{3.23}$$

for $t\in[0,T]$. In fact, this is the same supercloseness bound as that of Corollary 2.2 for the one-dimensional problem.

In this section, we provide a different approach to study the error (3.21). This will allow us to lessen the assumptions (3.22) while still preserving the supercloseness result (3.23). Besides, the complexity of this strategy is lesser than that of the conventional method. Our approach is as follows.

We start by noting that $e_h(t)$ satisfies the equality

$$\begin{aligned} \frac{1}{2}\partial_t\|e_h(t)\|_h^2 = (\partial_t P_h c(t), e_h(t))_h + a_h(c_h(t),e_h(t))\\ - \int_0^t b_h(s,t,c_h(s),e_h(t))\,ds - ((f(t))_h,e_h(t))_h. \end{aligned} \tag{3.24}$$

Note also that by (3.1)

$$((f(t))_h,e_h(t))_h = ((\partial_t c(t))_h,e_h(t))_h + ((Ac(t) - \int_0^t B(s,t)c(s)\,ds)_h,e_h(t))_h. \tag{3.25}$$

Hence, using the above expression in (3.24), we obtain

$$\frac{1}{2}\partial_t\|e_h(t)\|_h^2 + a_h(e_h(t),e_h(t)) = \int_0^t b_h(s,t,e_h(s),e_h(t))\,ds + \tau(e_h(t)), \tag{3.26}$$

with

$$\tau(e_h(t)) = \tau_d(e_h(t)) + \tau_A(e_h(t)) + \tau_{int}(e_h(t)) \tag{3.27}$$

and where

$$\begin{aligned} \tau_d(e_h(t)) &= (\partial_t P_h c(t),e_h(t))_h - ((\partial_t c(t))_h,e_h(t))_h,\\ \tau_{int}(e_h(t)) &= \int_0^t ((B(s,t)c(s))_h,e_h(t))_h - b_h(s,t,P_h c(s),e_h(t))\,ds,\\ \tau_A(e_h(t)) &= a_h(P_h c(t),e_h(t)) - ((Ac(t))_h,e_h(t))_h. \end{aligned}$$

Now we proceed to estimate (3.27). Let $\mathcal{T}_h^{obl}$ be the set of triangles that have one edge on the oblique part of $\partial\Omega$, and define Ω_h^{obl} as the region of the domain formed by those triangles. By C_{mix}^{obl}, we denote an indicator function that is equal to zero if $\Omega_h^{obl} = \emptyset$ or $a_{mix} = b_{mix} = 0$, and is equal to one if $\Omega_h^{obl} \neq \emptyset$ and $a_{mix} \neq 0$ or $b_{mix} \neq 0$. The following proposition is a direct consequence of Lemmas 5.1, 5.2, 5.4, 5.5, and 5.7 of [82].

Proposition 3.1 *Suppose that the coefficients of the differential operators A and $B(s,t)$ are in $W^{r,\infty}(\Omega)$, for $s,t \in [0,T]$, and let $r \in \{1,2\}$ and $h \in \mathrm{H}$. Then,*

$$|\tau(v_h)| \leq \tau^{(r)}(t)\|v_h\|_{H^1} \quad \textit{for } v_h \in S_h,$$

with

$$\begin{aligned}\tau^{(1)}(t) &\leq C\Big(\Big(\sum_{T\in\mathcal{T}_h} h_T^2\|c(t)\|_{H^2(T)}^2\Big)^{1/2} + \Big(\sum_{T\in\mathcal{T}_h} h_T^4\|\partial_t c(t)\|_{H^2(T)}^2\Big)^{1/2} \\ &\qquad + \int_0^t \Big(\sum_{T\in\mathcal{T}_h} h_T^2\|c(s)\|_{H^2(T)}^2\Big)^{1/2} ds\Big) \\ &\leq Ch_{max}\Big(\|c(t)\|_{H^2} + \|\partial_t c(t)\|_{H^2} + \int_0^t \|c(s)\|_{H^2}\, ds\Big), \end{aligned} \tag{3.28}$$

provided that $c \in L^\infty(0,T;H^2(\Omega)\cap H_0^1(\Omega))$ and $\partial_t c \in L^\infty(0,T;H^2(\Omega))$, and

$$\begin{aligned}\tau^{(2)}(t) &\leq C\Big(\Big(\sum_{T\in\mathcal{T}_h} h_T^4\|c(t)\|_{H^3(T)}^2\Big)^{1/2} + \Big(\sum_{T\in\mathcal{T}_h} h_T^4\|\partial_t c(t)\|_{H^2(T)}^2\Big)^{1/2} \\ &\qquad + \int_0^t \Big(\sum_{T\in\mathcal{T}_h} h_T^4\|c(s)\|_{H^3(T)}^2\Big)^{1/2} ds + C_{mix}^{obl}\Big(\Big(\sum_{T\in\mathcal{T}_h^{obl}} h_T^{4(1-1/p)}|c(t)|_{W^{2,p}(T)}^2\Big)^{1/2} \\ &\qquad\qquad + \int_0^t \Big(\sum_{T\in\mathcal{T}_h^{obl}} h_T^{4(1-1/p)}|c(s)|_{W^{2,p}(T)}^2\Big)^{1/2} ds\Big) \\ &\leq Ch_{max}^2\Big(\|c(t)\|_{H^3} + \|\partial_t c(t)\|_{H^2} + \int_0^t \|c(s)\|_{H^3}\, ds\Big) \\ &\qquad + C_{mix}^{obl}Ch_{max}^{3/2-1/p}\Big(|c(t)|_{W^{2,p}(\Omega_h^{obl})} + \int_0^t |c(s)|_{W^{2,p}(\Omega_h^{obl})}\, ds\Big), \end{aligned} \tag{3.29}$$

provided that $c \in L^\infty(0,T;H^3(\Omega)\cap H_0^1(\Omega))$ and $\partial_t c \in L^\infty(0,T;H^2(\Omega))$, for $p \in [2,\infty)$.

With the aid of Proposition 3.1 and equation (3.26), we can establish one of our main results for the error $e_h(t)$.

Theorem 3.1 *Assume that $a_h(\cdot,\cdot)$ and $b_h(s,t,\cdot,\cdot)$ satisfy (3.17) and (3.18), respectively. Then, for $r \in \{1,2\}$, and under the hypothesis of Proposition 3.1, it holds*

$$\|e_h(t)\|_h^2 + \int_0^t \|e_h(s)\|_{H^1}^2\, ds \leq C_1 e^{C_2 t}\Big(\|e_h(0)\|_h^2 + \frac{1}{2\eta^2}\int_0^t \tau^{(r)}(s)^2\, ds\Big),$$

with ϵ and η non-zero constants such that

$$C_{a,e} - \epsilon^2 - \eta^2 > 0, \tag{3.30}$$

and where

$$C_1 = \frac{1}{min\{1, 2(C_{a,e} - \epsilon^2 - \eta^2)\}}, \quad C_2 = C_1 max\{2C_{a,\lambda}, C_{b,c}^2 T/2\epsilon^2\}. \tag{3.31}$$

Moreover, one has

$$\tau^{(1)}(t)^2 \leq C h_{max}^2\Big(\|c(t)\|_{H^2}^2 + \|\partial_t c(t)\|_{H^2}^2 + \int_0^t \|c(s)\|_{H^2}^2\, ds\Big), \tag{3.32}$$

provided that $c \in L^\infty(0,T;H^2(\Omega)\cap H_0^1(\Omega))$ and $\partial_t c \in L^\infty(0,T;H^2(\Omega))$, and

$$\begin{aligned}\tau^{(2)}(t)^2 \leq{}& C h_{max}^4\Big(\|c(t)\|_{H^3}^2 + \|\partial_t c(t)\|_{H^2}^2 + \int_0^t \|c(s)\|_{H^3}^2\, ds\Big)\\ &+ C_{mix}^{obl} C h_{max}^{3-2/p}\Big(|c(t)|_{W^{2,p}(\Omega_h^{obl})}^2 + \int_0^t |c(s)|_{W^{2,p}(\Omega_h^{obl})}^2\, ds\Big),\end{aligned} \tag{3.33}$$

provided that $c \in L^\infty(0,T;H^3(\Omega)\cap H_0^1(\Omega))$ and $\partial_t c \in L^\infty(0,T;H^2(\Omega))$, for $p \in [2,\infty)$.

Proof: Using the bounds (3.17) and (3.18) in (3.26), we obtain

$$\begin{aligned}\partial_t\|e_h(t)\|_h^2 + 2(C_{a,e} - \epsilon^2 - \eta^2)\|e_h(t)\|_{H^1}^2 \leq{}& \frac{C_{b,c}^2 T}{2\epsilon^2}\int_0^t \|e_h(s)\|_{H^1}^2\, ds\\ &+ 2C_{a,\lambda}\|e_h(t)\|_h^2 + \frac{1}{2\eta^2}\tau^{(r)}(t)^2.\end{aligned}$$

Integrating over $[0,t]$ we find that under the conditions (3.30) and (3.31)

$$\begin{aligned}\|e_h(t)\|_h^2 + \int_0^t \|e_h(s)\|_{H^1}^2\, ds \leq{}& C_2\int_0^t\int_0^s \|e_h(\mu)\|_{H^1}^2\, d\mu + \|e_h(s)\|_h^2\, ds\\ &+ C_1\Big(\frac{1}{2\eta^2}\int_0^t \tau^{(r)}(s)^2\, ds + \|e_h(0)\|_h^2\Big).\end{aligned}$$

Then, by the Gronwall's lemma and the inequalities (3.28) and (3.29), we prove the theorem.

■

The previous theorem shows that when C_{mix}^{obl} is not zero, the order of convergence is lower. This loss of accuracy is due to the approximation used for the mixed derivatives near the oblique part of the boundary. In the next corollary, we assume that C_{mix}^{obl} is zero, i.e., the domain is rectangular or the coefficients of the mixed derivatives are equal to zero.

Corollary 3.1 *Let the assumptions of Theorem 3.1 hold. Assume that $C_{mix}^{obl} = 0$ and that $c_{h,0}$ satisfies an estimate of type (2.34). Then, for $t \in [0,T]$,*

$$\int_0^t \|P_h c(s) - c_h(s)\|_{H^1}^2 \, ds \leq C h_{max}^4 \Big(\int_0^t \|c(s)\|_{H^3}^2 \, ds + \|c(t)\|_{H^3}^2 + \|\partial_t c(t)\|_{H^2}^2 \Big),$$

provided that $c \in L^\infty(0,T; H^3(\Omega) \cap H_0^1(\Omega))$ and $\partial_t c \in L^\infty(0,T; H^2(\Omega))$.

The supercloseness estimate above is equivalent to the one obtained with the classical error analysis (see (3.23)). However, the regularity conditions imposed in Corollary 3.1 are more relaxed than (3.22). We remark that a similar result to Corollary 3.1 can be proved for the one-dimensional problem.

The following Corollary 3.2 is a consequence of Theorem 3.1 and Corollary 6.2 of [82]. It establishes, under some more restrictive assumptions on a solution c, that at least a convergence rate of $3/2$ is attained for the more general problem $C_{mix}^{obl} \neq 0$. We note that this is also a supercloseness result.

Corollary 3.2 *Let Ω^{obl} be a neighborhood of the oblique part of $\partial\Omega$ and, in addition to the assumptions of Theorem 3.1, take $c \in L^\infty(0,T; C^2(\bar{\Omega} \cup \Omega^{obl}))$. Then,*

$$\begin{aligned}\int_0^t \|P_h c(s) - c_h(s)\|_{H^1}^2 \, ds \leq C h_{max}^4 \Big(\int_0^t \|c(s)\|_{H^3}^2 \, ds + \|c(t)\|_{H^3}^2 + \|\partial_t c(t)\|_{H^2}^2 \Big) \\ + C h_{max}^3 \Big(\|c(t)\|_{C^2(\Omega_h^{obl})}^2 + \int_0^t \|c(s)\|_{C^2(\Omega_h^{obl})}^2 \, ds \Big),\end{aligned}$$

for $t \in [0,T]$, assuming also that $\sum_{T \in \mathcal{T}_h^{obl}} h_T \leq C$.

It is clear that the results of this section can be carried over to the equivalent FDM. For instance, in the conditions of Corollary 3.1 we have the supraconvergence estimate,

$$\int_0^t \|c(s) - c_h^F(s)\|_{1,h}^2 \, ds \leq C h_{max}^4 \Big(\int_0^t \|c(s)\|_{H^3}^2 \, ds + \|c(t)\|_{H^3}^2 + \|\partial_t c(t)\|_{H^2}^2 \Big),$$

where c_h^F is the approximation given by (3.20) and $\|\cdot\|_{1,h}$ is the norm (3.19).

3.2 A Fully Discrete Method

The aim of this section is to present a time integration method of the IMEX type for the differential system (3.14)-(3.16). In this way, we get a fully discrete scheme to approximate the integro-differential problem (3.1)-(3.3). The corresponding stability and convergence analysis is also provided. We remark that similar results can easily be obtained for the one-dimensional problem.

For a given fixed time step Δt on the interval $[0, T]$, we define the uniform grid $t_n = n\Delta t$, for $n = 0, \ldots, N$, with $t_N = T$. Further, we consider the operator

$$D_{-t} v_h^{n+1} = \frac{v_h^{n+1} - v_h^n}{\Delta t} \quad \text{for } v_h^n \in S_h.$$

The discretization in time is obtained by applying the implicit Euler method to the semi-discrete system (3.14)-(3.16) and the rectangular rule to the resulting integral term. Therefore, our fully discrete FEM for the integro-differential problem (3.1)-(3.3) reads as follows: for $n = 0, \ldots, N-1$, find $c_h^n \in S_h$ such that, for all $v_h \in S_h$,

$$\begin{cases} (D_{-t} c_h^{n+1}, v_h)_h + a_h(c_h^{n+1}, v_h) = \Delta t \sum_{l=0}^{n} b_h(t_l, t_{n+1}, c_h^l, v_h) + ((f)_h^{n+1}, v_h)_h, \\ \\ c_h^0 = c_{h,0}, \end{cases} \tag{3.34}$$

where $(f)_h^{n+1} = (f(t_{n+1}))_h$. Using the same time integration scheme on (3.20) we get the equivalent fully discrete finite difference formulation: for $n = 0, \ldots, N-1$, find $c_h^{F,n} \in W_h$ such that

$$\begin{cases} D_{-t} c_h^{F,n+1} + A_h c_h^{F,n+1} = \Delta t \sum_{l=0}^{n} B_h(t_l, t_{n+1}) c_h^{F,l} + (f)_h^{n+1}, \\ \\ c_h^{F,0} = c_{h,0}^F. \end{cases} \tag{3.35}$$

A solution of the problem (3.34) or (3.35) is then an approximation to a solution of (3.1)-(3.3) on the given time and spatial grids.

We now make some computational remarks. For our discussion, we consider the formulation (3.35), since it is the one used in practice. We first notice that this scheme is very memory-demanding, since we need all the values of $c_h^{F,l}$, for $l = 0, \ldots, n$, to compute $c_h^{F,n+1}$. However, in certain special cases, the method (3.35) can be rewritten as a three-time-level method. This means that at time level $n+1$ we only need two

previous time step solutions, $c_h^{F,n}$ and $c_h^{F,n-1}$, which is a drastic reduction of the memory storage. This reformulation is as follows. Taking $n \geq 1$, then we have

$$D_{-t}c_h^{F,n+1} + A_h c_h^{F,n+1} = \Delta t B_h(t_n, t_{n+1})c_h^{F,n} + \Delta t \sum_{l=0}^{n-1} B_h(t_l, t_{n+1})c_h^{F,l} + (f)_h^{n+1}$$

and

$$D_{-t}c_h^{F,n} + A_h c_h^{F,n} = \Delta t \sum_{l=0}^{n-1} B_h(t_l, t_n)c_h^{F,l} + (f)_h^{n}.$$

Moreover, if

$$B_h(t_l, t_{n+1})c_h^{F,l} = g(\Delta t)B_h(t_l, t_n)c_h^{F,l}, \tag{3.36}$$

where g is some function, we obtain the three-time-level method

$$\begin{aligned}(I + \Delta t A_h)c_h^{F,n+1} = {} & c_h^{F,n} + \Delta t^2 B_h(t_n, t_{n+1})c_h^{F,n} + \Delta t (f)_h^{n+1} \\ & + g(\Delta t)(c_h^{F,n} - c_h^{F,n-1} + \Delta t A_h c_h^{F,n} - \Delta t (f)_h^{n}),\end{aligned}$$

for $n = 1, \ldots, N-1$, with I the identity matrix and A_h and $B_h(\cdot,\cdot)$ sparse non-symmetric matrices with a bandwidth of four. Here we need a starting value, $c_h^{F,1}$, that may be obtained directly from (3.35). Note that the assumption (3.36) is satisfied, for instance, when $B(s,t)c(t) = K(t-s)Bc(t)$ and $K(\alpha+\lambda) = K(\alpha)K(\lambda)$, for $\alpha, \lambda \in \mathbb{R}$.

3.2.1 Stability and Convergence Analysis

We begin this section with a version of the discrete Gronwall's inequality (see Lemma 4.3 in [46]) that will be an essential tool to all subsequent analysis.

Lemma 3.1 *(Discrete Gronwall's inequality) Let $\{\eta_n\}$ be a sequence of non-negative real numbers satisfying*

$$\eta_n \leq \sum_{j=0}^{n-1} \omega_j \eta_j + \beta_n \quad \textit{for } n \geq 1,$$

where $\omega_j \geq 0$ and $\{\beta_n\}$ is a non-decreasing sequence of non-negative numbers. Then

$$\eta_n \leq \beta_n exp\big(\sum_{j=0}^{n-1} \omega_j\big) \quad \textit{for } n \geq 1.$$

We now give a general stability theorem for problem (3.34).

Theorem 3.2 *Let us suppose that $a_h(\cdot,\cdot)$ and $b_h(s,t,\cdot,\cdot)$ satisfy (3.17) and (3.18), respectively. Then, for c_h^n defined in (3.34), it holds that*

$$\|c_h^n\|_h^2 + \Delta t \sum_{m=0}^{n} \|c_h^m\|_{H^1}^2 \leq C_1 e^{C_2 T}\Big(\|c_h^0\|_h^2 + 2\Delta t(C_{a,e} - \epsilon^2)\|c_h^0\|_{H^1}^2 + \frac{\Delta t}{2\eta^2}\sum_{m=1}^{n}\|(f)_h^m\|_h^2\Big),$$

where

$$C_1 = \frac{1}{min\{1 - 2\Delta t(C_{a,\lambda} + \eta^2), 2(C_{a,e} - \epsilon^2)\}}, \quad C_2 = C_1 max\{2(C_{a,\lambda} + \eta^2), C_{b,c}^2 T/2\epsilon^2\},$$

the time step satisfies

$$1 - 2\Delta t(C_{a,\lambda} + \eta^2) > 0 \quad for\ \eta \neq 0, \tag{3.37}$$

and $\epsilon \neq 0$ is such that

$$C_{a,e} - \epsilon^2 > 0. \tag{3.38}$$

Proof: Substituting $n = m$ and $v_h = c_h^{m+1}$ in (3.34) and taking into account (3.17) and (3.18), we establish

$$(D_{-t}c_h^{m+1}, c_h^{m+1})_h + C_{a,e}\|c_h^{m+1}\|_{H^1}^2 - C_{a,\lambda}\|c_h^{m+1}\|_h^2 \leq C_{b,c}\Delta t \sum_{j=0}^{m}\|c_h^j\|_{H^1}\|c_h^{m+1}\|_{H^1} + ((f)_h^{m+1}, c_h^{m+1})_h. \tag{3.39}$$

Since

$$C_{b,c}\Delta t \sum_{j=0}^{m}\|c_h^j\|_{H^1}\|c_h^{m+1}\|_{H^1} \leq \frac{C_{b,c}^2 T\Delta t}{4\epsilon^2}\sum_{j=0}^{m}\|c_h^j\|_{H^1}^2 + \epsilon^2\|c_h^{m+1}\|_{H^1}^2$$

and

$$((f)_h^{m+1}, c_h^{m+1})_h \leq \frac{1}{4\eta^2}\|(f)_h^{m+1}\|_h^2 + \eta^2\|c_h^{m+1}\|_h^2,$$

for all $\epsilon \neq 0$ and $\eta \neq 0$, from (3.39), we estimate

$$\|c_h^{m+1}\|_h^2 - \|c_h^m\|_h^2 + 2\Delta t(C_{a,e} - \epsilon^2)\|c_h^{m+1}\|_{H^1}^2 \leq \frac{C_{b,c}^2 T\Delta t^2}{2\epsilon^2}\sum_{j=0}^{m}\|c_h^j\|_{H^1}^2 + \frac{\Delta t}{2\eta^2}\|(f)_h^{m+1}\|_h^2 + 2\Delta t(C_{a,\lambda} + \eta^2)\|c_h^{m+1}\|_h^2. \tag{3.40}$$

Summing (3.40) over $m = 0, \ldots, n-1$, we get

$$\|c_h^n\|_h^2 - \|c_h^0\|_h^2 + 2\Delta t(C_{a,e} - \epsilon^2)\sum_{m=0}^{n-1}\|c_h^{m+1}\|_{H^1}^2 \leq \frac{C_{b,c}^2 T\Delta t^2}{2\epsilon^2}\sum_{m=0}^{n-1}\sum_{j=0}^{m}\|c_h^j\|_{H^1}^2$$
$$+ \frac{\Delta t}{2\eta^2}\sum_{m=0}^{n-1}\|(f)_h^{m+1}\|_h^2 + 2\Delta t(C_{a,\lambda} + \eta^2)\sum_{m=0}^{n-1}\|c_h^{m+1}\|_h^2,$$

and consequently

$$(1 - 2\Delta t(C_{a,\lambda} + \eta^2))\|c_h^n\|_h^2 + 2\Delta t(C_{a,e} - \epsilon^2)\sum_{m=0}^{n}\|c_h^m\|_{H^1}^2 \leq \sum_{m=0}^{n-1}\frac{C_{b,c}^2 T\Delta t^2}{2\epsilon^2}\sum_{j=0}^{m}\|c_h^j\|_{H^1}^2$$
$$+ 2\Delta t(C_{a,\lambda} + \eta^2)\sum_{m=1}^{n-1}\|c_h^m\|_h^2 + \|c_h^0\|_h^2 + 2\Delta t(C_{a,e} - \epsilon^2)\|c_h^0\|_{H^1}^2 + \frac{\Delta t}{2\eta^2}\sum_{m=1}^{n}\|(f)_h^m\|_h^2.$$

Choosing ϵ satisfying (3.38), and Δt and η satisfying (3.37), we obtain

$$\|c_h^n\|_h^2 + \Delta t\sum_{m=0}^{n}\|c_h^m\|_{H^1}^2 \leq \Delta t C_2\sum_{m=0}^{n-1}\Big(\|c_h^m\|_h^2 + \Delta t\sum_{j=0}^{m}\|c_h^j\|_{H^1}^2\Big)$$
$$+ C_1\Big(\|c_h^0\|_h^2 + 2\Delta t(C_{a,e} - \epsilon^2)\|c_h^0\|_{H^1}^2 + \frac{\Delta t}{2\eta^2}\sum_{m=1}^{n}\|(f)_h^m\|_h^2\Big).$$

Finally, an application of the discrete Gronwall's inequality, completes the proof.

■

The next corollary follows from Theorem 3.2, and establishes the stability of the fully discrete method (3.34) under perturbations in the initial condition. It states that the scheme is unconditionally stable with respect to the H^1-norm, provided that $C_{a,\lambda} \leq 0$. Otherwise, when $C_{a,\lambda}$ is positive, the stability condition for the time step Δt must be respected (see (3.41)). We notice that we can draw the same conclusion for the scheme (3.35) with respect to the discrete norm (3.19).

Corollary 3.3 *Let c_h^n be a solution of (3.34), with $(f)_h^{n+1}$ equal to zero. Under the assumptions of Theorem 3.2,*

$$\|c_h^n\|_h^2 + \Delta t\sum_{m=0}^{n}\|c_h^m\|_{H^1}^2 \leq C_1 e^{C_2 T}\Big(\|c_h^0\|_h^2 + 2\Delta t(C_{a,e} - \epsilon^2)\|c_h^0\|_{H^1}^2\Big),$$

for $\epsilon \neq 0$ satisfying (3.38), with

$$C_1 = \frac{1}{min\{1 - 2\Delta t_0 C_{a,\lambda}, 2(C_{a,e} - \epsilon^2)\}}, \quad C_2 = max\{2C_{a,\lambda}, C_{b,c}^2 T^2/2\epsilon^2\}$$

and $\Delta t \in (0, \Delta t_0)$, where Δt_0 is such that

$$1 - 2\Delta t_0 C_{a,\lambda} > 0. \tag{3.41}$$

Now we turn our attention to the convergence problem. Again, let c be a solution of (3.4)-(3.6) and c_h^n the numerical approximation determined by (3.34). Denote by e_h^n the error

$$e_h^n = P_h c(t_n) - c_h^n.$$

We prove the following H^1-norm error estimate.

Theorem 3.3 *Assume the hypotheses of Theorem 3.2. If additionally $\partial_s b_h(s,t,\cdot,\cdot)$ is uniformly continuous, i.e.,*

$$|\partial_s b_h(s,t,w_h,v_h)| \le C_{b,d}\|w_h\|_{H^1}\|v_h\|_{H^1} \quad \textit{for all } w_h, v_h \in S_h,\ s,t \in [0,T], \tag{3.42}$$

then, we have

$$\|e_h^n\|_h^2 + \Delta t \sum_{m=0}^{n} \|e_h^m\|_{H^1}^2 \le C_2 e^{C_3 T}\Big(\Delta t C_1 \|e_h^0\|_{H^1}^2 + \|e_h^0\|_h^2 + \Delta t \sum_{m=1}^{n} \frac{1}{2\gamma_3^2}\tau^{(r)}(t_m)^2 + C\Delta t^2\Big(\frac{1}{2\gamma_1^2}\|P_h c\|_{H^2(0,T;S_h)}^2 + \frac{C_b^2 T}{2\gamma_2^2}\|P_h c\|_{H^1(0,T;H^1)}^2\Big)\Big), \tag{3.43}$$

where $\Delta t \in (0, \Delta t_0)$, with Δt_0 fixed by

$$1 - 2\Delta t_0(C_{a,\lambda} + \gamma_1^2) > 0,$$

the constants ϵ and $\gamma_i \neq 0$, for $i = 1,2,3$, are such that

$$C_1 = 2(C_{a,e} - \epsilon^2 - \gamma_2^2 - \gamma_3^2) > 0,$$

and where

$$C_2 = \frac{1}{min\{1 - 2\Delta t_0(C_{a,\lambda} + \gamma_1^2), C_1\}},$$

$$C_3 = C_2 max\{2(C_{a,\lambda} + \gamma_1^2), C_b^2 T/2\epsilon^2\}, \quad C_b = max\{C_{b,c}, C_{b,d}\}.$$

In (3.43), $\tau^{(r)}(t_m)^2$, for $r = 1$ and $r = 2$, respectively, satisfy the inequalities (3.32) and (3.33), with $t = t_m$.

Proof: In view of (3.34) and the definition of the error e_h^n, we find

$$(D_{-t}e_h^{m+1}, e_h^{m+1})_h = (D_{-t}P_h c(t_{m+1}), e_h^{m+1})_h + a_h(c_h^{m+1}, e_h^{m+1}) - \Delta t \sum_{j=0}^{m} b_h(t_j, t_{m+1}, c_h^j, e_h^{m+1}) - ((f)_h^{m+1}, e_h^{m+1})_h.$$

By virtue of (3.25), which holds with $t = t_{m+1}$, we deduce

$$(D_{-t}e_h^{m+1}, e_h^{m+1})_h + a_h(e_h^{m+1}, e_h^{m+1}) \\ = \Delta t \sum_{j=0}^{m} b_h(t_j, t_{m+1}, e_h^j, e_h^{m+1}) + \tau_{cd}(e_h^{m+1}), \tag{3.44}$$

where

$$\tau_{cd}(e_h^{m+1}) = \tau(e_h^{m+1}) + \tau_n(e_h^{m+1}).$$

Here, $\tau(e_h^{m+1})$ is defined by (3.27) with $e_h(t)$ replaced by e_h^{m+1} and

$$\tau_n(e_h^{m+1}) = \tau_{n,1}(e_h^{m+1}) + \tau_{n,2}(e_h^{m+1}),$$

with

$$\tau_{n,1}(e_h^{m+1}) = (D_{-t}P_hc(t_{m+1}) - \partial_t P_h c(t_{m+1}), e_h^{m+1})_h,$$
$$\tau_{n,2}(e_h^{m+1}) = \int_0^{t_{m+1}} b_h(s, t_{m+1}, P_hc(s), e_h^{m+1})\, ds - \Delta t \sum_{j=0}^{m} b_h(t_j, t_{m+1}, P_hc(t_j), e_h^{m+1}).$$

Now we estimate these terms. By using the Taylor's expansion we easily obtain

$$|\tau_{n,1}(e_h^{m+1})| \le C \int_{t_m}^{t_{m+1}} \|\partial_t^2 P_h c(s)\|_h \, ds \|e_h^{m+1}\|_h \\ \le C\Delta t \frac{1}{4\gamma_1^2} \|P_hc\|^2_{H^2(t_m, t_{m+1}; S_h)} + \gamma_1^2 \|e_h^{m+1}\|_h^2, \tag{3.45}$$

where $\gamma_1 \neq 0$ is an arbitrary constant. For $\tau_{n,2}(e_h^{m+1})$, we can use the Bramble-Hilbert lemma (see Theorem 4.1.3 in [47]) to get

$$|\tau_{n,2}(e_h^{m+1})| \le C\Delta t \sum_{j=0}^{m} \int_{t_j}^{t_{j+1}} |\partial_s b_h(s, t_{m+1}, P_hc(s), e_h^{m+1})| \\ + |b_h(s, t_{m+1}, \partial_t P_h c(s), e_h^{m+1})|\, ds,$$

and the assumptions (3.42) and (3.18) to find

$$|\tau_{n,2}(e_h^{m+1})| \le C\Delta t C_b \sum_{j=0}^{m} \int_{t_j}^{t_{j+1}} \|P_hc(s)\|_{H^1} + \|\partial_t P_h c(s)\|_{H^1} \, ds \|e_h^{m+1}\|_{H^1} \\ \le \frac{1}{4\gamma_2^2} C\Delta t^2 C_b^2 \|P_hc\|^2_{H^1(0,T;H^1)} + \gamma_2^2 \|e_h^{m+1}\|^2_{H^1}, \tag{3.46}$$

where $\gamma_2 \neq 0$ is an arbitrary constant.

Combining (3.45) and (3.46) with the estimates for $\tau(e_h^{m+1})$ established in Proposition 3.1 yields

$$\tau_{cd}(e_h^{m+1}) \leq \frac{1}{4\gamma_3^2}\tau^{(r)}(t_{m+1})^2 + (\gamma_3^2+\gamma_2^2)\|e_h^{m+1}\|_{H^1}^2 + \gamma_1^2\|e_h^{m+1}\|_h^2 + C\Big(\frac{1}{4\gamma_1^2}\Delta t\|P_h c\|_{H^2(t_m,t_{m+1};S_h)}^2 + \frac{1}{4\gamma_2^2}C_b^2\Delta t^2\|P_h c\|_{H^1(0,T;H^1)}^2\Big). \tag{3.47}$$

Returning to (3.44), using the inequality (3.47) and proceeding like in the proof of Theorem 3.2, we verify that

$$\begin{aligned}\|e_h^{m+1}\|_h^2 - \|e_h^m\|_h^2 + 2\Delta t(C_{a,e} - \epsilon^2 - \gamma_2^2 - \gamma_3^2)\|e_h^{m+1}\|_{H^1}^2 &\leq \frac{\Delta t}{2\gamma_3^2}\tau^{(r)}(t_{m+1})^2 \\ &+ C\Delta t\Big(\frac{1}{2\gamma_1^2}\Delta t\|P_h c\|_{H^2(t_m,t_{m+1};S_h)}^2 + \frac{C_b^2}{2\gamma_2^2}\Delta t^2\|P_h c\|_{H^1(0,T;H^1)}^2\Big) \\ &+ 2\Delta t(C_{a,\lambda}+\gamma_1^2)\|e_h^{m+1}\|_h^2 + \Delta t^2\frac{C_b^2 T}{2\epsilon^2}\sum_{j=0}^{m}\|P_h e_h^j\|_{H^1}^2.\end{aligned}$$

Following again the proof of Theorem 3.2, we get the desired result.

■

We remark that the assumption (3.42) holds, e.g., for $B(s,t)c(s) = K(t-s)Bc(s)$, whenever the kernel K satisfies $|\partial_t K(t-s)| \leq C$, for $s,t \in [0,T]$, and B is a second-order differential operator such that $b(\cdot,\cdot)$ is continuous.

The next corollary, a direct consequence of Theorem 3.3, states that the fully discrete FEM (3.34) is first-order accurate in time. This is an expected result, since our scheme is based on two first-order methods in time, the implicit Euler and the rectangular rule. Here, for brevity of presentation, we only consider the case when $r = 2$ and C_{mix}^{obl} is null.

Corollary 3.4 *Let the assumptions of Theorem 3.3 be verified, and assume that $c_{h,0}$ satisfies an estimate of type (2.34). Then, the upper bound*

$$\|e_h^n\|_h^2 + \Delta t\sum_{m=1}^{n}\|e_h^m\|_{H^1}^2 \leq C\Big(h_{max}^4\Big(\|c\|_{W^{1,\infty}(0,T;H^2)}^2 + \|c\|_{L^2(0,T;H^3)}^2 + \|c\|_{L^\infty(0,T;H^3)}^2\Big) + \Delta t^2\Big(\|P_h c\|_{H^2(0,T;S_h)}^2 + \|P_h c\|_{H^1(0,T;H^1)}^2\Big)\Big), \tag{3.48}$$

is attained, provided that $c \in L^\infty(0,T;H^3(\Omega)\cap H_0^1(\Omega))$, $\partial_t c \in L^\infty(0,T;H^2(\Omega))$, and $\partial_t^2 c \in L^2(0,T;C(\Omega))$.

A estimate like (3.48) holds true for the approximation $c_h^{F,n}$ defined by (3.35) as well, with the error function e_h^n given by $e_h^n = c(t_n) - c_h^{F,n}$ and substituting $\|\cdot\|_{1,h}$ for $\|\cdot\|_{H^1}$.

3.3 Numerical Experiments

The purpose of this section is to illustrate the theoretical convergence rates proved for the semi-discrete approximation. For that, we consider two problems, one a with rectangular domain, the other with a polygonal domain and mixed derivatives.

Example 3.1 *Consider the integro-differential problem (3.1)-(3.3) with* $\Omega = (0,1)^2$*,*

$$A_2(x,y) = \begin{bmatrix} 1 & y-x \\ y-x & 1 \end{bmatrix}, \quad A_1(x,y) = \begin{bmatrix} -x \\ -y \end{bmatrix}, \quad a_0 = 0,$$

$$B_2(s,t) = e^{-(t-s)} \begin{bmatrix} -1 & 0 \\ 0 & -1 \end{bmatrix}, \quad B_1(s,t) = 0, \quad b_0(s,t) = 0,$$

and initial condition and f *chosen so that*

$$c(x,y,t) = e^t xy(x-1)(y-1)$$

is the exact solution.

Example 3.2 *Let* Ω *be the polygonal domain in Figure 3.3. In this domain, we*

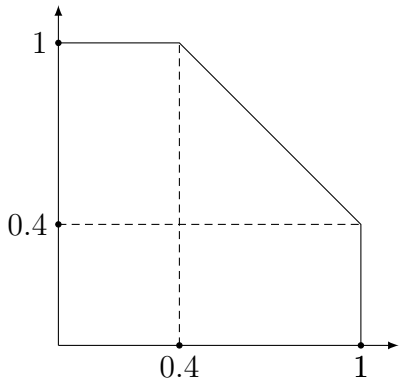

Figure 3.3: Polygonal domain Ω.

consider the integro-differential problem (3.1)-(3.3) with

$$A_2(x,y) = \begin{bmatrix} 1 & xy \\ xy & 1 \end{bmatrix}, \quad A_1 = 0, \quad a_0 = 0,$$

$$B_2(x,y,s,t) = e^{-(t-s)} \begin{bmatrix} 0 & -xy \\ -xy & 0 \end{bmatrix}, \quad B_1(s,t) = 0, \quad b_0(s,t) = 0,$$

and initial condition and f *chosen so that*

$$c(x,y,t) = e^t xy(x-1)(y-1)(-x+7/5-y)$$

is the exact solution.

Using the FDM (3.35) we solved each problem on a sequence of grids, starting with a random grid that is successively refined by taking $h_i^x = h_i^x/2$ and $h_l^y = h_l^y/2$. The results are presented in Tables 3.1 and 3.2, where

$$\text{Error} = \left(\|e_h^N\|_h^2 + \Delta t \sum_{n=1}^{N} \|e_h^n\|_{1,h}^2 \right)^{1/2},$$

and N_x and N_y denote the number of nodes in the x and y direction, respectively. We

h_{max}	N_x	N_y	Error	Rate
1.2998×10^{-1}	9	8	4.9148×10^{-4}	1.9065
6.4989×10^{-2}	18	16	1.3110×10^{-4}	1.9425
3.2494×10^{-2}	36	32	3.4107×10^{-5}	1.9781
1.6247×10^{-2}	72	64	8.6572×10^{-6}	1.9932
8.1236×10^{-3}	144	128	2.1745×10^{-6}	2.0031
4.0618×10^{-3}	288	256	5.4248×10^{-7}	2.0254
2.0309×10^{-3}	576	512	1.3325×10^{-7}	-

Table 3.1: Discrete norm errors and convergence rates for Example 3.1.

observe that the estimated convergence rates for both examples is approximately 2 for Example 3.1 and 3/2 for Example 3.2. This behavior is exactly as predicted by Corollaries 3.1 and 3.2.

h_{max}	N_x	N_y	Error	Rate
1.3466×10^{-1}	9	8	2.9878×10^{-4}	1.5541
6.7329×10^{-2}	18	16	1.0175×10^{-4}	1.5597
3.3665×10^{-2}	36	32	3.4513×10^{-5}	1.5390
1.6832×10^{-2}	72	64	1.1876×10^{-5}	1.5219
8.4162×10^{-3}	144	128	4.1358×10^{-6}	1.5114
4.2081×10^{-3}	288	256	1.4507×10^{-6}	1.5059
2.1040×10^{-3}	576	512	5.1081×10^{-7}	-

Table 3.2: Discrete norm errors and convergence rates for Example 3.2.

In the experiments, we have taken $T = 0.1$ and $\Delta t = 10^{-6}$, a very small time step to minimize the error due to the time discretization.

Chapter 4

A Parabolic-Elliptic Coupled Problem

In this chapter, we extend the analysis of FEMs with quadrature to systems of equations. However, as explained in the introduction, we move away from integro-differential equations and turn our attention to coupled problems consisting of an elliptic equation of the form

$$-\nabla(a(c)\nabla p) = q_1 \quad \text{in } \Omega \times (0,T], \tag{4.1}$$

and a parabolic PDE of the form

$$\partial_t c + \nabla(b(c,\nabla p)c) - \nabla(d(c,\nabla p)\nabla c) = q_2 \quad \text{in } \Omega \times (0,T]. \tag{4.2}$$

This quasilinear system of equations is complemented with the initial conditions,

$$p(0) = p_0, \quad c(0) = c_0 \quad \text{in } \Omega, \tag{4.3}$$

and with homogeneous Dirichlet boundary conditions

$$p = 0, \quad c = 0 \quad \text{on } \partial\Omega \times (0,T]. \tag{4.4}$$

We assume that $a \in W^{1,\infty}(\mathbb{R})$, $b \in W^{2,\infty}(\mathbb{R}^2)$ and $d \in W^{1,\infty}(\mathbb{R}^2)$, and all with codomain lying in $\mathbb{R}$. Additionally, we assume that the initial conditions and q_1 and q_2 are regular enough and, without loss of generality, that the domain Ω is the open interval $(0,1)$.

The organization of this chapter is straightforward and very similar to previous chapters. The fundamental result is the supercloseness of the gradient of a finite element approximation. The proof of this is given in Section 4.1, together with the description of the numerical method. In Section 4.2, we study a fully discrete scheme and we finish in Section 4.3 with a numerical test that illustrates the theory developed.

4.1 A Semi-Discrete Galerkin Method

To obtain our semi-discrete FEM for (4.1)-(4.4), we start with a variational formulation of the problem which is given by: find $p, c : [0,T] \to H_0^1(\Omega)$ such that the conditions (4.3) are fulfilled and

$$\begin{cases} (a(c)\nabla p, \nabla v) = (q_1, v), \\ \\ (\partial_t c, w) + (d(c, \nabla p)\nabla c, \nabla w) - (b(c, \nabla p)c, \nabla w) = (q_2, w), \end{cases} \tag{4.5}$$

for all $v, w \in H_0^1(\Omega)$ and $t \in (0,T]$. A standard finite element approximation problem is the following: find $p, c : [0,T] \to S_h$ satisfying the conditions (4.3) and such that

$$\begin{cases} (a(c_h)\nabla p_h, \nabla v_h) = (q_1, v_h), \\ \\ (\partial_t c_h, w_h) + (d(c_h, \nabla p_h)\nabla c_h, \nabla w_h) - (b(c_h, \nabla p_h)c_h, \nabla w_h) = (q_2, w_h), \end{cases} \tag{4.6}$$

for all $v_h, w_h \in S_h$ and $t \in (0,T]$. The FEM that we study in this chapter is based on the numerical integration of the equations (4.6). We notice that many of the numerical tools to be used here are identical to the ones employed in Chapter 2, and we refer to that chapter for notation and definitions.

Thus, our semi-discrete approximation to the weak solution of (4.1)-(4.4), defined by (4.5), is a solution of the following problem: find

$$p_h, c_h : [0,T] \to S_h,$$

satisfying the initial conditions

$$p_h(0) = p_{h,0}, \quad c_h(0) = c_{h,0}, \tag{4.7}$$

and moreover, that for all $v_h, w_h \in S_h$ and $t \in (0,T]$,

$$\begin{cases} (a_h \nabla p_h, \nabla v_h) = ((q_1)_h, v_h)_h, & (4.8) \\ \\ (\partial_t c_h, w_h)_h + (d_h \nabla c_h, \nabla w_h) - (M^*(b_h c_h), \nabla w_h) = ((q_2)_h, w_h)_h. & (4.9) \end{cases}$$

Here, we have denoted

$$\begin{aligned} a_h(x,t) &= a(M^*(c_h(x,t))), \\ d_h(x,t) &= d(M^*(c_h(x,t)), \nabla p_h(x_{i-1/2}, t)), \end{aligned}$$

for $x \in (x_{i-1}, x_i]$, and

$$b_h(x_i,t) = \begin{cases} b(c_h(x_0,t), \nabla p_h(x_{1-1/2},t)) & \text{for } i=0, \\ b(c_h(x_i,t), D_h p_h(x_i,t)) & \text{for } i=1,\ldots,N-1, \\ b(c_h(x_N,t), \nabla p_h(x_{N-1/2},t)) & \text{for } i=N, \end{cases}$$

with

$$D_h p_h(x_i,t) = (h_i \nabla p_h(x_{i+1/2},t) + h_{i+1}\nabla p_h(x_{i-1/2},t))/(h_i + h_{i+1}).$$

Once again, it can be proved that the FEM (4.7)-(4.9) is equivalent, in the same sense as Chapter 2, to a FDM. The approximations given by this method, represented by $p_h^F, c_h^F : [0,T] \to W_h$, are solutions of the following ordinary differential problem

$$\begin{cases} -D(a_h D p_h^F) = (q_1)_h, \\ \partial_t c_h^F - D(d_h D p_h^F) + D_c(b_h c_h^F) = (q_2)_h, \end{cases} \tag{4.10}$$

for $t \in (0,T]$, together with suitable initial conditions in accordance with (4.3). In order to simplify our presentation, we have considered here that $a_h(x_{i\pm1/2},t) = a_h(x_{i\pm1},t)$ and $d_h(x_{i\pm1/2},t) = d_h(x_{i\pm1},t)$.

As we mention in the introduction, the system (4.1)-(4.4) is closely related to some porous media problems. Therefore, for the remainder of this chapter, we will sometimes refer to p as pressure and c as concentration.

4.1.1 Stability Analysis

This section presents two theorems that together prove energy stability of a solution of the variational problem (4.7)-(4.9). We start with the pressure.

Theorem 4.1 *If $C_a \le a$, then*

$$\|p_h(t)\|_{H^1} \le C_p \|(q_1(t))_h\|_h \quad \textit{for } t \in [0,T]. \tag{4.11}$$

Proof: Taking in (4.8) $v_h = p_h(t)$, and using the Poincaré-Friedrichs' inequality $\|v_h\|_h \le \|\nabla v_h\|_{L^2}^2$, for $v_h \in S_h$, we easily get (4.11).

■

The next corollary is obvious.

Corollary 4.1 *In the conditions of Theorem 4.1, if*

$$\|q_1(t)\|_{L^2} \leq C_{q_1} \quad \textit{for } t \in [0,T], \tag{4.12}$$

then

$$\|p_h(t)\|_{H^1} \leq C_p \quad \textit{for } t \in [0,T]. \tag{4.13}$$

Moreover, the inequality (4.13) implies that

$$\|p_h(t)\|_{L^\infty} \leq C_p \quad \textit{for } t \in [0,T].$$

In the following theorem we consider the concentration equation.

Theorem 4.2 *Suppose that $c_h \in C^1([0,T]; S_h)$ and that*

$$\max_{i=1,\ldots,N} |\nabla p_h(x_{i-1/2}, t)| \leq C_p. \tag{4.14}$$

Suppose also that $C_a \leq a$, $C_d \leq d$ and

$$|b(\alpha,\lambda)| \leq C_b|\lambda| \quad \textit{for } (\alpha,\lambda) \in \mathbb{R}^2. \tag{4.15}$$

Then, there holds

$$\|c_h(t)\|_h^2 + \int_0^t \|c_h(s)\|_{H^1}^2\, ds \leq C_1 e^{C_2 t}\Big(\|c_{h,0}\|_h^2 + \frac{1}{2\eta^2}\int_0^t \|(q_2(s))_h\|_h^2\, ds\Big),$$

for $t \in [0,T]$, with

$$C_1 = \frac{1}{min\{1, 2(C_d - \epsilon^2)\}}, \qquad C_2 = \frac{1}{2\epsilon^2} C_b^2 C_p^2 + 2\eta^2,$$

$\epsilon \neq 0$ such that $C_d - \epsilon^2 > 0$ and $\eta \neq 0$ an arbitrary constant.

Proof: On replacing w_h in (4.9) by $c_h(t)$, we estimate

$$\frac{1}{2}\partial_t \|c_h(t)\|_h^2 + C_d\|c_h(t)\|_{H^1}^2 - (M^*(b_h(t)c_h(t)), \nabla c_h(t)) \leq \frac{1}{4\eta^2}\|(q_2(t))_h\|_h^2 + \eta^2\|c_h(t)\|_h^2,$$

for arbitrary $\eta \neq 0$. As obtained from (4.14) and (4.15)

$$|(M^*(b_h(t)c_h(t)), \nabla c_h(t))| \leq C_b C_p \|c_h(t)\|_h \|\nabla c_h(t)\|_{L^2}, \tag{4.16}$$

it follows that

$$\partial_t \|c_h(t)\|_h^2 + 2(C_d - \epsilon^2)\|c_h(t)\|_{H^1}^2 \leq C_2\|c_h(t)\|_h^2 + \frac{1}{2\eta^2}\|(q_2(t))_h\|_h^2,$$

where ϵ is a non-zero constant. This inequality leads to

$$\|c_h(t)\|_h^2 + 2(C_d - \epsilon^2)\int_0^t \|c_h(s)\|_{H^1}^2\,ds \le C_2\int_0^t \|c_h(s)\|_h^2\,ds + \|c_{h,0}\|_h^2 + \frac{1}{2\eta^2}\int_0^t \|(q_2(s))_h\|_h^2\,ds,$$

and the desired result follows by Gronwall's lemma.

■

A comment about condition (4.14) is in order here. Observe that

$$\begin{aligned} a_h(x_{i+1},t)\nabla p_h(x_{i+1/2},t) &= \sum_{j=1}^{i} h_{j+1/2} D(a_h(t)\nabla p_h(t))(x_j) + a_h(x_1,t)\nabla p_h(x_{1-1/2},t) \\ &= -\sum_{j=1}^{i} h_{j+1/2}(q_1(x_j,t))_h + a_h(x_1,t)\nabla p_h(x_{1-1/2},t), \end{aligned}$$

for $i = 1,\dots,N-1$, and by (4.12) we get

$$\max_{i=2,\dots,N} |a_h(x_i,t)\nabla p_h(x_{i-1/2},t)| \le C_{q_1} + |a_h(x_1,t)\nabla p_h(x_{1-1/2},t)|,$$

provided that $q_1 \in L^\infty(0,T;L^2(\Omega))$. It is then plausible to assume that (4.14) holds.

4.1.2 Error Estimates

In the first part of this section we introduce and study two auxiliary problems. The results derived for these problems are essential for the forthcoming analysis.

Let $\tilde{p}_h(t), \tilde{c}_h(t) \in S_h$ be solutions of the variational problems

$$(\tilde{a}_h(t)\nabla\tilde{p}_h(t), \nabla w_h) = ((q_1(t))_h, w_h)_h \quad \text{for } w_h \in S_h \tag{4.17}$$

and

$$(\tilde{d}_h(t)\nabla\tilde{c}_h(t), \nabla w_h) - (M^*(\tilde{b}_h(t)\tilde{c}_h(t)), \nabla w_h)_h = ((\tilde{q}_2(t))_h, w_h)_h \quad \text{for } w_h \in S_h, \tag{4.18}$$

where $\tilde{q}_2(t) = q_2(t) - \partial_t c(t)$ and where the other coefficient functions are defined by

$$\begin{aligned} \tilde{a}_h(x,t) &= a(M(c(x,t))), \\ \tilde{d}_h(x,t) &= d(M(c(x,t)), \nabla p(x_{i-1/2},t)), \end{aligned}$$

for $x \in (x_{i-1}, x_i]$, and

$$\tilde{b}_h(x_i,t)\tilde{c}_h(x_i,t) = \begin{cases} b(c(x_i,t), \nabla p(x_i,t))\tilde{c}_h(x_i,t) & \text{for } i = 1,\dots,N-1, \\ 0 & \text{for } i = 0, N. \end{cases}$$

It can be shown that $\tilde{p}_h(t)$ and $\tilde{c}_h(t)$ are solutions of a coupled finite difference problem analogous to system (4.10).

The following proposition can be established by Theorem 3.1 of [16].

Proposition 4.1 *If $C_a \leq a$, then for $\tilde{p}_h(t)$ defined by (4.17) the following estimate holds:*

$$\|P_h p(t) - \tilde{p}_h(t)\|_{H^1}^2 \leq C_{\tilde{p}} \sum_{i=1}^{N} h_i^{2r} \|p(t)\|_{H^{1+r}(x_{i-1},x_i)}^2, \tag{4.19}$$

provided that $h \in \mathrm{H}$ and $p(t) \in H^{1+r}(\Omega) \cap H_0^1(\Omega)$, for $r \in \{1, 2\}$.

As a consequence of this result, we prove that

$$\max_{i=1,\ldots,N} |\nabla \tilde{p}_h(x_{i-1/2}, t)| \leq C_{\tilde{p}}. \tag{4.20}$$

In fact, from (4.19) we have

$$|\nabla (P_h p(x_{i-1/2}, t) - \tilde{p}_h(x_{i-1/2}, t))| \leq C h_{max}^{r-1/2},$$

and so, using Taylor's expansion, we obtain

$$\begin{aligned} |\nabla \tilde{p}_h(x_{i-1/2}, t)| &\leq |\nabla (P_h p(x_{i-1/2}, t) - \tilde{p}_h(x_{i-1/2}, t))| + \frac{1}{h_i} \int_{x_{i-1}}^{x_i} |\nabla p(x, t)| \, dx \\ &\leq C h_{max}^{r-1/2} + \|\nabla p(t)\|_{L^\infty}, \end{aligned}$$

which means that (4.20) is valid, provided that $p \in L^\infty(0, T; H^2(\Omega) \cap H_0^1(\Omega))$.

We now proceed to establish an estimate like (4.19) for $\tilde{c}_h(t)$. We follow again the proof of Theorem 3.1 in [16], but we need a more precise result here. First we must guarantee the stability of the bilinear form

$$a_{\tilde{c}_h}(v_h, w_h) = (\tilde{d}_h(t) \nabla v_h, \nabla w_h) - (M^*(\tilde{b}_h(t) v_h), \nabla w_h)_h \quad \text{for } v_h, w_h \in S_h.$$

The next proposition states this result and the conditions under which it occurs (see Proposition 3.1 in [16]).

Proposition 4.2 *Define $\tilde{d}(t) = d(c(t), \nabla p(t))$ and $\tilde{b}(t) = b(c(t), \nabla p(t))$, where p and c are solutions of the variational problem (4.5). If the variational problem: find $v \in H_0^1(\Omega)$ such that $(\tilde{d}(t) \nabla v, \nabla w) - (\tilde{b}(t) v, \nabla w) = 0$, for $w \in H_0^1(\Omega)$, has only a null solution, then, for $h \in \mathrm{H}$, it holds the following stability inequality*

$$\|v_h\|_{H^1} \leq C_{e,c} \sup_{0 \neq w_h \in S_h} \frac{|a_{\tilde{c}_h}(v_h, w_h)|}{\|w_h\|_{H^1}} \quad \text{for } v_h \in S_h.$$

Now, by virtue of Theorem 3.1 in [16], to estimate the error $P_h c(t) - \tilde{c}_h(t)$, it suffices to estimate

$$T_d = \sum_{i=1}^{N} h_i d(x_{i-1/2}, t)\Big(\nabla P_h c(x_{i-1/2}, t) - \nabla c(x_{i-1/2}, t)\Big)\nabla w_h(x_{i-1/2}) \tag{4.21}$$

and

$$T_b = \sum_{i=1}^{N} h_i \Big(b(x_{i-1/2}, t) - \frac{b(x_{i-1}, t) + b(x_i, t)}{2}\Big)\nabla w_h(x_{i-1/2}), \tag{4.22}$$

where

$$d(x,t) = d(c(x,t), \nabla p(x,t)) \quad \text{and} \quad b(x,t) = b(c(x,t), \nabla p(x,t)).$$

To obtain bounds for (4.21) and (4.22), we apply the Bramble-Hilbert lemma. This gives

$$|T_d| \le C\|d(c(t), \nabla p(t))\|_{L^\infty} \Big(\sum_{i=1}^{N} h_i^{2r} \|c(t)\|^2_{H^{1+r}(x_{i-1}, x_i)}\Big)^{1/2} \|w_h\|_{H^1},$$

and

$$|T_b| \le C\Big(\sum_{i=1}^{N} h_i^{2r} |b(c(t), \nabla p(t))c(t)|^2_{H^r(x_{i-1}, x_i)}\Big)^{1/2} \|w_h\|_{H^1}. \tag{4.23}$$

Denote by $C^r_B(\Omega)$ the set of functions on Ω having bounded, continuous derivatives up to order r. As the imbedding of $H^{1+r}(\Omega)$ into $C^r_B(\Omega)$ is continuous (see Theorem 4.12 in [5]), we get from (4.23)

$$|T_b| \le C\Big(\sum_{i=1}^{N} h_i^2 \|c(t)\|^2_{L^\infty} \Big(\|c(t)\|^2_{H^1(x_{i-1}, x_i)} + \|p(t)\|^2_{H^2(x_{i-1}, x_i)}\Big)\Big)^{1/2} \|w_h\|_{H^1},$$

for $r = 1$, and for $r = 2$

$$\begin{aligned} |T_b| \le C\Big(\sum_{i=1}^{N} h_j^4 \Big(&\|c(t)\|^2_{W^{1,\infty}} \Big(\|c(t)\|^2_{L^\infty} + 1\Big)\Big(\|c(t)\|^2_{H^1(x_{i-1}, x_i)} + \|p(t)\|^2_{H^2(x_{i-1}, x_i)}\Big) \\ &+ \|c(t)\|^2_{L^\infty} \Big(\|p(t)\|^2_{W^{2,\infty}} \|p(t)\|^2_{H^2(x_{i-1}, x_i)} + \|p(t)\|^2_{H^3(x_{i-1}, x_i)}\Big) \\ &+ \|c(t)\|^2_{H^2(x_{i-1}, x_i)}\Big)\Big)^{1/2} \|w_h\|_{H^1}. \end{aligned}$$

We summarize the previous results in the following proposition.

Proposition 4.3 *Let the assumptions of Proposition 4.2 be valid. Then for $\tilde{c}_h(t)$ defined by (4.18) there holds the following*

$$\|P_h c(t) - \tilde{c}_h(t)\|_{H^1}^2 \leq C_{\tilde{c}} \sum_{i=1}^{N} h_i^{2r} \Big(\|c(t)\|_{H^{1+r}(x_{i-1},x_i)}^2 + \|p(t)\|_{H^{1+r}(x_{i-1},x_i)}^2 \Big),$$

provided that $p(t), c(t) \in H^{1+r}(\Omega) \cap H_0^1(\Omega)$, for $r \in \{1, 2\}$.

Before proceeding, we point out that Proposition 4.3 implies that $\|\tilde{c}_h(t)\|_{H^1} \leq C_{\tilde{c}}$, from which we can conclude

$$\|\tilde{c}_h(t)\|_{L^\infty} \leq C_{\tilde{c}}. \tag{4.24}$$

Also, as for (4.20), from Proposition 4.3 we still have

$$\max_{i=1,\ldots,N} |\nabla \tilde{c}_h(x_{i-1/2}, t)| \leq C_{\tilde{c}}, \tag{4.25}$$

provided that $p, c \in L^\infty(0, T; H^2(\Omega) \cap H_0^1(\Omega))$.

In the next proposition, we establish an upper bound for the error $p_h(t) - \tilde{p}_h(t)$.

Proposition 4.4 *Suppose $C_a \leq a$. Then, for $h \in \mathrm{H}$,*

$$\|p_h(t) - \tilde{p}_h(t)\|_{H^1} \leq C_{p,\tilde{p}} \Big(\|P_h c(t) - c_h(t)\|_h + \Big(\sum_{i=1}^{N} h_i^{2r} \|c(t)\|_{H^r(x_{i-1},x_i)}^2 \Big)^{1/2} \Big),$$

provided that $p \in L^\infty(0, T; H^2(\Omega) \cap H_0^1(\Omega))$ and $c(t) \in H^r(\Omega) \cap H_0^1(\Omega)$, for $r \in \{1, 2\}$.

Proof: From (4.8) and (4.17), it can be shown that

$$\begin{aligned}(a_h(t)\nabla(p_h(t) - \tilde{p}_h(t)), \nabla w_h) = &((\tilde{a}_h(t) - a_h^*(t))\nabla \tilde{p}_h(t), \nabla w_h) \\ &+ ((a_h^*(t) - a_h(t))\nabla \tilde{p}_h(t), \nabla w_h),\end{aligned} \tag{4.26}$$

for $w_h \in S_h$, where $a_h^*(t)$ is defined as $a_h(t)$, but with $c_h(t)$ replaced by $P_h c(t)$.

By (4.20), we have for the second term of the second member of (4.26) that

$$|((a_h^*(t) - a_h(t))\nabla \tilde{p}_h(t), \nabla w_h)| \leq C \|P_h c(t) - c_h(t)\|_h \|w_h\|_{H^1}, \tag{4.27}$$

while for the first term, by the Bramble-Hilbert lemma, we deduce

$$|((\tilde{a}_h(t) - a_h^*(t))\nabla \tilde{p}_h(t), \nabla w_h)| \leq C \Big(\sum_{i=1}^{N} h_i^{2r} \|c(t)\|_{H^r(x_{i-1},x_i)}^2 \Big)^{1/2} \|w_h\|_{H^1}. \tag{4.28}$$

We can conclude the proof taking $w_h = p_h(t) - \tilde{p}_h(t)$ in (4.26) and using the inequalities (4.27) and (4.28).

■

One important result is stated in the following corollary.

Corollary 4.2 *If $C_a \leq a$, then for p_h and c_h defined by (4.7)-(4.9) it holds that for $h \in \mathrm{H}$ and $r \in \{1,2\}$*

$$\|P_h p(t) - p_h(t)\|_{H^1} \leq C\Big(\|P_h c(t) - c_h(t)\|_h + \Big(\sum_{i=1}^{N} h_i^{2r} \|c(t)\|^2_{H^r(x_{i-1},x_i)}\Big)^{1/2} + \Big(\sum_{i=1}^{N} h_i^{2r} \|p(t)\|^2_{H^{1+r}(x_{i-1},x_i)}\Big)^{1/2}\Big),$$

provided that $c(t) \in H^r(\Omega) \cap H_0^1(\Omega)$ and $p \in L^\infty(0,T; H^{1+r}(\Omega) \cap H_0^1(\Omega))$.

The next three lemmas will play a fundamental role in the sequel.

Lemma 4.1 *Assume $p, c \in L^\infty(0,T; H^{1+r}(\Omega) \cap H_0^1(\Omega))$, for $r \in \{1,2\}$. Let $\tilde{c}_h(t)$ be defined by (4.18) and let the conditions of Proposition 4.2 and Corollary 4.2 hold. Then, for the functional defined on S_h by*

$$\tau_d(t, w_h) = (\tilde{d}_h(t)\nabla\tilde{c}_h(t), \nabla w_h) - (d_h(t)\nabla c_h(t), \nabla w_h),$$

we have

$$\tau_d(t, w_h) = (d_h(t)\nabla(P_h c(t) - c_h(t)), \nabla w_h) + \tau_{d,h}(t, w_h), \tag{4.29}$$

where for $w_h \in S_h$

$$|\tau_{d,h}(t, w_h)| \leq C_d\Big(\|P_h c(t) - c_h(t)\|_h + \Big(\sum_{i=1}^{N} h_i^{2r} \|p(t)\|^2_{H^{1+r}(x_{i-1},x_i)}\Big)^{1/2} + \Big(\sum_{i=1}^{N} h_i^{2r} \|c(t)\|^2_{H^{1+r}(x_{i-1},x_i)}\Big)^{1/2}\Big)\|w_h\|_{H^1}. \tag{4.30}$$

Proof: The representation (4.29) holds with

$$\tau_{d,h}(t, w_h) = \tau_{d,h}^{(1)}(t, w_h) + \tau_{d,h}^{(2)}(t, w_h) + \tau_{d,h}^{(3)}(t, w_h),$$

where

$$\begin{aligned}
\tau_{d,h}^{(1)}(t, w_h) &= ((\tilde{d}_h(t) - d_h^*(t))\nabla\tilde{c}_h(t), \nabla w_h),\\
\tau_{d,h}^{(2)}(t, w_h) &= ((d_h^*(t) - d_h(t))\nabla\tilde{c}_h(t), \nabla w_h),\\
\tau_{d,h}^{(3)}(t, w_h) &= (d_h(t)\nabla(\tilde{c}_h(t) - P_h c(t)), \nabla w_h),
\end{aligned}$$

and $d_h^*(t)$ is defined as $d_h(t)$ replacing $c_h(t)$ and $p_h(t)$ by $P_hc(t)$ and $P_hp(t)$, respectively. Let us estimate each term separately (recall (4.25)). First, using the Bramble-Hilbert lemma, it can be shown that

$$|\tau_{d,h}^{(1)}(t,w_h)| \le C\Big(\Big(\sum_{i=1}^{N} h_i^{2r}\|c(t)\|^2_{H^r(x_{i-1},x_i)}\Big)^{1/2} + \Big(\sum_{i=1}^{N} h_i^{2r}\|p(t)\|^2_{H^{1+r}(x_{i-1},x_i)}\Big)^{1/2}\Big)\|w_h\|_{H^1} \quad \text{for } w_h \in S_h.$$

Next, we find

$$|\tau_{d,h}^{(2)}(t,w_h)| \le C(\|P_hc(t)-c_h(t)\|_h + \|\nabla(P_hp(t)-p_h(t))\|_{L^2})\|w_h\|_{H^1}$$

from which, by Corollary 4.2,

$$|\tau_{d,h}^{(2)}(t,w_h)| \le C\Big(\|P_hc(t)-c_h(t)\|_h + \Big(\sum_{i=1}^{N} h_i^{2r}\|c(t)\|^2_{H^r(x_{i-1},x_i)}\Big)^{1/2} + \Big(\sum_{i=1}^{N} h_i^{2r}\|p(t)\|^2_{H^{1+r}(x_{i-1},x_i)}\Big)^{1/2}\Big)\|w_h\|_{H^1} \quad \text{for } w_h \in S_h.$$

For the last term, by Proposition 4.3, we have

$$|\tau_{d,h}^{(3)}(t,w_h)| \le C\Big(\Big(\sum_{i=1}^{N} h_i^{2r}\|c(t)\|^2_{H^{1+r}(x_{i-1},x_i)}\Big)^{1/2} + \Big(\sum_{i=1}^{N} h_i^{2r}\|p(t)\|^2_{H^{1+r}(x_{i-1},x_i)}\Big)^{1/2}\Big)\|w_h\|_{H^1} \quad \text{for } w_h \in S_h.$$

The inequality (4.30) follows from the previous estimates.

■

Lemma 4.2 *Assume $p, c \in L^\infty(0,T;H^{1+r}(\Omega)\cap H_0^1(\Omega))$, for $r \in \{1,2\}$. Let $\tilde{c}_h(t)$ be defined by (4.18) and let the conditions of Proposition 4.2 hold. If $C_a \le a$, the assumption (4.14) holds and the coefficient function b satisfies (4.15) then, for the functional defined on S_h by*

$$\tau_b(t,w_h) = (M^*(b_h(t)c_h(t)),\nabla w_h) - (M^*(\tilde{b}_h(t)\tilde{c}_h(t)),\nabla w_h),$$

we have

$$\tau_b(t,w_h) = (M^*(b_h(t)(c_h(t)-P_hc(t))),\nabla w_h) + \tau_{b,h}(t,w_h), \tag{4.31}$$

where for $w_h \in S_h$

$$|\tau_{b,h}(t,w_h)| \le C_{b,2}\Big(\|P_hc(t)-c_h(t)\|_h + \Big(\sum_{i=1}^{N} h_i^{2r}\|c(t)\|^2_{H^{1+r}(x_{i-1},x_i)}\Big)^{1/2} + \Big(\sum_{i=1}^{N} h_i^{2r}\|p(t)\|^2_{H^{1+r}(x_{i-1},x_i)}\Big)^{1/2}\Big)\|w_h\|_{H^1}. \tag{4.32}$$

Proof: The representation (4.31) holds with

$$\tau_{b,h}(t,w_h) = \tau^{(1)}_{b,h}(t,w_h) + \tau^{(2)}_{b,h}(t,w_h) + \tau^{(3)}_{b,h}(t,w_h),$$

where

$$\begin{aligned}
\tau^{(1)}_{b,h}(t,w_h) &= (M^*(b_h(t)(P_hc(t)-\tilde{c}_h(t))),\nabla w_h),\\
\tau^{(2)}_{b,h}(t,w_h) &= (M^*((b_h(t)-b^*_h(t))\tilde{c}_h(t)),\nabla w_h),\\
\tau^{(3)}_{b,h}(t,w_h) &= (M^*((b^*_h(t)-\tilde{b}_h(t))\tilde{c}_h(t)),\nabla w_h),
\end{aligned}$$

being $b^*_h(t)$ defined as $b_h(t)$ replacing $c_h(t)$ and $p_h(t)$ by $P_hc(t)$ and $P_hp(t)$, respectively. Consider the first term. By (4.14), (4.15), and Proposition 4.3, we estimate

$$|\tau^{(1)}_{b,h}(t,w_h)| \le C\Big(\Big(\sum_{i=1}^{N} h_i^{2r}\|c(t)\|^2_{H^{1+r}(x_{i-1},x_i)}\Big)^{1/2} + \Big(\sum_{i=1}^{N} h_i^{2r}\|p(t)\|^2_{H^{1+r}(x_{i-1},x_i)}\Big)^{1/2}\Big)\|w_h\|_{H^1}.$$

As for the second term, since $\tilde{c}_h(t)$ satisfies (4.24), we find

$$|\tau^{(2)}_{b,h}(t,w_h)| \le C(\|P_hc(t)-c_h(t)\|_h + \|\nabla(P_hp(t)-p_h(t))\|_{L^2})\|w_h\|_{H^1}.$$

Furthermore, from Corollary 4.2, one concludes that

$$|\tau^{(2)}_{b,h}(t,w_h)| \le C\Big(\|P_hc(t)-c_h(t)\|_h + \Big(\sum_{i=1}^{N} h_i^{2r}\|c(t)\|^2_{H^{r}(x_{i-1},x_i)}\Big)^{1/2} + \Big(\sum_{i=1}^{N} h_i^{2r}\|p(t)\|^2_{H^{1+r}(x_{i-1},x_i)}\Big)^{1/2}\Big)\|w_h\|_{H^1}. \tag{4.33}$$

To obtain the bound for the last term, we first notice that

$$\nabla p(x_i,t) - D_hp(x_i,t) = \frac{1}{h_i+h_{i+1}}\lambda(v),$$

with

$$\lambda(v) = \nabla v(\rho) - \hat{\rho}(v(1) - v(\rho)) + \frac{1}{\hat{\rho}}(v(\rho) - v(0)),$$

and

$$v(\xi) = p(x_{i-1} + \xi(h_i + h_{i+1}), t), \quad \rho = \frac{h_i}{h_i + h_{i+1}}, \quad \hat{\rho} = \frac{h_i}{h_{i+1}}.$$

Applying the Bramble-Hilbert lemma to $\lambda(v)$ we obtain

$$\begin{aligned} |\lambda(v)| &\le C \int_0^1 |\nabla^r v(\xi)|\, d\xi \\ &\le C(h_i + h_{i+1})^{r-1} \int_{x_{i-1/2}}^{x_{i+1/2}} |\nabla^r p(x,t)|\, dx \quad \text{for } r \in \{1,2\}, \end{aligned} \tag{4.34}$$

with ∇^r the derivative of order r. Therefore, the last term can be estimated as follows

$$|\tau_{b,h}^{(3)}(t, w_h)| \le C\Big(\sum_{i=1}^{N} h_i^{2r} \|p(t)\|^2_{H^{1+r}(x_{i-1},x_i)} \Big)^{1/2} \|w_h\|_{H^1}. \tag{4.35}$$

The proof now follows from (4.33)-(4.35).

■

The next lemma is given without proof. It can be found as Remark 3.4 to Theorem 3.1 in [16].

Lemma 4.3 *Let $g(t)$ be a function in the space $H^2(\Omega)$. Then, for $h \in \mathrm{H}$, it holds*

$$|(P_h g(t) - (g(t))_h, w_h)_h| \le C_{in}\Big(\sum_{i=1}^{N} h_i^4 \|g(t)\|^2_{H^2(x_{i-1},x_i)} \Big)^{1/2} \|w_h\|_{H^1} \quad \textit{for } w_h \in S_h.$$

For the semi-discretization (4.7)-(4.9) define the errors

$$e_{c,h}(t) = P_h c(t) - c_h(t) \quad \text{and} \quad e_{p,h}(t) = P_h p(t) - p_h(t).$$

We are now in position to establish the main results of this chapter, namely the supercloseness of the approximations. We start with the concentration.

Theorem 4.3 *Let p and c be solutions of the coupled quasi-linear problem (4.5) and let p_h and c_h be the approximations defined by (4.7)-(4.9). Assume that the variational problem: find $v \in H_0^1(\Omega)$ such that $(\tilde{d}(t)\nabla v, \nabla w) - (\tilde{b}(t)v, \nabla w) = 0$, for $w \in H_0^1(\Omega)$, has only the null solution, where $\tilde{d}(t) = d(c(t), \nabla p(t))$ and $\tilde{b}(t) = b(c(t), \nabla p(t))$.*

Moreover, assume that $C_a \leq a$, $C_d \leq d$, b *satisfies (4.15) and that the assumption (4.14) holds. Then, for* $r \in \{1,2\}$ *and* $h \in \mathrm{H}$, *we have*

$$\|e_{c,h}(t)\|_h^2 + \int_0^t \|e_{c,h}(s)\|_{H^1}^2\, ds \leq C_1 e^{C_2 t}\Big(C_e \sum_{i=1}^{N} \int_0^t h_i^{2r}\Big(\|p(s)\|_{H^{1+r}(x_{i-1},x_i)}^2 + \|c(s)\|_{H^{1+r}(x_{i-1},x_i)}^2\Big) + h_i^4 \|\partial_t c(s)\|_{H^2(x_{i-1},x_i)}^2\, ds + \|e_{c,h}(0)\|_h^2\Big),$$

where ϵ *is a non-zero constant satisfying* $C_d - 4\epsilon^2 > 0$,

$$C_1 = \frac{1}{min\{1, 2(C_d - 4\epsilon^2)\}}, \quad C_2 = \frac{1}{\epsilon^2}\Big(C_d^2 + C_{b,2}^2 + \frac{1}{2}C_b^2 C_p^2\Big) + 2\epsilon^2$$

and provided that $p, c \in L^\infty(0,T; H^{1+r}(\Omega) \cap H_0^1(\Omega))$ *and* $\partial_t c \in L^2(0,T; H^2(\Omega))$.

Proof: It is easy to show that $e_{c,h}(t)$ is a solution of the variational problem

$$(\partial_t e_{c,h}(t), w_h)_h = (d_h(t)\nabla c_h(t), \nabla w_h) - (M^*(b_h(t)c_h(t)), \nabla w_h) - ((q_2(t))_h, w_h)_h + (\partial_t P_h c(t), w_h)_h$$

and, as $\tilde{c}_h(t)$ satisfies (4.18), we obtain

$$\begin{aligned}(\partial_t e_{c,h}(t), w_h)_h = &-(\tilde{d}_h(t)\nabla \tilde{c}_h(t), \nabla w_h) + (d_h(t)\nabla c_h(t), \nabla w_h) \\ &- (M^*(b_h(t)c_h(t)), \nabla w_h) + (M^*(\tilde{b}_h(t)\tilde{c}_h(t)), \nabla w_h) \\ &- (\partial_t (c_h(t))_h, w_h)_h + (\partial_t P_h c(t), w_h)_h. \end{aligned} \tag{4.36}$$

By setting $w_h = e_{c,h}(t)$ in (4.36) and taking into account Lemmas 4.1 and 4.2, we get

$$\begin{aligned}(\partial_t e_{c,h}(t), e_{c,h}(t))_h = &-(d_h(t)\nabla e_{c,h}(t), \nabla e_{c,h}(t)) + (M^*(b_h(t)e_{c,h}(t)), \nabla e_{c,h}(t)) \\ &+ (\partial_t P_h c(t) - \partial_t (c_h(t))_h, e_{c,h}(t))_h - \tau_{d,h}(t, e_{c,h}(t)) - \tau_{b,h}(t, e_{c,h}(t)). \end{aligned} \tag{4.37}$$

For $(\partial_t P_h c(t) - \partial_t (c_h(t))_h, e_{c,h}(t))_h$, it follows from Lemma 4.3 that

$$|(\partial_t P_h c(t) - \partial_t (c_h(t))_h, e_{c,h}(t))_h| \leq \frac{C_{in}^2}{4\sigma^2} \sum_{i=1}^{N} h_i^4 \|\partial_t c(t)\|_{H^2(x_{i-1},x_i)}^2 + \sigma^2 \|e_{c,h}(t)\|_{H^1}^2, \tag{4.38}$$

provided that $\partial_t c(t) \in H^2(\Omega)$. Here, $\sigma \neq 0$ is an arbitrary constant.

For $\tau_{d,h}(t, e_{c,h}(t))$ and $\tau_{b,h}(t, e_{c,h}(t))$, we use the estimates (4.30) and (4.32), respectively, to obtain

$$\begin{aligned}|\tau_{d,h}(t, e_{c,h}(t))| \leq &\frac{1}{2\epsilon^2} C_d^2 \|e_{c,h}(t)\|_h^2 + \epsilon^2 \|e_{c,h}(t)\|_{H^1}^2 \\ &+ \frac{1}{2\epsilon^2} C_d^2 \sum_{i=1}^{N} h_i^{2r}\Big(\|p(t)\|_{H^{1+r}(x_{i-1},x_i)}^2 + \|c(t)\|_{H^{1+r}(x_{i-1},x_i)}^2\Big), \end{aligned} \tag{4.39}$$

and

$$|\tau_{b,h}(t, e_{c,h}(t))| \leq \frac{1}{2\eta^2} C_{b,2}^2 \|e_{c,h}(t)\|_h^2 + \eta^2 \|e_{c,h}(t)\|_{H^1}^2 + \frac{1}{2\eta^2} C_{b,2}^2 \sum_{i=1}^{N} h_i^{2r} \Big(\|p(t)\|_{H^{1+r}(x_{i-1},x_i)}^2 + \|c(t)\|_{H^{1+r}(x_{i-1},x_i)}^2 \Big), \quad (4.40)$$

where $\epsilon \neq 0$ and $\eta \neq 0$ are arbitrary constants.

Hence, by (4.38)-(4.40), from (4.37) we find

$$\frac{1}{2}\partial_t \|e_{c,h}(t)\|_h^2 + (d_h(t)\nabla e_{c,h}(t), \nabla e_{c,h}(t)) \leq (\epsilon^2 + \eta^2 + \sigma^2)\|e_{c,h}(t)\|_{H^1}^2 + (M^*(b_h(t)e_{c,h}(t)), \nabla e_{c,h}(t)) + \Big(\frac{1}{2\epsilon^2} C_d^2 + \frac{1}{2\eta^2} C_{b,2}^2 + \sigma^2\Big)\|e_{c,h}(t)\|_h^2 + \tau_h(t)^2, \quad (4.41)$$

where

$$\tau_h(t)^2 \leq \Big(\frac{1}{2\epsilon^2} C_d^2 + \frac{1}{2\eta^2} C_{b,2}^2\Big)\Big(\sum_{i=1}^{N} h_i^{2r} \Big(\|p(t)\|_{H^{1+r}(x_{i-1},x_i)}^2 + \|c(t)\|_{H^{1+r}(x_{i-1},x_i)}^2 \Big)\Big) + \frac{1}{4\sigma^2} C_{in}^2 \sum_{i=1}^{N} h_i^4 \|\partial_t c(t)\|_{H^2(x_{i-1},x_i)}^2.$$

Now, we have

$$(d_h(t)\nabla e_{c,h}(t), \nabla e_{c,h}(t)) \geq C_d \|e_{c,h}(t)\|_{H^1}^2, \quad (4.42)$$

and, since (4.16) holds with $c_h(t)$ replaced by $e_{c,h}(t)$, we can write

$$|(M^*(b_h(t)e_{c,h}(t)), \nabla e_{c,h}(t))| \leq \frac{1}{4\gamma^2} C_b^2 C_p^2 \|e_{c,h}(t)\|_h^2 + \gamma^2 \|e_{c,h}(t)\|_{H^1}^2, \quad (4.43)$$

with $\gamma \neq 0$ an arbitrary constant.

Joining estimates (4.41)-(4.43) and setting $\epsilon = \eta = \gamma = \sigma$, one obtains

$$\partial_t \|e_{c,h}(t)\|_h^2 + 2(C_d - 4\epsilon^2)\|e_{c,h}(t)\|_{H^1}^2 \leq C_2 \|e_{c,h}(t)\|_h^2 + \tau_h(t)^2.$$

Therefore, we have

$$\|e_{c,h}(t)\|_h^2 + 2(C_d - 4\epsilon^2) \int_0^t \|e_{c,h}(s)\|_{H^1}^2 \, ds \leq \|e_{c,h}(0)\|_h^2 + C_2 \int_0^t \|e_{c,h}(s)\|_h^2 \, ds + \int_0^t \tau_h(s)^2 \, ds,$$

which yields the desired result using Gronwall's lemma.

■

The Corollary 4.3 below gives the supercloseness of the pressure. It is a consequence of Corollary 4.2 and Theorem 4.3.

Corollary 4.3 *Under the assumptions of Theorem 4.3, it holds*

$$\|e_{p,h}(t)\|_{H^1}^2 \leq C_{p,n}\Big(\|P_h c_0 - c_{h,0}\|_h^2 + C_e \sum_{i=1}^{N} \int_0^t \Big(h_i^{2r}\Big(\|p(s)\|_{H^{1+r}(x_{i-1},x_i)}^2 + \|c(s)\|_{H^{1+r}(x_{i-1},x_i)}^2\Big) + h_i^4 \|\partial_t c(s)\|_{H^2(x_{i-1},x_i)}^2\Big) ds\Big).$$

The following corollary summarizes our main findings.

Corollary 4.4 *Let the assumptions of Theorem 4.3 hold, and assume that $c_{h,0}$ satisfies an estimate of type (2.34). Then, for $t \in [0,T]$,*

$$\|e_{p,h}(t)\|_{H^1}^2 + \int_0^t \|e_{c,h}(s)\|_{H^1}^2 \, ds \leq C h_{max}^4 \int_0^t \|c(s)\|_{H^3}^2 + \|p(s)\|_{H^3}^2 + \|\partial_t c(s)\|_{H^2}^2 \, ds,$$

provided that $p, c \in L^\infty(0,T; H^3(\Omega) \cap H_0^1(\Omega))$ and $\partial_t c \in L^2(0,T; H^2(\Omega))$.

The analogue of Corollary 4.4 for the FDM (4.10) can be established as in the previous chapters. It is important to enhance the fact that the supercloseness result, Corollary 4.4, or the equivalent supraconvergence result, are valid without any assumption on the mesh. We also observe that the error analysis introduced in Chapter 3 was used to study the error of the finite element approximation. Again, this permits us to relax the smoothness requirements on a solution of (4.5).

4.2 A Fully Discrete Method

We are going to discuss in this section the full discretization of the coupled problem (4.1)-(4.4). First a scheme is presented, then a convergence result is provided.

We consider full discretizations by applying a time integration method to the finite element differential system (4.7)-(4.9). On $[0,T]$, let us introduce the uniform grid $t_n = t_{n-1} + \Delta t$, for $n = 1, \ldots, N$, with $t_0 = 0$, $t_N = T$ and fixed step size Δt. Let $p_h^{n+1}, c_h^{n+1} \in S_h$ be the numerical approximations for $p_h(t_{n+1})$ and $c_h(t_{n+1})$, respectively. Then, for $w_h \in S_h$, our fully discrete FEM is described by

$$\begin{cases} (a_h^n \nabla p_h^{n+1}, \nabla w_h) = ((q_1)_h^{n+1}, w_h)_h, \\ \\ (D_{-t} c_h^{n+1}, w_h)_h + (d_h^{n,n+1} \nabla c_h^{n+1}, \nabla w_h) \\ \qquad\qquad - (M^*(b_h^{n,n+1} c_h^{n+1}), \nabla w_h) = ((q_2)_h^{n+1}, w_h)_h, \end{cases} \tag{4.44}$$

for $n = 0, \ldots, N-1$, and with the initial conditions

$$p_h^0 = p_{h,0}, \quad c_h^0 = c_{h,0}. \tag{4.45}$$

Recall that the function a_h depends only on the concentration c_h, while d_h and b_h depend also on the pressure p_h. Here, a_h^n, $d_h^{n,n+1}$, and $b_h^{n,n+1}$ mean that we are evaluating the concentration at time level n and the pressure at time level $n+1$. Therefore, the time integration method is of IMEX type. In the porous media context, this kind of method is known as IMPES (implicit pressure, explicit saturation/concentration).

4.2.1 Convergence Analysis

In this section, we prove linear convergence in time of the IMEX method (4.44)-(4.45). Most of the analysis is similar to Section 4.1.2, so we merely outline the main steps.

Let $\tilde{p}_h^{n+1}$ and $\tilde{c}_h^{n+1}$ be solutions of the auxiliary problems (4.17)-(4.18) where the source terms and the coefficient functions are defined using $t = t_{n+1}$. As in the semi-discrete case, we consider that

$$\max_{i=1,\dots,N} |\nabla \tilde{p}_h^n(x_{i-1/2})| \leq C_{\tilde{p}}, \tag{4.46}$$

$$\max_{i=1,\dots,N} |\nabla \tilde{c}_h^n(x_{i-1/2})| \leq C_{\tilde{c}}, \tag{4.47}$$

$$\max_{i=1,\dots,N} |\nabla p_h^n(x_{i-1/2})| \leq C_p. \tag{4.48}$$

Under the conditions of Proposition 4.4 and assuming (4.46) we can prove that

$$\|p_h^{n+1} - \tilde{p}_h^{n+1}\|_{H^1} \leq C\Big(\|P_h c(t_n) - c_h^n\|_h + \Big(\sum_{i=1}^N h_i^{2r} \|c(t_{n+1})\|^2_{H^r(x_{i-1},x_i)} \Big)^{1/2} + \Big(\Delta t^2 \|\partial_t P_h c(t_n)\|_h^2 + \Delta t^3 \|P_h c\|^2_{H^2(t_n,t_{n+1};S_h)} \Big)^{1/2} \Big).$$

for $r \in \{1,2\}$. Hence, since (4.19) holds with $t = t_{n+1}$, we get

$$\|e_{p,h}^{n+1}\|_{H^1} \leq C\Big(\|e_{c,h}^n\|_h + \Delta t \Big(\|\partial_t P_h c(t_n)\|_h^2 + \Delta t \|P_h c\|^2_{H^2(t_n,t_{n+1};S_h)} \Big)^{1/2} + \Big(\sum_{i=1}^N h_i^{2r} \|c(t_{n+1})\|^2_{H^r(x_{i-1},x_i)} \Big)^{1/2} + \Big(\sum_{i=1}^N h_i^{2r} \|p(t_{n+1})\|^2_{H^{1+r}(x_{i-1},x_i)} \Big)^{1/2} \Big), \tag{4.49}$$

where

$$e_{c,h}^{n+1} = P_h c(t_{n+1}) - c_h^{n+1} \quad \text{and} \quad e_{p,h}^{n+1} = P_h p(t_{n+1}) - p_h^{n+1}.$$

Now, proceeding as in Theorem 4.3 and assuming that (4.47) and (4.48) are satisfied, we obtain

$$(D_{-t} e_{c,h}^{m+1}, w_h)_h = (M^*(b_h^{m,m+1} e_{c,h}^{m+1}), \nabla w_h) - (d_h^{m,m+1} \nabla e_{c,h}^{m+1}, \nabla w_h) - \tau_h^{m+1}(w_h), \tag{4.50}$$

with

$$\tau_h^{m+1}(w_h) = \tau_{d,h}^{m+1}(w_h) + \tau_{b,h}^{m+1}(w_h) + \tau_{c,h}^{m+1}(w_h).$$

Moreover, we have the bounds

$$|\tau_{d,h}^{m+1}(w_h)| \le C_{d,d}\Big(\|e_{c,h}^m\|_h + \Delta t\Big(\|\partial_t P_h c(t_m)\|_h^2 + \Delta t\|P_h c\|^2_{H^2(t_m,t_{m+1};S_h)}\Big)^{1/2} + \Big(\sum_{i=1}^N h_i^{2r}\|p(t_{m+1})\|^2_{H^{1+r}(x_{i-1},x_i)}\Big)^{1/2} + \Big(\sum_{i=1}^N h_i^{2r}\|c(t_{m+1})\|^2_{H^{1+r}(x_{i-1},x_i)}\Big)^{1/2}\Big)\|w_h\|_{H^1}$$

and

$$|\tau_{b,h}^{m+1}(w_h)| \le C_{b,d}\Big(\|e_{c,h}^m\|_h + \Delta t\Big(\|\partial_t P_h c(t_m)\|_h^2 + \Delta t\|P_h c\|^2_{H^2(t_m,t_{1+r};S_h)}\Big)^{1/2} + \Big(\sum_{i=1}^N h_i^{2r}\|c(t_{m+1})\|^2_{H^{1+r}(x_{i-1},x_i)}\Big)^{1/2} + \Big(\sum_{i=1}^N h_i^{2r}\|p(t_{m+1})\|^2_{H^{1+r}(x_{i-1},x_i)}\Big)^{1/2}\Big)\|w_h\|_{H^1}$$

and

$$|\tau_{c,h}^{m+1}(w_h)| \le C_{in,d}\Big(\Delta t\|P_h c\|_{W^{2,\infty}(t_m,t_{m+1};S_h)} + \Big(\sum_{i=1}^N h_i^4\|\partial_t c(t_{m+1})\|^2_{H^2(x_{i-1},x_i)}\Big)^{1/2}\Big)\|w_h\|_{H^1}.$$

Taking $w_h = e_{c,h}^{m+1}$ in equation (4.50), we find

$$\|e_{c,h}^{m+1}\|_h^2 + 2\Delta t(C_d - 4\epsilon^2)\|e_{c,h}^{m+1}\|^2_{H^1} \le (1+\theta_2\Delta t)\|e_{c,h}^m\|_h^2 + \theta_1\Delta t\|e_{c,h}^{m+1}\|_h^2 + \Delta t(\tau_s^{m+1})^2, \tag{4.51}$$

with ϵ a non-zero constant,

$$\theta_1 = \frac{1}{2\epsilon^2}C_p^2C_b^2, \quad \theta_2 = \frac{1}{2\epsilon^2}(C_{d,d}^2 + C_{b,d}^2 + C_{in,d}^2)$$

and

$$(\tau_s^{m+1})^2 \le \frac{1}{2\epsilon^2}\Big(C_{d,d}^2 + C_{b,d}^2\Big)\Big(\Delta t\|\partial_t P_h c(t_m)\|_h + \Delta t\|P_h c\|^2_{H^2(t_m,t_{m+1};S_h)} + \Big(\sum_{i=1}^N h_i^{2r}\|c(t_{m+1})\|^2_{H^{1+r}(x_{i-1},x_i)}\Big)^{1/2} + \Big(\sum_{i=1}^N h_i^{2r}\|p(t_{m+1})\|^2_{H^{1+r}(x_{i-1},x_i)}\Big)^{1/2}\Big)^2 + \frac{1}{2\epsilon^2}C_{in,d}^2\Big(\Delta t\|P_h c\|_{W^{2,\infty}(t_m,t_{m+1};S_h)} + \Big(\sum_{i=1}^N h_i^4\|\partial_t c(t_{m+1})\|^2_{H^2(x_{i-1},x_i)}\Big)^{1/2}\Big)^2.$$

By summing in (4.51) over the index m from 0 to $n-1$, we deduce that

$$(1-\theta_1\Delta t)\|e_{c,h}^n\|_h^2 + 2\Delta t(C_d-4\epsilon^2)\sum_{m=0}^{n}\|e_{c,h}^m\|_{H^1}^2 \le (1-\theta_1\Delta t)\|e_{c,h}^0\|_h^2 + 2\Delta t(C_d-4\epsilon^2)\|e_{c,h}^0\|_{H^1}^2 + (\theta_1+\theta_2)\Delta t\sum_{m=0}^{n-1}\|e_{c,h}^m\|_h^2 + \Delta t\sum_{m=1}^{n}(\tau_s^m)^2,$$

which implies

$$\|e_{c,h}^n\|_h^2 + \Delta t\sum_{m=0}^{n}\|e_{c,h}^m\|_{H^1}^2 \le C_1((1-\theta_1\Delta t)\|e_{c,h}^0\|_h^2 + 2\Delta t(C_d-4\epsilon^2)\|e_{c,h}^0\|_{H^1}^2) + C_2\Delta t\sum_{m=0}^{n-1}\|e_{c,h}^m\|_h^2 + \Delta t\sum_{m=1}^{n}(\tau_s^m)^2, \tag{4.52}$$

with

$$C_1 = \frac{1}{\min\{1-\theta_1\Delta t, 2(C_d-4\epsilon^2)\}}, \quad C_2 = C_1(\theta_1+\theta_2)$$

and provided that $C_d - 4\epsilon^2 > 0$ and

$$1-\theta_1\Delta t > 0. \tag{4.53}$$

Applying the discrete Gronwall's inequality to (4.52) gives

$$\|e_{c,h}^n\|_h^2 + \Delta t\sum_{m=0}^{n}\|e_{c,h}^m\|_{H^1}^2 \le C_1 e^{C_2 n\Delta t}\Big((1-\theta_1\Delta t)\|e_{c,h}^0\|_h^2 + 2(C_d-4\epsilon^2)\Delta t\|e_{c,h}^0\|_{H^1}^2 + \Delta t\sum_{m=1}^{n}(\tau_s^m)^2\Big). \tag{4.54}$$

Moreover, if p and c are smooth enough, we have

$$\Delta t\sum_{m=1}^{n}(\tau_s^m)^2 \le C\Big(\sum_{i=1}^{N}\Big(h_i^{2r}\Big(\|c\|^2_{L^\infty(0,T;H^{1+r}(x_{i-1},x_i))} + \|p\|^2_{L^\infty(0,T;H^{1+r}(x_{i-1},x_i))}\Big) + h_i^4\|\partial_t c\|^2_{L^\infty(0,T;H^2(x_{i-1},x_i))}\Big) + \Delta t^2\Big(\|\partial_t P_h c\|^2_{L^\infty(0,T;S_h)} + \|P_h c\|^2_{W^{2,\infty}(0,T;S_h)}\Big)\Big).$$

In Theorem 4.4 below, we present our convergence result. It is a direct consequence of the previous estimate and (4.49) and (4.54). We remark that a similar result can be obtained applying the same time integration procedure to the semi-discrete finite difference scheme (4.10).

Theorem 4.4 *Let $c_{h,0}$ satisfy condition (2.34) with respect to $\|\cdot\|_{H^1}$ and let Δt verify (4.53). For $r \in \{1,2\}$, there holds*

$$\|e_{p,h}^{n+1}\|_{H^1}^2 + \|e_{c,h}^n\|_h^2 + \Delta t \sum_{m=1}^{n} \|e_{c,h}^m\|_{H^1}^2 \leq C\Big(\Delta t^2 \|P_h c\|_{W^{2,\infty}(0,T;S_h)}^2 + h_{max}^{2r}\Big(\|c\|_{L^\infty(0,T;H^{1+r})}^2 + \|p\|_{L^\infty(0,T;H^{1+r})}^2\Big) + h_{max}^4 \|\partial_t c\|_{L^\infty(0,T;H^2)}^2\Big),$$

provided that $p, c \in L^\infty(0,T;H^{1+r}(\Omega) \cap H_0^1(\Omega))$, $\partial_t c \in L^\infty(0,T;H^2(\Omega))$, and $\partial_t^2 c \in L^\infty(0,T;C(\Omega))$.

4.3 Numerical Experiments

In this section we illustrate our convergence result by one example.

Example 4.1 *Consider the coupled problem (4.1)-(4.4) with*

$$a(c) = 1 + c, \quad b(c, \nabla p) = (c\nabla p)^2, \quad \textit{and} \quad d(c, \nabla p) = c + \nabla p + 2.$$

We choose q_1, q_2, and the initial conditions so that the exact solution is

$$p(x,t) = e^t x(x-1) \quad \textit{and} \quad c(x,t) = e^t(1 - cos(2\pi x))sin(x).$$

The pressure and concentration errors are measured by

$$\text{Error}_\text{p} = \|e_{p,h}^N\|_{1,h} \quad \text{and} \quad \text{Error}_\text{c} = \Big(\|e_{c,h}^N\|_h^2 + \Delta t \sum_{n=1}^{N} \|e_{c,h}^n\|_{1,h}^2\Big)^{1/2}.$$

The numerical results are presented in Table 4.1, and they confirm the theoretically predicted convergence rates.

h_{max}	Error_c	Rate	Error_p	Rate
1.3174×10^{-1}	5.5435×10^{-2}	1.9492	1.1099×10^{-2}	1.5048
6.5869×10^{-2}	1.4355×10^{-2}	2.0010	3.9113×10^{-3}	1.5808
3.2934×10^{-2}	3.5863×10^{-3}	2.0024	1.3075×10^{-3}	1.8337
1.6467×10^{-2}	8.9511×10^{-4}	2.0008	3.6682×10^{-4}	1.9296
8.2336×10^{-3}	2.2366×10^{-4}	2.0029	9.6288×10^{-5}	1.9671
4.1168×10^{-3}	5.5804×10^{-5}	2.0109	2.4628×10^{-5}	1.9866
2.0584×10^{-3}	1.3846×10^{-5}	2.0301	6.2144×10^{-6}	2.0015
1.0292×10^{-3}	3.3899×10^{-6}	-	1.5520×10^{-6}	-

Table 4.1: Discrete norm errors and estimated convergence rates for Example 4.1.

For the computations, we have chosen $T = 0.1$ and a very small time step to reduce the buildup of time integration errors.

Chapter 5

Applications: Non-Fickian Tracer Transport in Porous Media

This chapter is totally dedicated to our mathematical model for non-Fickian tracer transport in porous media. In the first section, considering the one-dimensional version, we test and validate the model by fitting breakthrough curves (BTCs) resulting from laboratory tracer tests. Comparisons with the traditional PDE model are also presented and, as we will see, the proposed model allows a better fitting of the observations. In fact, the BTCs presented here exhibit some non-Fickian features, such as asymmetric profiles and long tails, that are not captured by the traditional model. For completeness, we also compare our model to the continuous time random walk (CTRW) model, which has been shown to be very effective in describing non-Fickian transport. In the second and last section, we develop an efficient discretization scheme in two dimensions for the solution of the concentration PIDE equation and the velocity system. Some numerical experiments illustrate the applicability and the feasibility of our approach.

5.1 Model Validation: Breakthrough curve analysis

The objective of this section is to test the proposed integro-differential model, designated as the PIDE model, against real data and to compare its effectiveness with the usual PDE model. We restrict attention to the one-dimensional case. Additional simplifications included the absence of source or sink terms. In this manner, the PIDE model (1.30) reduces to

$$\partial_t c + \nabla \cdot (vc) - d_f \Delta c = d_{nf} \int_0^t K(t-s)\Delta c(s)\, ds \quad \text{in } \Omega \times (0,T], \tag{5.1}$$

while the PDE model (1.20) takes the form

$$\partial_t c + \nabla \cdot (vc) = d\Delta c \quad \text{in } \Omega \times (0, T]. \tag{5.2}$$

Here, we have written $v = v/\phi$ as the average velocity, d as a dispersion coefficient and d_f and d_{nf} as Fickian and non-Fickian dispersion coefficients, respectively. We emphasize that the parameters d_f and d have a different physical meaning in each of the above models.

In order to better illustrate the performance of the PIDE model, we also compare it against the CTRW model in the truncated power law (TPL) form. Such a model, designated TPL, is based on the CTRW theory and has been proved quite accurate for modeling tracer transport [49,88,109]. In the CTRW perspective, tracer transport can be seen as a series of particle jumps in space and time that can be characterized by a probability density function (pdf) $\psi(x,t)$. For a given initial position x_0 at time t_0, this function gives the probability that the particle is at position x at time t, i.e., the probability of making a jump of length $h = x - x_0$ after a time $\Delta t = t - t_0$. Assuming that this process is uncorrelated in space and time, we can write $\psi(x,t) = \psi_x(x)\psi_t(t)$, where ψ_x denotes the jump length pdf and ψ_t the waiting time pdf. Assuming moreover that ψ_x is Gaussian, the general one-dimensional version of such CTRW models is given in the Laplace domain by

$$p\tilde{c}(p) - c_0 = \tilde{M}(p)(d\Delta\tilde{c}(p) - \nabla \cdot (v\tilde{c}(p))), \tag{5.3}$$

where $\tilde{M}(p)$ is the memory function defined by

$$\tilde{M}(p) = \tilde{t}p\frac{\tilde{\psi}_t(p)}{1 - \tilde{\psi}_t(p)}$$

with $\tilde{t}$ some characteristic time. The particular case of the TPL model is obtained, assuming that ψ_t follows a TPL distribution function

$$\psi_t(t) = \frac{r^\beta(1 + t/t_1)^{-1-\beta}}{t_1\Gamma(-\beta, r)}\exp(-r - t/t_2), \quad r = \frac{t_1}{t_2},\ 0 \le \beta \le 2,$$

where Γ is the incomplete Gamma function and $t_1 = \tilde{t}$. Although, for simplicity, we have used the same notation as in (5.2) it should be noted that the parameters d and v have a different physical meaning in this approach. For a detail discussion on this model we refer to [29, 56].

We observe that the proposed PIDE model can also be interpreted in the language of CTRWs. For that, we first note that considering the Poissonian waiting time pdf

$$\psi_t(t) = \lambda\exp(-\lambda t),$$

taking $\tilde{t} = \lambda^{-1}$ and writing (5.3) in the time domain, we get an equation that is formally identical to the classical PDE model (5.2). On the other hand, if we take the waiting time pdf of the Gamma family defined by

$$\psi_t(t) = \frac{t}{4\tau^2} \exp(-t/2\tau), \quad \tau > 0,$$

and considering also $\tilde{t} = 4\tau$, we obtain the equation

$$\partial_t c = \int_0^t K(t-s)(d\Delta c(s) + \nabla \cdot (vc))\, ds, \tag{5.4}$$

where K is precisely the memory function of the PIDE model (5.1). Therefore the PIDE model can be regarded as a compromise between the Gamma model (5.4) and the PDE model.

Now we specify the boundary and initial conditions for the PIDE model. In the following simulations, the outlet boundary condition is open, while at the inlet we adopt the Dirichlet condition,

$$c(0,t) = c_I(t) \quad \text{for } t \leq t_I \leq T. \tag{5.5}$$

Furthermore, the initial condition $c(0) = 0$ is used, i.e., the initial concentration is assumed to be zero. There is a lot of discussion about the correct type of boundary conditions to be used in these problems and also on the closely related notation of flux-averaged concentration. For that, we refer to [106, 135, 145], where this is more deeply explored. Here, we do not address this question.

As mentioned before, we test the models by comparing simulated and measured BTCs. The quality of the fitting is quantified using the root mean square error (RMSE), which is defined by

$$\text{RMSE} = \Big(\frac{1}{N}\sum_{n=1}^{N}(c^n - c_h^n)^2\Big)^{1/2},$$

with N the number of observations, c^n the measured concentration at time t_n, and c_h^n the estimated concentration at time t_n. The best-fit BTCs based on the PDE and TPL models are generated using the publicly available CTRW toolbox [50]. For the PIDE model, the minimization procedure was carried out using built-in routines of Matlab [1].

5.1.1 Data Set 1

In an already classical experiment, Scheidegger [144] used homogeneous Berea sandstone core columns to investigate the accuracy of the PDE model in simulating tracer transport in porous media. During the experiment, columns of different lengths were first fully saturated with tracer and subsequently flushed with clean liquid. The resulting tracer BTCs at the outflow boundary were measured and compared with the ones predicted by the PDE model. Scheidegger concluded that the PDE model was inadequate for describing the BTCs, in his own words: *"The deviations are systematic which appears to point towards an additional, hitherto unknown effect"*.

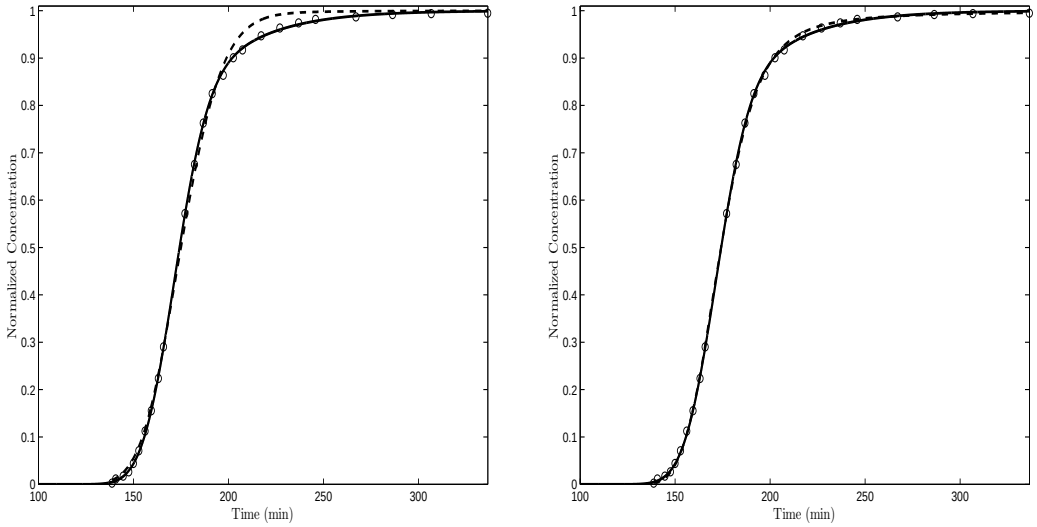

(a) PIDE (solid line) and PDE (dash line). (b) PIDE (solid line) and TPL (dash line).

Figure 5.1: Experimental data set 1 and the best-fit BTCs.

We test the models using typical data from one of these experiments. In this case, the column was 7.62×10^{-1} meters (m) long and 5.08×10^{-2} m in diameter, the clean liquid was injected at a rate equal to 1.73 cubic centimeters per minute (cm^3/min), and the porosity of the core was 0.204. This gives an average velocity of 4.18×10^{-3} m/min. Observe that in order to simulate this experiment we solve equations (5.1) and (5.2) for the liquid concentration, and so the appropriate boundary condition at the inlet (5.5) is of step type, i.e., $c_I = 1$, for $t \in (0, T]$. In Figure 5.1 (a), we show the experimental data and the best-fit curves obtained with the PIDE and the PDE models. A quick observation of Figure 5.1 (a) indicates that the PIDE model captures the transport dynamics quite well. The PDE model, however, fails to describe the data, especially at late times, since it can not reproduce the long tail, a typical indication of non-Fickian transport. This result for the PDE model is in line with the findings of

Scheidegger. The values of the two models constants and the RMSE are listed in Table 5.1. As indicated by the given results, the application of the proposed model leads to a reduction of about 79% in the RMSE.

PDE	PIDE		TPL	
v (m/min)	v (m/min)	d_f (m^2/min)	v (m/min)	
4.65×10^{-3}	4.27×10^{-3}	1.08×10^{-5}	7.23×10^{-3}	
d (m^2/min)	d_{nf} (m^2/min)	τ (min)	d (m^2/min)	β
1.35×10^{-5}	1.76×10^{-5}	25.52	7.86×10^{-6}	1.58
RMSE	RMSE		RMSE	
1.72×10^{-2}	3.66×10^{-3}		5.11×10^{-3}	

Table 5.1: Fitting parameters for the models plotted in Figure 5.1 and the corresponding RMSE values.

Now we compare the results obtained for the PIDE model with the results for the TPL model. As shown in Figure 5.1 (b), there is only a small discrepancy between them. The RMSE values, 3.66×10^{-3} and 5.11×10^{-3}, respectively, suggest that the PIDE model fits the data slightly better. This same data have been analyzed in [49] using the PDE and TPL models, with similar conclusions. Here and in the following, we omitted the values of t_1 and t_2 in the TPL model. They are consistently very small, and very large, respectively, when compared to the time scale; therefore, its exact value is not relevant.

5.1.2 Data Set 2

The second group of data is the result of tracer displacement experiments through homogeneous sand columns reported in [36]. Next, we briefly describe the setup and we refer to that paper for all other experimental details. The columns were incrementally packed with sand particles of different sizes. The diameter of most of the sand particles lie in the range of $0.1 - 0.71$ millimeters. We consider the results for two columns: Column 1, 11 cm in diameter and 10 cm long; and Column 2, also 11 cm in diameter but 40 cm long. The transport experiment was conducted under initially unsaturated conditions, with the water content of 0.24 for Column 1 and of 0.18 for Column 2. A pulse tracer at the flow rate of 4.20×10^{-2} cm/min was applied at the top of both columns within the time period of 140 seconds (s) for the smaller column and of 107 s for the longer one. The respective average velocities were

1.86×10^{-1} cm/min and 2.28×10^{-1} cm/min. After the pulse, water was injected at the same rate.

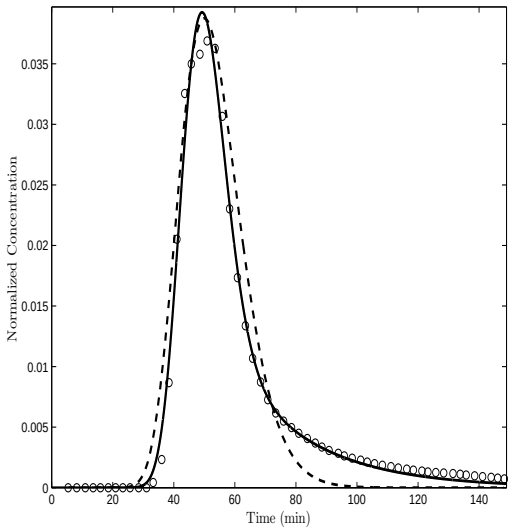

(a) PIDE (solid line) and PDE (dash line).

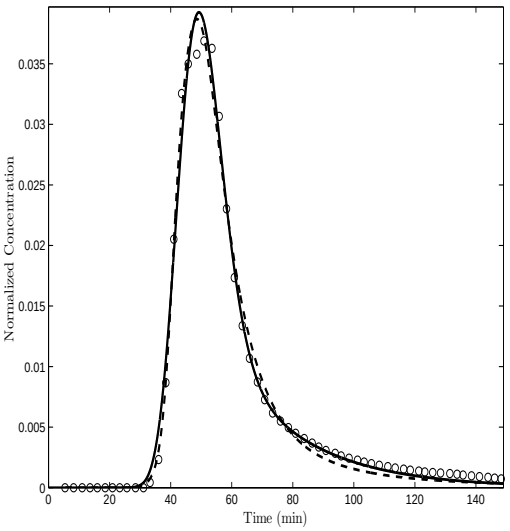

(b) PIDE (solid line) and TPL (dash line).

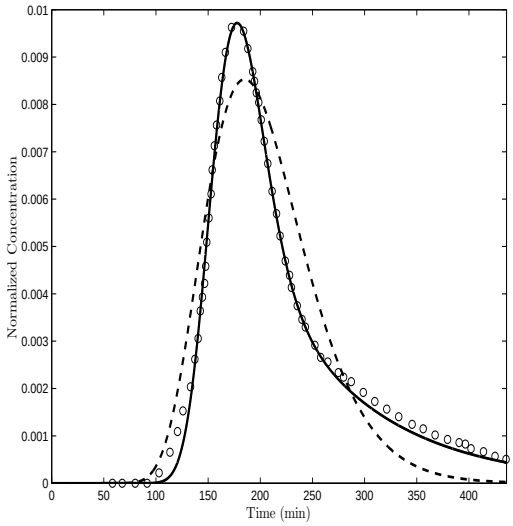

(c) PIDE (solid line) and PDE (dash line).

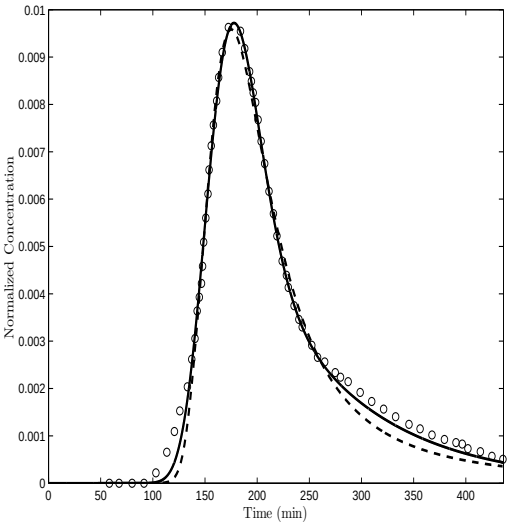

(d) PIDE (solid line) and TPL (dash line).

Figure 5.2: Experimental data set 2 and the best-fit BTCs for Column 1 in (a) and (b) and for Column 2 in (c) and (d).

To simulate this scenario, we set at the inlet boundary $c_I = 4.16 \times 10^{-2}$ and $t_I = 2.33$ min for Column 1, and $c_I = 5.77 \times 10^{-2}$ and $t_I = 1.78$ min for Column 2. These values of c_I correct the small mass imbalance. The observed and fitted BTCs for the models are plotted in Figure 5.2. In particular, Figures 5.2 (a) and (c) show that the agreement for the PDE model is very poor. This is especially true at later times, where the BTC possesses a heavy tail. On the other hand, the PIDE model

captures the BTC behavior much better. The RMSEs presented in Tables 5.2 and 5.3 prove this conclusion. Using the PIDE model results in a reduction in the RMSE of

PDE	PIDE		TPL	
v (cm/min)	v (cm/min)	d_f (cm^2/min)	v (cm/min)	
1.88×10^{-1}	1.69×10^{-1}	2.59×10^{-2}	1.10	
d (cm^2/min)	d_{nf} (cm^2/min)	τ (min)	d (cm^2/min)	β
3.69×10^{-2}	1.00×10^{-1}	15.95	2.92×10^{-2}	1.10
RMSE	RMSE		RMSE	
2.50×10^{-3}	9.57×10^{-4}		9.77×10^{-4}	

Table 5.2: Fitting parameters for the models plotted in Figures 5.2 (a) and (b) and the corresponding RMSE values (Column 1).

about 62% for Column 1 and 80% for Column 2. The difference between the RMSE of the PIDE model and that of the TPL model is not significant for Column 1, but it is more pronounced for Column 2. In this case the PIDE model presents a smaller error.

PDE	PIDE		TPL	
v (cm/min)	v (cm/min)	d_f (cm^2/min)	v (cm/min)	
1.90×10^{-1}	1.74×10^{-1}	1.16×10^{-1}	2.88	
d (cm^2/min)	d_{nf} (cm^2/min)	τ (min)	d (cm^2/min)	β
2.37×10^{-1}	4.25×10^{-1}	42.14	1.88×10^{-1}	0.97
RMSE	RMSE		RMSE	
9.64×10^{-4}	1.91×10^{-4}		3.43×10^{-4}	

Table 5.3: Fitting parameters for the models plotted in Figures 5.2 (c) and (d) and the corresponding RMSE values (Column 2).

These two models are compared in Figures 5.2 (b) and (d). In [36], the PDE and TPL models, among others, were tested against these data, and the authors considered the TPL one of two best-fitting models.

5.1.3 Data Set 3

In this section, we confront the models with tracer data from a laboratory experiment described in [96]. This was a large-scale experiment, using soil columns with a length of 1250 cm and a cross section of 10×10 cm^2. The tracer tests were conducted under

homogeneous and heterogeneous conditions. Here, we only analyze the data obtained in the heterogeneous column. This column was randomly packed with various soil

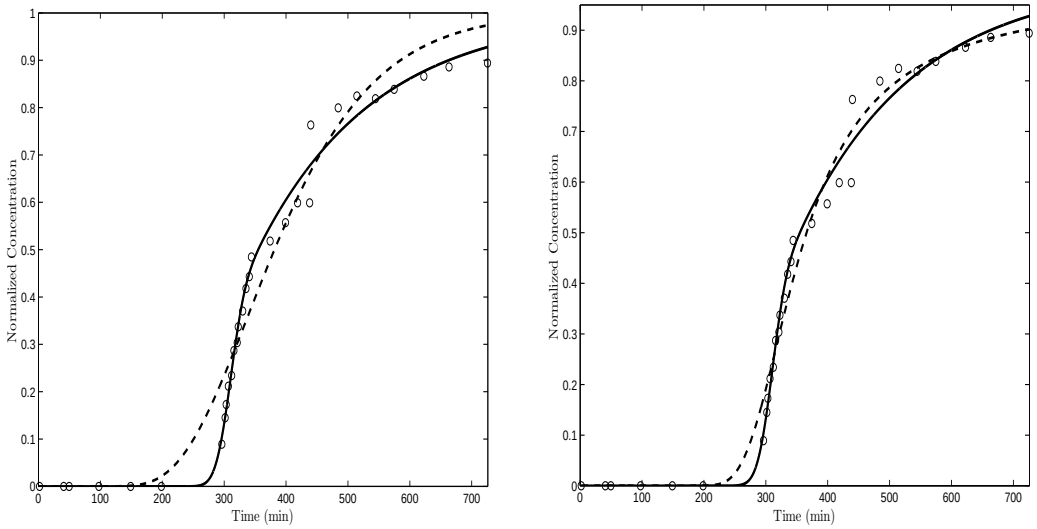

(a) PIDE (solid line) and PDE (dash line). (b) PIDE (solid line) and TPL (dash line).

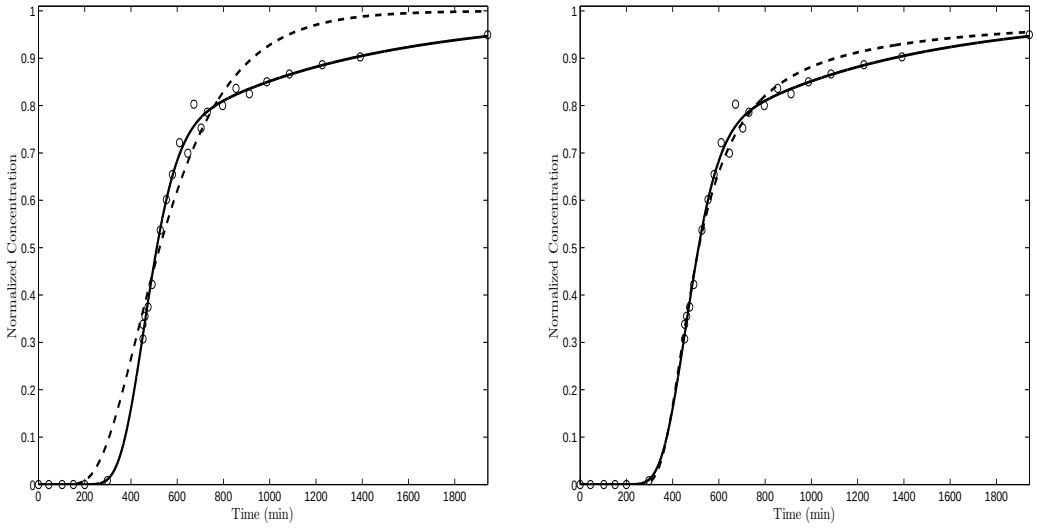

(c) PIDE (solid line) and PDE (dash line). (d) PIDE (solid line) and TPL (dash line).

Figure 5.3: Best-fit BTCs for the data set 3 at the distances of 400 and 600 cm away from the inlet in (a) and (b) and in (c) and (d), respectively.

materials with different shapes and sizes. The study was conducted under saturated conditions and at the constant flow rate of 2.39×10^{-1} cm/min. The estimated porosity was 0.37, leading to an average velocity of 6.45×10^{-1} cm/min. The tracer was injected as a step input and the concentration along the column was measured by installing 12 electrical conductivity probes that were 100 cm apart. The collected data and a detailed analysis of the experiment are given in [96]. Note that because of the

difference between the length and diameter of the column, the use of one-dimensional models is justified.

PDE	PIDE		TPL	
v (cm/min)	v (cm/min)	d_f (cm^2/min)	v (cm/min)	
9.39×10^{-1}	9.30×10^{-1}	1.15	26.61	
d (cm^2/min)	d_{nf} (cm^2/min)	τ (min)	d (cm^2/min)	β
19.82	31.43	67.71	40.34	0.95
RMSE	RMSE		RMSE	
5.63×10^{-2}	2.97×10^{-2}		3.96×10^{-2}	

Table 5.4: Fitting parameters for the models plotted in Figures 5.3 (a) and (b) and the corresponding RMSE values (400 cm).

For our study, we consider the BTCs measured at the distances of 400 and 600 cm. Because of the normalization used in [96] to report the results, we set $c_I = 1$ at the inlet boundary (5.5). The best-fit BTCs by the models and the experimental observations are given in Figure 5.3. We observe that the measured BTCs are highly asymmetric with long tails, and it is clear (Figures 5.3 (a) and (c)) that these non-Fickian features are better captured by the PIDE model than the PDE model. The

PDE	PIDE		TPL	
v (cm/min)	v (cm/min)	d_f (cm^2/min)	v (cm/min)	
9.43×10^{-1}	8.25×10^{-1}	20.67	29.27	
d (cm^2/min)	d_{nf} (cm^2/min)	τ (min)	d (cm^2/min)	β
50.32	187.65	383.09	79.08	0.93
RMSE	RMSE		RMSE	
5.23×10^{-2}	1.51×10^{-2}		2.30×10^{-2}	

Table 5.5: Fitting parameters for the models plotted in Figures 5.3 (c) and (d) and the corresponding RMSE values (600 cm).

modeling parameters and the RMSEs are shown in Tables 5.4 and 5.5. The proposed model provided a reduction in the RMSE of 43% at distance 400 cm and of 71% at distance 600 cm. In Figures 5.3 (b) and (d), we compare again the PIDE model with the TPL model. As before, they have a similar performance, but the PIDE model appears to have smaller RMSE values. This is corroborated by other results

not shown here. The same data was used used in [88, 95] to test various transport models including the PDE model. In [88], the TPL model provided the best results among all five models considered.

5.1.4 Scale-Dependent Prediction

An important aspect that we have not explored so far is the prediction capacity of the PIDE model. Our results show that the average velocity is always in good agreement with experiments, suggesting that the mean velocity of the tracer can be correctly predicted. Unfortunately, the other parameters of the model seem to be scale-dependent. For instance, for data set 2, the values of d_{nf} and d_f clearly increase with distance. A possible solution to mitigate this problem is to insert scale-dependent coefficients in the PIDE model, similar to those proposed for the PDE model [115, 124, 164, 170].

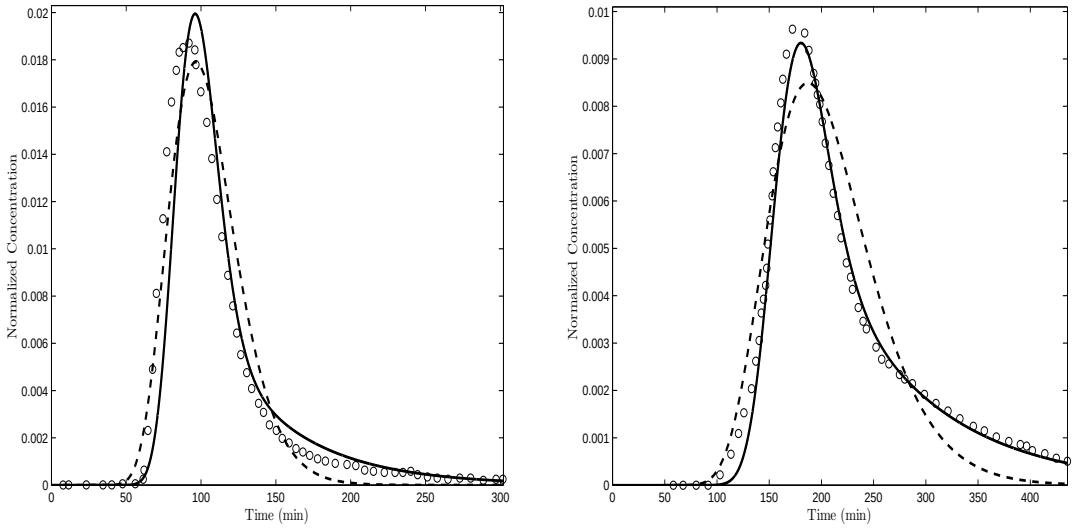

(a) PIDE (solid line) and PDE (dash line). (b) PIDE (solid line) and PDE (dash line).

Figure 5.4: Predicted BTCs for Column 3 in (a) and for Column 2 in (b).

Keeping the discussion in the data set 2, we note that the values of d, d_f, and d_{nf} in the PDE and PIDE models seem to vary linearly with the distance L, while the value of τ seem to vary linearly with time T. Using the data displayed in Tables 5.2 and 5.3, we establish the power-law approximations

$$d_f = 2.14 \times 10^{-3} L^{1.08}, \quad d_{nf} = 9.11 \times 10^{-3} L^{1.04},$$
$$\tau = 1.72 \times 10^{-1} T^{0.90}, \qquad d = 2.06 \times 10^{-3} L^{1.28}.$$

From these relations and the parameters obtained for Column 1, we attempted to predict the BTC for Column 2 and also for another column with a 20 cm length, designated Column 3. As it is shown in Figure 5.4, a good agreement was obtained for the PIDE model. The results presented in [36, 88] suggest that the TPL model is less scale-dependent, but we recall that in the PIDE model, we only have four parameters, as opposed to the TPL model, which has five.

5.2 Numerical Experiments in Two Dimensions

It should be noted that whether and how the previous one-dimensional results can translate to two or three dimensions needs further study. The intent of this section is to illustrate the applicability and computational feasibility of the proposed model to simulate two-dimensional transport problems. On the other hand, this type of equation arises in many problems, and so, the following discussion may also be useful in a different context. We begin with a brief explanation of the numerical procedure used to discretize the model equations. Then, we validate the code by comparing it with analytical solutions for a number of simple problems, and we close with a few realistic examples.

5.2.1 The Numerical Scheme

As we have already discussed, our two-dimensional model for flow and tracer transport in porous media is governed by a PIDE for the concentration

$$\phi\partial_t c + \nabla\cdot(vc) - \nabla\cdot(D_f\nabla c) = \int_0^t K(t-s)\nabla\cdot(D_{nf}\nabla c(s))\,ds + qc^* \tag{5.6}$$

and an elliptic system for the velocity and pressure

$$\nabla\cdot v = q, \tag{5.7}$$

$$v = -\bar{K}\nabla p. \tag{5.8}$$

The system of equations (5.6)-(5.8) is complemented with initial and Dirichlet or Neumann boundary conditions as given by (1.33)-(1.37).

The numerical strategy adopted to discretize this uncoupled problem pays special attention to the flow system (5.7)-(5.8). In fact, the equation (5.6) is usually advection dominated and, therefore, an accurate approximation of v is required. Due to the presence of the full tensor $\bar{K}$ in (5.8) this can be a challenging task, especially when the medium is highly heterogeneous. We address this issue by using MFEMs,

a method that has proved very effective for this kind of problems [7, 10, 27, 73, 114]. In particular, we employed the RT_0 elements [35, 60, 137]. The mixed formulation is natural for this kind of problem, since it approximates both variables p and v simultaneous. This is not the case, e.g., for FEMs, where the variable v is obtained from p by some kind of numerical approximation. The advantages of the RT_0 mixed approach over the traditional piecewise linear FEMs is well documented in [136]. We note that some post-processing techniques can be applied to enhance the finite element solution [118]. One of the keys behind the success of the mixed method is the continuity of the numerical fluxes between two adjacent elements. This ensures the local conservation of mass, a property that is shared with the exact solution of (5.7)-(5.8). Another key property is the discontinuous tangential component of the approximate velocities. This feature is well-suited for this problem since when $\bar{K}$ is discontinuous the tangential component of v is also discontinuous. The relevance of this aspect is discussed in [98]. Noteworthy among alternative methods are the multipoint flux MFEM [3, 161, 162], the mixed method with divergence-free RT_0 elements [48, 143], and mimetic FDMs [34, 113].

Now, we discuss the numerical procedure for the solution of the PIDE (5.6). This equation describes the spatial and temporal development of the concentration. Thus, obtaining an accurate and stable solution is of crucial interest for our purpose. For the approximation in space, a higher-order Godunov FVM is applied to handle the dominant advective term. More precisely, we use the second-order MUSCL scheme described by Barth and Jespersen in [19]. Other suitable alternatives can be found in [21, 37, 97, 134]. This method combines naturally with the RT_0 mixed method that is also used for approximating the dispersion terms. These schemes, called Godunov-mixed methods, have been successfully applied in the simulation of Fickian transport in porous media [7, 27, 53, 54, 121, 127]. At last, we would like to mention that, recently, discontinuous Galerkin methods have gained great popularity in this field [22, 65, 138, 141, 147, 152].

In the time integration, we use a second-order multistep BDF method [51] combined with a numerical quadrature rule for the integral term. This scheme is applied in a natural IMEX fashion where the non-stiff advective term is treated explicitly and the remaining stiff terms are treated implicitly. One attractive aspect of this approach is that the computationally expensive advective term only needs to be evaluated once every time step. The reliability of this kind of IMEX method has been proved for the solution of advection-dominated PDE problems [58, 99, 100, 156].

The proposed scheme is implemented over triangular elements, as they provide the greater geometric flexibility, a crucial aspect in porous media simulation, allied with good stability and convergence properties. Moreover, while not yet available, our implementation can be easily modified to support adaptive mesh refinement procedures. In the following, we describe in more detail the numerical approach presented above.

The Concentration Equation: Time Discretization

In order to simplify the presentation the PIDE (5.6) is discretized first in time. Notice that it would be equivalent to go the other way around, i.e., first discretize in space and then in time. Let Δt be a fixed time step with $t_n = n\Delta t$, for $n = 0, \ldots, N$, and such that $t_N = T$. Denote by c^n the numerical approximation at time level t_n and by $\bar{c}^n$ the linear extrapolation for c^{n+1} defined by $\bar{c}^n = 2c^n - c^{n-1}$. The IMEX method yields the following approximation

$$\frac{\phi}{2\Delta t}\Big(3c^{n+1} - 4c^n + c^{n-1}\Big) + \nabla \cdot (v\bar{c}^n) \\ - \nabla \cdot (D_f \nabla c^{n+1}) = \int_0^{t_{n+1}} K(t_{n+1}, s)\nabla \cdot (D_{nf}\nabla c(s))\, ds,$$

for $n \geq 1$ and where, for simplicity of exposition, we consider no source or sink terms. Applying the composite trapezoidal rule to the integral term, and using the same strategy as outlined at the beginning of Section 3.2, we can obtain the following three-time-level solution scheme

$$\frac{3\tau\phi}{\Delta t^2}c^{n+1} - \frac{2\tau}{\Delta t}\nabla \cdot (D_f \nabla c^{n+1}) - \nabla \cdot (D_{nf}\nabla c^{n+1}) = G^n \quad \text{for } n \geq 2, \tag{5.9}$$

with

$$\Delta t^2 G^n = \tau\phi(4c^n - c^{n-1}) - 2\tau\Delta t\nabla \cdot (v\bar{c}^n + \exp(-\Delta t/\tau)v\bar{c}^{n-1}) \\ + \tau\phi(3c^n - 4c^{n-1} + c^{n-2}) + \Delta t^2\nabla \cdot (D_{nf}\nabla c^n - 2\tau\Delta t D_f \nabla c^n). \tag{5.10}$$

Here we have assumed, again for simplicity of exposition, that $c(0) = 0$.

One of the shortcomings of multistep methods is that they are not self-starting. In this work, the starting value c^1 is computed by the one-step IMEX Euler method combined with the rectangular rule,

$$\frac{\tau\phi}{\Delta t^2}c^1 - \frac{\tau}{\Delta t}\nabla \cdot (D_f \nabla c^1) - \nabla \cdot (D_{nf}\nabla c^1) = -\frac{\tau}{\Delta t}\nabla \cdot (vc^0). \tag{5.11}$$

Ideally, this should be done using a higher-order method or variable step sizes [101, 158]. Note that c^2 can be obtained from the equation

$$\frac{3\tau\phi}{\Delta t^2}c^2 - \frac{2\tau}{\Delta t}\nabla\cdot(D_f\nabla c^2) - \nabla\cdot(D_{nf}\nabla c^2) = \exp(-2\Delta t/\tau)\nabla\cdot(D_{nf}\nabla c^0) + \exp(-\Delta t/\tau)\nabla\cdot(D_{nf}\nabla c^1) + \frac{4\tau\phi}{\Delta t^2}c^1 - \frac{2\tau}{\Delta t}\nabla\cdot(v\bar{c}^1). \tag{5.12}$$

This is nothing more than a direct application of the proposed method, i.e., without using the formulation (5.9)-(5.10).

One major drawback of the method is the stability restriction that limits the time step, since we expect this to be determined by the CFL restriction coming from the explicit treatment of advection. It is given by

$$\Delta t \leq C\frac{1}{3}\frac{\phi T_{min}}{||v||_{L^\infty}}, \tag{5.13}$$

with $C = 5/8$ and where T_{min} represents the minimum ratio between the measure and the perimeter of the triangles in the triangulation [21,102]. A possible solution to mitigate this restrictive condition would be to use variable step sizes in the domain, as done for PDEs in [55]. Also worth mentioning are the characteristic methods, which allow for large time steps and that have shown promising results in the simulation of Fickian transport in porous media [11, 62, 64, 159, 165].

The Concentration Equation: Spatial Discretization

Now we proceed to the discretization in space. Defining, for $n \geq 2$, the variables

$$\tilde{z}^{n+1} = -D_f\nabla c^{n+1} \quad \text{and} \quad z^{n+1} = -D_{nf}\nabla c^{n+1},$$

we rewrite the equation (5.9) in the mixed form

$$\beta c^{n+1} + \alpha\nabla\cdot\tilde{z}^{n+1} + \nabla\cdot z^{n+1} = G^n, \tag{5.14}$$

$$z^{n+1} + D_{nf}\nabla c^{n+1} = 0, \tag{5.15}$$

$$\tilde{z}^{n+1} + D_f\nabla c^{n+1} = 0, \tag{5.16}$$

with $\beta = 3\tau\phi/\Delta t^2$ and $\alpha = 2\tau/\Delta t$. Consider the Sobolev space

$$H(div;\Omega) = \left\{u \in (L^2(\Omega))^2 : \nabla\cdot u \in L^2(\Omega)\right\},$$

with the norm

$$\|u\|^2_{H(div)} = \|u\|^2_{L^2} + \|\nabla\cdot u\|_{L^2},$$

and the subspace

$$H_0(div;\Omega) = \big\{u \in H(div;\Omega) : u \cdot \eta = 0 \text{ on } \partial\Omega_N\big\}.$$

Assuming, for simplicity, homogeneous boundary conditions, the system (5.14)-(5.16) has the mixed variational formulation: find $z^{n+1}, \tilde{z}^{n+1} \in H_0(div;\Omega)$ and $c^{n+1} \in L^2(\Omega)$, such that, for $n \geq 2$,

$$\beta(c^{n+1}, w) + \alpha(\nabla \cdot \tilde{z}^{n+1}, w) + (\nabla \cdot z^{n+1}, w) = (G^n, w), \tag{5.17}$$

$$(D_{nf}^{-1} z^{n+1}, u) - (c^{n+1}, \nabla \cdot u) = 0, \tag{5.18}$$

$$(D_f^{-1} \tilde{z}^{n+1}, u) - (c^{n+1}, \nabla \cdot u) = 0, \tag{5.19}$$

for all $u \in H_0(div;\Omega)$ and $w \in L^2(\Omega)$.

Let $\mathcal{T}_h = \{T_i : i = 1, \ldots, N_T\}$ be an admissible triangulation of the domain Ω and $\mathcal{E}_h = \{E_i : E_i \in \Omega \cup \partial\Omega, i = 1, \ldots, M_E\}$, the set of edges associated with the triangulation. In order to discretize the variational problem (5.17)-(5.19) with respect to the space variables we introduce the elements $RT_0 = W_h \times V_h$. The space $W_h \subset L^2(\Omega)$ is used to approximate the concentration and consists of scalar functions that are constant in each triangle T. For approximating the flux variables, we use the space $V_h \subset H(div;\Omega)$. This means that the flux is represented by piecewise linear functions with continuous normal components across the interior boundaries in $\mathcal{T}_h$. Therefore, the fully-discrete variational formulation for problem (5.17)-(5.19) reads: find $z_h^{n+1}, \tilde{z}^{n+1} \in V_h$ and $c_h^{n+1} \in W_h$, such that, for $n \geq 2$ and for all $u_h \in V_h$ and $w_h \in W_h$,

$$\beta(c_h^{n+1}, w_h) + \alpha(\nabla \cdot \tilde{z}_h^{n+1}, w_h) + (\nabla \cdot z_h^{n+1}, w_h) = (G_h^n, w_h), \tag{5.20}$$

$$(D_{nf}^{-1} z_h^{n+1}, u_h) - (c_h^{n+1}, \nabla \cdot u_h) = 0, \tag{5.21}$$

$$(D_f^{-1} \tilde{z}_h^{n+1}, u_h) - (c_h^{n+1}, \nabla \cdot u_h) = 0. \tag{5.22}$$

Denote by ϕ_m, for $m = 1, \ldots, N_T$, and ψ_j, for $j = 1, \ldots, M_E$, the usual basis functions of the spaces W_h and V_h, respectively [35]. Hence, any function $w_h \in W_h$ can be expressed via the equality

$$w_h(x,y) = \sum_{m=1}^{N_T} w_m \phi_m(x,y) \quad \text{for } (x,y) \in \Omega, \tag{5.23}$$

where w_m is value of w_h at the centroid of each triangle. While any function $u_h \in V_h$ can be written as

$$u_h(x,y) = \sum_{j=1}^{M_E} u_j \psi_j(x,y) \quad \text{for } (x,y) \in \Omega \cup \partial\Omega, \tag{5.24}$$

with u_j being the value of the normal component of the flux at the midpoint of the corresponding edge. Using the representations (5.23) and (5.24) we can transform the variational problem (5.20)-(5.22) into the equivalent linear system

$$\begin{bmatrix} B & 0 & -C \\ 0 & \tilde{B} & -C \\ C^{\mathrm{T}} & \alpha C^{\mathrm{T}} & E \end{bmatrix} \begin{bmatrix} z_h^{n+1} \\ \tilde{z}_h^{n+1} \\ c_h^{n+1} \end{bmatrix} = \begin{bmatrix} 0 \\ 0 \\ b \end{bmatrix} \quad \text{for } n \geq 2, \tag{5.25}$$

where z_h^{n+1}, $\tilde{z}_h^{n+1}$ and c_h^{n+1} are the vectors of unknown coefficients in the basis, with the diagonal matrix

$$[E_{mm}] = \beta |T_m| \quad \text{for } m = 1, \ldots, N_T,$$

the matrices B, $\tilde{B}$, and C defined by

$$[B_{ij}] = \int_{T_m} D_{nf}^{-1} \psi_i \cdot \psi_j \, dxdy \quad \text{for } i, j = 1, \ldots, M_E, \tag{5.26}$$

$$[\tilde{B}_{ij}] = \int_{T_m} D_f^{-1} \psi_i \cdot \psi_j \, dxdy \quad \text{for } i, j = 1, \ldots, M_E, \tag{5.27}$$

$$[C_{im}] = \int_{T_m} \nabla \cdot \psi_i \, dxdy \quad \text{for } i = 1, \ldots, M_E, \tag{5.28}$$

for $m = 1, \ldots, N_T$, and with the vector

$$b_m = \int_{T_m} G^n \, dxdy \quad \text{for } m = 1, \ldots, N_T. \tag{5.29}$$

Proceeding just as above, an analogous linear system can be found from the equations (5.11) and (5.12). We also mention that the calculation of the integrals (5.26)-(5.28), which is not shown here, was obtained using the reference element approach.

To finish the spatial discretization, we must only apply the MUSCL scheme to the advective term

$$F = \int_{T_m} \nabla \cdot (v \bar{c}_m^n) \, dxdy. \tag{5.30}$$

Note that this term is now included in the expression (5.29). For a detailed description of this scheme, we refer to [18, 19]; here we give only the basic steps. In the sequel, we write for brevity c_m instead of $\bar{c}_m^n$.

Applying the divergence theorem to (5.30), we get

$$F = \sum_{j=1}^{3} \int_{E_j} c_m v \cdot \eta_{E_j} \, dS,$$

where E_j is the edge j of the triangle T_m and η_{E_j} is the exterior normal to E_j. Assume now that T_m is an interior triangle, i.e., $T_m \subset \Omega$. Assume also that the triangle T_m is adjacent with the triangles T_p, T_q and T_r as represented in Figure 5.5. Denote by c_{m1} and c_{p1} an approximation of c_m and c_p, respectively, at the midpoint of edge E_1 and define with an analogous meaning the elements c_{q2}, c_{r3}, c_{m2}, and c_{m3}.

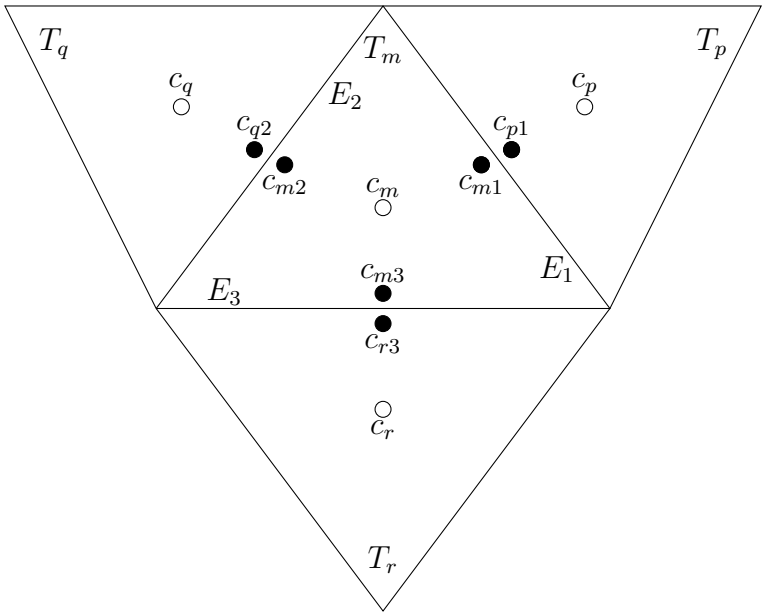

Figure 5.5: The MUSCL scheme and the notation.

Noting that we also restrict v to the space V_h, we can write the used scheme as follows,

$$F \approx \sum_{j=1}^{3} |E_j| f(c_{mj}, c_{nj}) \quad \text{for } n \in \{p, q, r\},$$

with $|E_j|$ the measure of the edge and f the Godunov numerical flux function,

$$f(c_{mj}, c_{nj}) = \begin{cases} c_{mj} & \text{if } v_j > 0, \\ \\ c_{nj} & \text{if } v_j \leq 0. \end{cases}$$

The main question now is how to calculate the approximations c_{mj} and c_{nj}. In the classical first-order upwind scheme, we simply use the values c_m and c_n. This method is very stable; however, it is a well-known fact that is not very accurate and introduces excessive numerical diffusion. The main idea behind the MUSCL technique is to improve the accuracy of the upwind scheme by using higher-order

approximations. Here, we use a second-order linear reconstruction method. With this procedure c_{mj}, for instance, is given by

$$c_{mj} = c_m + \theta_m \nabla c_{T_m}(x_{E_j} - x_{T_m}), \quad \theta_m \in [0,1]. \tag{5.31}$$

where x_{E_j} and x_{T_m} are the middle point of the edge E_j and the centroid of the triangle T_m, respectively, and where ∇c_{T_m} is an approximate gradient of c on the triangle T_m. In this case, we differ from the method proposed by Barth and Jespersen, where the gradient is given by the plane through the three nearby centroids, c_q, c_p, and c_r, in the notation of Figure 5.5. Instead, we use the least-squares technique, which is more robust because it is less sensitive to the triangulation [120]. By θ, we represent the so-called slope limiter. These limiting functions are essential to avoid the introduction of non-physical oscillations during this reconstruction step. Here we implemented the Barth-Jespersen limiter; it is defined by

$$\theta_m = \min(\theta_{mj}) \quad \text{for } j = 1,2,3,$$

with

$$\theta_{mj} = \begin{cases} \min\left(1, \dfrac{c_m^{max} - c_m}{c_{mj}^* - c_m}\right) & \text{if } c_{mj}^* - c_m > 0, \\ \min\left(1, \dfrac{c_m^{min} - c_m}{c_{mj}^* - c_m}\right) & \text{if } c_{mj}^* - c_m < 0, \\ 1 & \text{if } c_{mj}^* - c_m = 0. \end{cases} \tag{5.32}$$

where c_{mj}^* represents the value obtained using the unconstrained version of (5.31), i.e., fixing $\theta_m = 1$, and where $c_m^{max} = \max(c_m, c_p, c_q, c_r)$ and $c_m^{min} = \min(c_m, c_p, c_q, c_r)$. For other options, we refer to [18, 97] and also to [20], where an improved version of (5.32) is presented.

The Flow System: Numerical Discretization

As we mention before, the RT_0 space is also employed in the approximation of the flow system (5.7)-(5.8). In the space variables, this system can be seen as a particular case of (5.14)-(5.16). Considering homogeneous boundary conditions, and proceeding in a similar way as before, one obtains

$$\begin{bmatrix} \hat{B} & -C \\ -C^{\mathrm{T}} & 0 \end{bmatrix} \begin{bmatrix} v_h \\ p_h \end{bmatrix} = \begin{bmatrix} 0 \\ -d \end{bmatrix}, \tag{5.33}$$

where $\hat{B}$ is as defined in (5.26) (or (5.27)) with the permeability tensor $\bar{K}$ in the place of the tensor D_{nf}, and where d is the vector with components

$$d_m = \int_{T_m} q(x,y)\,dxdy \quad \text{for } m = 1,\ldots,N_T.$$

These integrals are evaluated by numerical integration. Next, we briefly discuss the numerical techniques used to solve the linear systems (5.25) and (5.33).

The Linear Systems

First, we turn our attention to the linear system (5.25). To solve this system we use the following decomposition,

$$Ac^{n+1} = b, \quad (A = E + C^{\mathrm{T}}B^{-1}C + \alpha C^{\mathrm{T}}\tilde{B}^{-1}C) \tag{5.34}$$

$$\tilde{B}\tilde{z}^{n+1} = Cc^{n+1}, \tag{5.35}$$

$$Bz^{n+1} = Cc^{n+1}. \tag{5.36}$$

The advantages of this approach are evident; namely, it largely reduces the dimension of the problem, and only symmetric and positive definite matrices are involved in the solution process. Furthermore, the matrices $\tilde{B}$ and B are well-conditioned, in the sense that the spectral condition number is independent of the mesh size when the triangulation is regular [142], and if the entries of the diagonal matrix E are very big, like in our case, we expect the matrix A to be also well-conditioned. For this class of matrices, the conjugate gradient method (CGM) should converge rapidly and is the one adopted. Simple diagonal preconditioning is used in (5.35) and (5.36) to speed up the convergence. One may notice in (5.34) that $\tilde{B}^{-1}$ is required, and $\tilde{B}$ is not easily invertible. Moreover, $\tilde{B}^{-1}$ is not a sparse matrix. However, since the CGM only need to calculate the action of $\tilde{B}^{-1}$, we tackle this problem by solving a system of the form $Br = p$. This is realized using the CGM with diagonal preconditioning and a small stopping tolerance. This same observation holds for B^{-1}.

Now, we discuss the linear system (5.33). The matrix involved in this system is strongly indefinite [35] and it is well-known that iterative methods for indefinite systems are not so efficient as those for problems with positive definite matrices. On the other hand, because of the dimension of real problems, direct solvers are computationally prohibitive. This challenging problem is actually one of the major drawbacks to MFEMs. Many different approaches have been proposed to address this issue. Without being exhaustive, we refer to [8, 9, 30, 33, 73] and also to the survey

article [26], where the focus is on numerical methods for solving this kind of linear system.

Here, we solve the system (5.33) using again a decoupling method and obtaining in this way the following system of equations,

$$Ap = q, \quad (A = C^{\mathrm{T}}\hat{B}^{-1}C) \tag{5.37}$$

$$\hat{B}v = C\bar{p}. \tag{5.38}$$

Now, since $\hat{B}$ holds the properties of B, we can efficiently solve (5.38) using the same strategy adopted for (5.35). As for (5.37), the CGM is again employed. This choice is justified by the fact that A is symmetric and positive definite. Unfortunately, the spectral condition number of A increases quadratically when the triangulation is refined [142]. The matrix A is then very ill-conditioned and so the efficiency of the CGM is strongly dependent on a suitable preconditioning matrix. One option is to use the matrix $M = C^{\mathrm{T}}D_{\hat{B}}^{-1}C$, where $D_{\hat{B}}$ is the main diagonal of $\hat{B}$, a choice that is optimal from a spectral point of view. Identical or similar diagonalization procedures for the approximation of B^{-1} have been suggested in the literature [2, 28, 72]. However, with this approach, we obtain a matrix that is also ill-conditioned; therefore, preconditioning is again of high importance. The CGM with diagonal preconditioning will be used, but the convergence is often very slow, especially when the medium is very heterogeneous. For a comprehensive survey on preconditioning techniques, we refer to [25]. Lastly, it should be noted that decoupled strategies, as the ones presented here, and also the type of decoupling, can decrease the accuracy of the numerical solution [103].

We finish this section with some more observations. In order to avoid the indefinite linear system, MFEMs are usually implemented using the so-called mixed-hybrid method [35]. This formulation reduces to a matrix analogue to $\hat{B}$ that is easy to invert and consequently to a symmetric and positive definite system of equations; but, generally, the dimension of the system increases, the system is still ill-conditioned and the accuracy can deteriorate. In fact, it has been observed that in the presence of an irregular triangulation or a high heterogeneity, this formulation is not as accurate as the one presented here [94].

5.2.2 Code Validation

In this section we present some numerical results to validate the code. First, we test its accuracy using problems with known analytical solutions. All analytical problems

are set on the unit square $\Omega = (0,1)^2$. The tolerance on the relative error for the CGM was taken to be 10^{-15} for the actions of B, $\tilde{B}$, and $\hat{B}$, 10^{-3} for the actions of M, and 10^{-10} elsewhere. The numerical error and the convergence rates were obtained on a sequence of five mesh refinements. The initial mesh, shown in Figure 5.6, was generated by a conformed Delaunay triangulation.

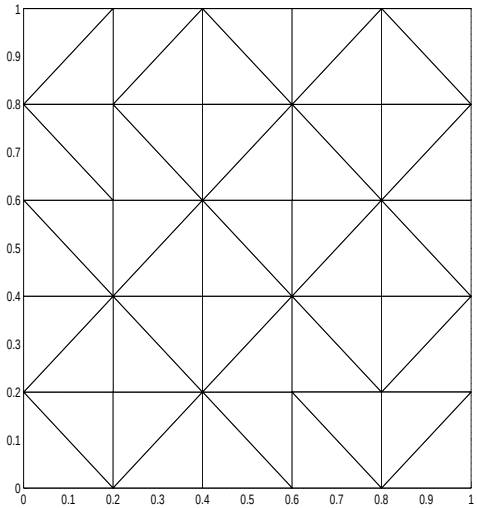

Figure 5.6: Initial Delaunay mesh.

The concentration and pressure errors are measured by the $L^2(\Omega)$ discrete norm

$$\|w - w_h\|_h^2 = \sum_{n=1}^{N_T} |T_n|(w(x_{T_n}) - w_h(x_{T_n}))^2, \tag{5.39}$$

while the flux error is calculated with the $H(div;\Omega)$ discrete norm

$$\|u - u_h\|_{div,h}^2 = \|u - u_h\|_{0,h}^2 + \|u - u_h\|_{1,h}^2$$

where

$$\|u - u_h\|_{0,h}^2 = \sum_{n=1}^{N_T} |T_n| \sum_{i=1}^{3} ((u(x_{E_i}) - u_h(x_{E_i})) \cdot \eta_{E_i})^2, \tag{5.40}$$

$$\|u - u_h\|_{1,h}^2 = \sum_{n=1}^{N_T} \sum_{i=1}^{3} |E_i|((u(x_{E_i}) - u_h(x_{E_i})) \cdot \eta_{E_i})^2, \tag{5.41}$$

with $E_i \in T_n$, for $i = 1, 2, 3$.

With the first two examples, we pretend to analyze the error of the spatial discretization of the PIDE (5.6). In Example 5.1, we present a problem that involves only dispersion, while Example 5.2 is pure advection.

Example 5.1 *In this example we consider* $\tau = 1$, $T = 0.5$ *and the fixed time step* $\Delta t = 5 \times 10^{-4}$. *The parameters for the integro-differential equation (5.6) are*

$$v = 0, \quad D_f = \begin{bmatrix} 0.25 & 0.1 \\ 0.1 & 0.2 \end{bmatrix}, \quad \textit{and} \quad D_{nf} = \begin{bmatrix} 0.5 & 0.1 \\ 0.1 & 0.4 \end{bmatrix}.$$

The remaining undefined terms are such that it has the solution

$$c(x, y, t) = e^{2t} xy(x-1)(y-1)\sin(xy).$$

In Example 5.1, where advection is not present, the convergence rate should be governed by the mixed method. Therefore, we predict a convergence rate equal to two for the scalar variable in the norm (5.39) and a convergence rate equal to one for the flux variable in the norms (5.40) and (5.41). Convergence of, at most, two in the

$\|c - c_h\|_h$	Rate	$\|z - z_h\|_{div,h}$	Rate	$\|\tilde{z} - \tilde{z}_h\|_{div,h}$	Rate
1.2358×10^{-3}	1.6878	3.1111×10^{-2}	1.1254	1.9625×10^{-2}	9.2069
3.8358×10^{-4}	1.8436	1.4260×10^{-2}	1.1326	1.0367×10^{-2}	1.1035
1.0688×10^{-4}	1.9323	6.5040×10^{-3}	1.1193	4.8247×10^{-3}	1.2490
2.8002×10^{-5}	1.9736	2.9939×10^{-3}	1.0778	2.0300×10^{-3}	1.2949
7.1296×10^{-6}	-	1.4183×10^{-3}	-	8.2735×10^{-4}	-

Table 5.6: Discrete norm errors and numerical convergence rates for Example 5.1.

norm (5.40) can also be expected in some situations. This expectations are based on known results for second-order elliptic problems [4, 8, 31, 63, 89, 137]. We observe in Table 5.6 that the numerical convergence rates are in agreement with our predictions.

Example 5.2 *In this example, we consider equation (5.6), with*

$$v = (1, 1) \quad \textit{and} \quad D_f = D_{nf} = q = 0.$$

The initial condition is defined as

$$c_0(x, y) = sin(2\pi x) sin(2\pi y)$$

and periodic boundary conditions are imposed. The solution for this problem is then given by

$$c(x, y, t) = sin(2\pi(x - T)) sin(2\pi(y - T)).$$

The time step is the maximum allowed by the CFL condition (5.13), and the results for $T = 0.1$ *are shown in Table 5.7. For comparison, we also present the results obtained with the upwind method, which we identify with the subscript up.*

In Example 5.2, dispersion is null; therefore, the error is dominated by the MUSCL method. Depending on the problem, we could expect this numerical scheme to have an order of accuracy between one and two. However, it is a well-known fact that second-

$\|c - c_h\|_h$	Rate	$\|c - c_{h,up}\|_h$	Rate
1.2997×10^{-1}	1.0328	1.9471×10^{-1}	0.65960
6.3523×10^{-2}	1.4492	1.2326×10^{-1}	0.77846
2.3264×10^{-2}	1.4861	7.1861×10^{-2}	0.86229
8.3047×10^{-3}	1.5206	3.9529×10^{-2}	0.90935
2.8946×10^{-3}	-	2.1046×10^{-2}	-

Table 5.7: Discrete norm errors and numerical convergence rates for Example 5.2.

order MUSCL schemes like the one proposed here rarely, if ever, achieve second-order convergence rate. Nevertheless, the option for higher-order MUSCL methods over first-order upwind scheme is justified since they present less numerical dispersion, smaller error and higher-order of accuracy [37,97,134]. The results exhibit in Table 5.7 confirm these predictions.

$\|p - p_h\|_h$	Rate	$\|v - v_h\|_{div,h}$	Rate	$\|v - v_h\|_{0,h}$	Rate
4.0019×10^{-3}	1.9822	1.6759×10^{-1}	1.2358	4.7619×10^{-2}	1.7009
1.0129×10^{-3}	1.9915	7.1160×10^{-2}	1.2850	1.4647×10^{-2}	1.7703
2.5473×10^{-4}	1.9966	2.9203×10^{-2}	1.3443	4.2939×10^{-3}	1.8367
6.3832×10^{-5}	1.9989	1.1502×10^{-2}	1.3752	1.2021×10^{-3}	1.8713
1.5971×10^{-5}	-	4.4340×10^{-3}	-	3.2858×10^{-4}	-

Table 5.8: Discrete norm errors and numerical convergence rates for Example 5.3.

In the next example, we test the numerical method for solving the flow problem (5.7)-(5.8). The numerical results are given in Table 5.8, and they are as expected (see the discussion following Example 5.1).

Example 5.3 *In this example we analyze the flow system (5.7)-(5.8) with a full tensor, defined by*

$$\bar{K} = \begin{bmatrix} (x+1)^2 + y & sin(xy) \\ sin(xy) & 2 \end{bmatrix}$$

and where q is such that it admits the solution

$$p(x, y) = x + y + sin(xy)cos(y).$$

The boundary conditions are of Neumann type on $x = 1$ and $y = 1$ and of Dirichlet type on $x = 0$ and $y = 0$.

Next, to illustrate the discussion of the resolution of the linear systems (5.25) and (5.33), respectively, we present in Table 5.9 the maximum number of iterations of the CGM observed in the resolution of Examples 5.1 and 5.3. As predicted, the results show that the numerical strategy is effective except for the matrix M of the flow system. In fact, the CGM performs well with a low number of iterations in the mesh refinement for all the other cases. However, for the matrix M, diagonal preconditioning is clearly inefficient, since the number of iterations is high and approximately doubled when the value of h_{max} is halved. We also observe an increase in the number

Concentration			Flow		
Iter_A	Iter_B	$\text{Iter}_{\tilde{B}}$	Iter_A	$\text{Iter}_{\hat{B}}$	Iter_M
5	19	22	17	18	23
7	21	24	19	20	45
11	21	25	22	21	89
20	21	25	24	23	164
38	20	25	26	23	311

Table 5.9: Number of CGM iterations in Example 5.1 and Example 5.3.

of iterations for the matrix A of the concentration system. The explanation is that, because of the constant α, the ill-conditioning of the matrix $C^{\mathrm{T}}\tilde{B}^{-1}C$ can influence the condition number of A, particularly when the coefficients of D_f are relatively high, and in those situations, preconditioning can also be required. In the interpretation of these results, we should take into account that, in this case, the tensors $\bar{K}$, D_f, and D_{nf} are smooth and the triangulation is regular.

Δt	$\|c - c_h\|_h$	Rate
5.0000×10^{-1}	2.7460×10^{-1}	1.2872
2.5000×10^{-1}	1.1251×10^{-1}	1.6416
1.2500×10^{-1}	3.6062×10^{-2}	1.8555
6.2500×10^{-2}	9.9650×10^{-3}	2.0259
3.1250×10^{-2}	2.4470×10^{-3}	-

Table 5.10: Discrete norm error and estimated order of accuracy in time.

Finally, we examine the rate of convergence in time. In order to do that, we consider the problem of Example 5.1, but with $v = (1, 0.5)$ and $T = 3$. We successively solve this problem, for different time steps, in the last refinement level. The results present in Table 5.10 indicate that the time integration scheme is second-order accurate.

5.2.3 Numerical Simulation

To further assess the performance of our method, we conclude the chapter with some more realistic examples of tracer transport in porous media. A typical porous medium is characterized by rapid changes in the permeability. Therefore, in the following examples, we attempted to replicate this situation. In all of the simulations, the computational domain $\Omega = (0,1)^2$ is discretized using a conforming Delaunay triangulation with 3200 elements, and the time step is taken in accordance with the CFL restriction (5.13). Let us note, that physical units are omitted since we are mostly interested in the numerical behavior of the scheme.

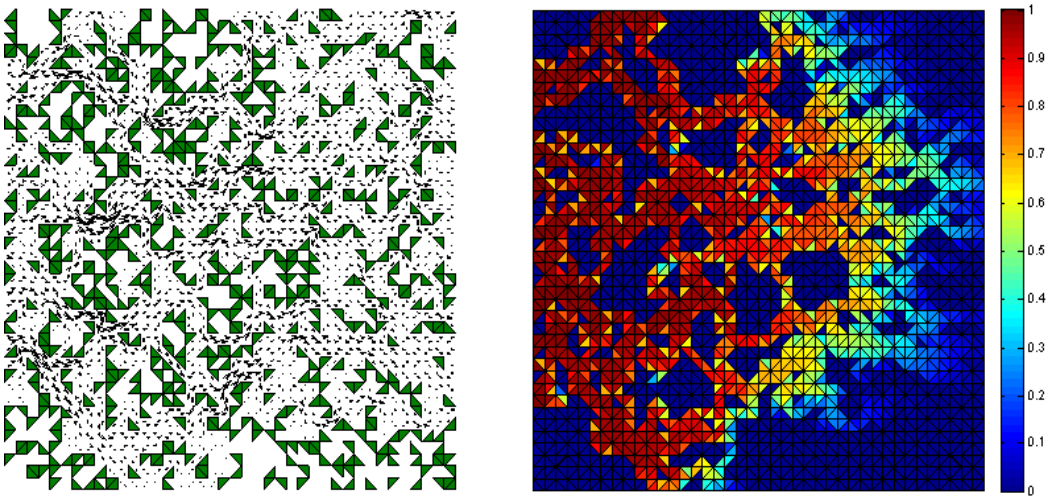

Figure 5.7: Computed velocity (left) and concentration profile (right).

For the first example, we consider the permeability field shown in Figure 5.7. The structure of the heterogeneity consists of two zones that differ in six orders of magnitude. The white zone has a high permeability, $\bar{K} = I$, while the green zone has a very low permeability, $\bar{K} = 10^{-6} I$. No flow conditions are imposed at the horizontal boundaries, while in the vertical boundaries the pressure is set $p = 1$ and $p = 0.1$ at the left and right boundaries, respectively. The resulting velocity field is also shown in Figure 5.7 and it seems to represent very well the heterogeneities pattern.

We also consider a tracer transport process that obeys the PIDE (5.6). We define the tensors $D_f = D_{nf}$ as in (1.21), with the molecular diffusion $d_m = 0$ and the dispersivities $d_l = 5 \times 10^{-4}$ and $d_t = 2 \times 10^{-5}$. We take the porosity $\phi = 0.3$, the parameter $\tau = 10$, and no source or sink terms $q = 0$. We impose zero initial condition for concentration, $c = 1$ on the left boundary, $c = 0$ on the right boundary, and impermeable conditions on the remaining ones. In Figure 5.7, we observe that

the concentration profile is in good agreement with that expected from the proposed permeability field. Note that the low permeability zones are not invaded by the tracer.

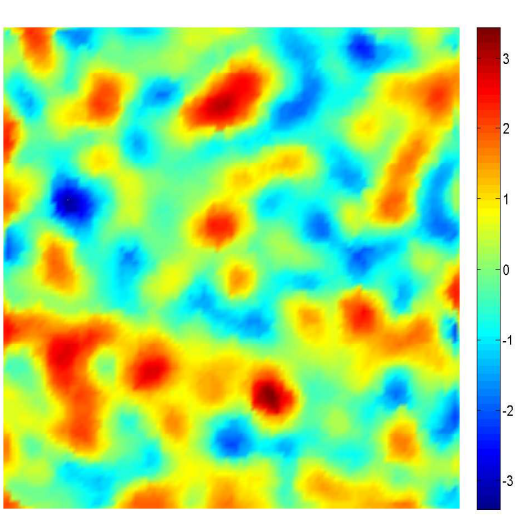

(a) The log-permeability field.

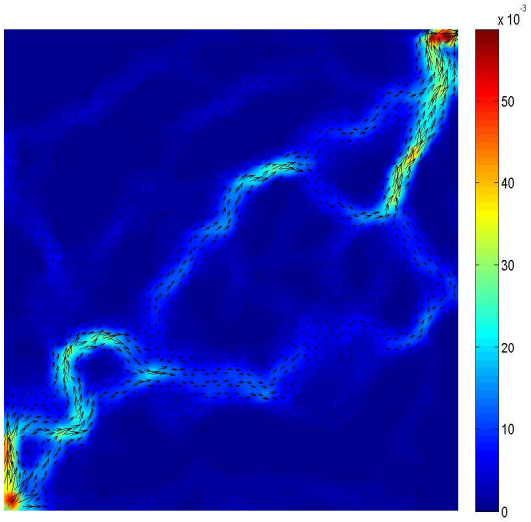

(b) Vectors and Euclidean norm of the velocity field.

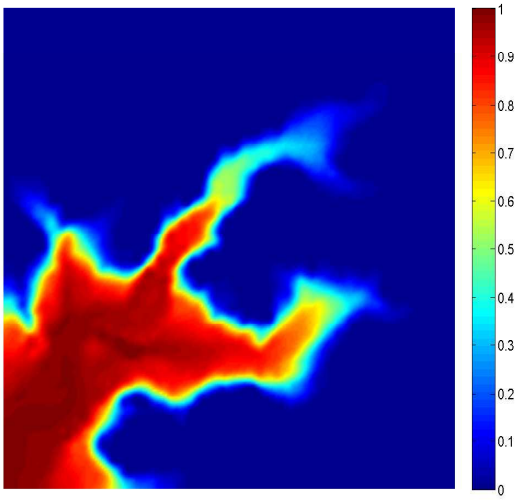

(c) The concentration at $T = 30$.

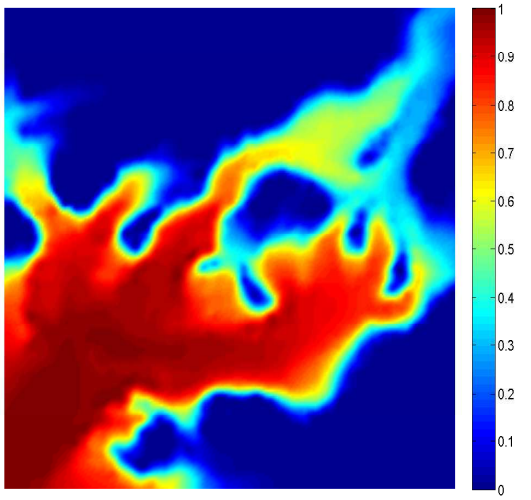

(d) The concentration at $T = 60$.

Figure 5.8: Surf plots obtained by interpolation of the simulation results.

For the final simulation (Figure 5.8), we consider a transport problem with a source and a sink term. The source covers one triangle near the lower-left corner with a rate of $q = 6.4$. The injected tracer concentration c^* is equal to one. The sink also covers one triangle and is located near the upper-right corner with an opposite rate to the source. No flow boundary conditions are assumed both for velocity and concentration. Also, we take $\tau = 50$, $\phi = 0.3$, and $D_f = D_{nf}/10$ defined as in (1.21)

with $d_m = 10^{-6}$, $d_l = 4 \times 10^{-3}$, and $d_t = 2 \times 10^{-3}$. The random permeability field is shown in Figure 5.8 (a), and was generated using a Gaussian distribution. As we can see, there are jumps of about four orders of magnitude throughout the domain. The computed velocity field and the estimated tracer concentration at $T = 30$ and $T = 60$ are also presented in Figure 5.8. Again, the numerical results seem consistent with respect to the permeability field. Finally, with the aim of testing the effect of the parameter τ, we solved the same problem but with $\tau = 0.1$. In Figure 5.9, we display the concentration profiles at $T = 30$ for the two different scenarios. For the

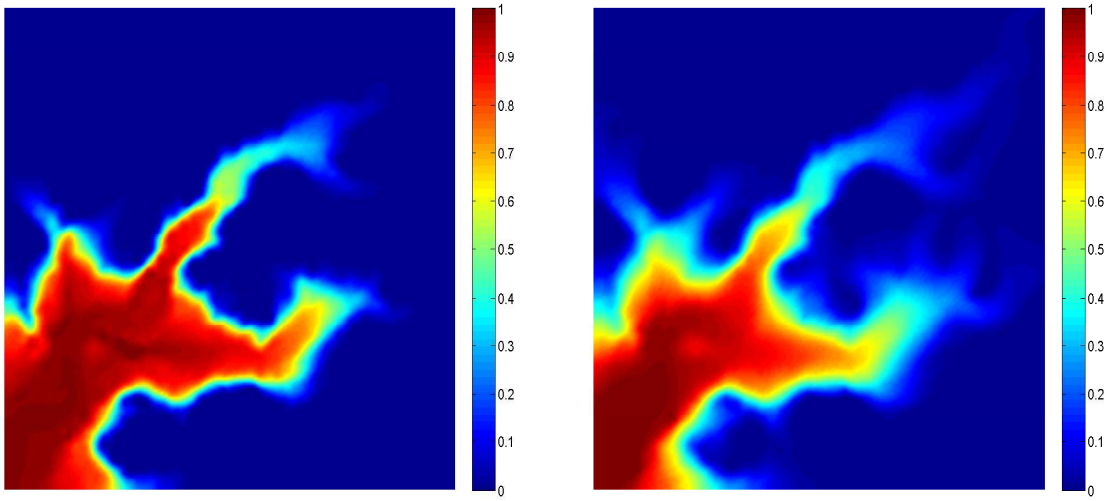

Figure 5.9: Concentration at $T = 30$ for $\tau = 50$ (left) and $\tau = 0.1$ (right).

lower value of τ, the transport seems to be more dispersive, the plume of tracer is less compressed and more widespread.

We remark that the vast majority of the computer code used in this chapter was written by the author in the programming language Matlab.

Chapter 6

Conclusions and Future Work

In this thesis we mainly focus on parabolic partial integro-differential equations of the form

$$\partial_t c + Ac = \int_0^t B(s,t)c(s)\,ds + f \quad \text{in } \Omega \times (0,T], \tag{6.1}$$

where A and $B(s,t)$ represents elliptic operators. Semi-discrete approximations by FEMs were studied and new superconvergence results were established. Real-life applications were also considered with the introduction of a model to describe non-Fickian tracer transport in porous media. Below, we give a brief summary and discussion of our findings and some future work direction.

In Chapter 2, a space discretization of the one-dimensional version of (6.1) by a piecewise linear FEM with numerical quadrature was presented and analyzed. The crucial result of this chapter is the supercloseness of the approximation in the H^1-norm with respect to the usual interpolation operator,

$$\int_0^t \|P_h c(s) - c_h(s)\|_{H^1}^2\,ds \le Ch^4. \tag{6.2}$$

Moreover, this supercloseness estimate naturally leads to the supraconvergence of the equivalent FDM in a discrete H^1-norm,

$$\int_0^t \|c(s) - c_h(s)\|_{1,h}^2\,ds \le Ch^4. \tag{6.3}$$

These results hold with no restrictions of any kind on the mesh.

In Chapter 3, we extended our spatially discrete method to the two-dimensional case, and we were able to establish superconvergence results identical to (6.2)-(6.3). However, in the convergence analysis we introduced a different approach from the one that is usually followed in the literature. Such a strategy enabled us to assume

lower regularity on the continuous solution. For polygonal domains, we provided an error estimate with half-order loss of accuracy due to the interpolation in the oblique boundary. It would be interesting to try to overcome this defect. We note that in the two-dimensional case no mesh restrictions are imposed for the supraconvergence estimate (6.3). In this chapter, we also introduced a fully discrete scheme based on the method of lines approach, combining the FEM with a first-order time integrator. The stability and the convergence of method was also discussed. We point out that the analysis presented here can be followed if we use in the time integration methods of higher-order such as the Crank-Nicolson method. This remark holds if we replace the rectangular rule, considered in the approximation of the time integral, by one of higher-order.

It is important to note that, in these chapters, the results concerning the stability and convergence of the numerical schemes depend on an exponential that can be unbounded in time. This means that the results hold only in bounded time intervals. For particular classes of integro-differential problems, long time stability with respect to the L^2-norm was established, for instance, in [12,153]. Another challenging question is whether the results presented can be generalized to problems involving non-linear or other type of integro-differential equations.

In Chapter 4, we presented preliminary results of ongoing work. There, a simplified version of equation (6.1) was coupled with a elliptic equation. The resulting system, defined by

$$\nabla(a(c)\nabla p) = q_1 \quad \text{in } \Omega \times (0,T], \tag{6.4}$$

and

$$\partial_t c + \nabla(b(c,\nabla p)c) - \nabla(d(c,\nabla p)\nabla c) = q_2 \quad \text{in } \Omega \times (0,T], \tag{6.5}$$

can model, e.g., classical Fickian tracer transport in one-dimensional porous media in the absence of source and sink terms. A piecewise linear FEM with numerical quadrature for the discretization of (6.4)-(6.5) was proposed. In the error analysis that followed, we proved superconvergence results like (6.2)-(6.3) for both variables c and p. These estimates were established for arbitrary non-uniform meshes. The convergence study for a full discretization with an IMEX scheme was also included. Natural future work will be to replace the parabolic PDE in (6.4)-(6.5) by a parabolic PIDE of type (6.1). Some preliminary results on this topic have been published in [83]. Other directions include the replacement of the Dirichlet boundary conditions by Neumann boundary conditions, the inclusion of source and sink terms and the generalization to

other dimensions. Another possible direction for future research would be the study of stabilized FEMs [87]. The goal would be to extended the superconvergence results presented in Chapters 2 through 4 to this class of methods. As it is known, these methods have a wider range of applicability.

In Chapter 5, we proposed and tested an integro-differential model to describe non-Fickian tracer movement. The results presented for the one-dimensional version suggest that this model can overcome the limitations of the traditional Fickian PDE-based model. A numerical scheme for the two-dimensional model, using a Godunov-mixed method in space and a second-order IMEX integrator in time, was also developed. Allowing an efficient implementation as a three-time-level scheme, the numerical procedure avoids a typical problem in the numerical solution of integro-differential models, namely, the storage required by the quadrature formula. To validate the code, we performed some numerical experiments, including comparisons with analytical solutions. We saw that the method is accurate and generates numerical solutions that are stable and physically reasonable. These results prove the computational feasibility of the proposed non-Fickian model. However, the theoretical analysis of this numerical scheme was left open.

In order to address more complex fluid problems, we plan to further modify the model and to improve the performance of the numerical method. Future modifications include reactive and multiphase tracer transport, compressible porous media, efficient preconditioning of the linear systems, adaptive mesh refinement and time stepping, higher-order numerical schemes and three-dimensional simulations. Another enhancement would be provided by a time marching method, for which the time step is not severely restricted by a CFL condition, as in (5.13). However, one of the largest problems regarding the applicability of our model is related to the model parameters. A better understanding of the physical meaning of τ, D_f, and D_{nf}, and the development of an automatic estimation of their values are crucial directions of investigation.

Bibliography

[1] MATLAB Release 2008a, The MathWorks, Inc., Natick, Massachusetts, United States.

[2] J. Aarnes, V. Kippe, and K.-A. Lie. Mixed multiscale finite elements and streamline methods for reservoir simulation of large geomodels. *Advances in Water Resources*, 28:257–271, 2005.

[3] I. Aavatsmark. An introduction to multipoint flux approximations for quadrilateral grids. *Computational Geosciences*, 6:405–432, 2002.

[4] G. Acosta and R. Duran. The maximum angle condition for mixed and nonconforming elements: Application to the Stokes equations. *SIAM Journal on Numerical Analysis*, 37:18–36, 2000.

[5] R. Adams and J. Fournier. *Sobolev spaces, second edition.* Academic Press, 2003.

[6] M. Ainsworth and J. Oden. A posteriori error estimation in finite element analysis. *Computer Methods in Applied Mechanics and Engineering*, 142:1–88, 1997.

[7] T. Arbogast, S. Bryant, C. Dawson, F. Saaf, C. Wang, and M. Wheeler. Computational methods for multiphase flow and reactive transport problems arising in subsurface contaminant remediation. *Journal of Computational and Applied Mathematics*, 74:19–32, 1996.

[8] T. Arbogast, C. Dawson, and P. Keenan. Efficient mixed methods for groundwater flow on triangular or tetrahedral meshes. *Computational Methods in Water Resources X*, 1:3–10, 1994.

[9] T. Arbogast, C. Dawson, P. Keenan, M. Wheeler, and I. Yotov. Enhanced cell-centered finite differences for elliptic equations on general geometry. *SIAM Journal on Scientific Computing*, 19:404–425, 1998.

[10] T. Arbogast and C. Huang. A fully mass and volume conserving implementation of a characteristic method for transport problems. *SIAM Journal on Scientific Computing*, 28:2001–2022, 2006.

[11] T. Arbogast and W. Wang. Stability, monotonicity, maximum and minimum principles, and implementation of the volume corrected characteristic method. *SIAM Journal on Scientific Computing*, 33:1549–1573, 2011.

[12] N. Bakaev, S. Larsson, and V. Thomée. Long time behavior of backward difference type methods for parabolic equations with memory in Banach space. *East-West Journal of Numerical Mathematics*, 6:185–206, 1998.

[13] R. Bank and J. Xu. Asymptotically exact a posteriori error estimators, part I: grids with superconvergence. *SIAM Journal on Numerical Analysis*, 41:2294–2312, 2003.

[14] R. Bank and J. Xu. Asymptotically exact a posteriori error estimators, part II: general unstructured grids. *SIAM Journal on Numerical Analysis*, 41:2313–2332, 2003.

[15] S. Barbeiro, J. Ferreira, and J. Brandts. Superconvergence of piecewise linear semi-discretizations for parabolic equations with nonuniform triangulations. *Journal of Mathematical Fluid Mechanics*, 7:192–214, 2005.

[16] S. Barbeiro, J. Ferreira, and R. Grigorieff. Supraconvergence of a finite difference scheme for solutions in $H^s(0, L)$. *IMA Journal of Numerical Analysis*, 25:797–811, 2005.

[17] S. Barbeiro, J. Ferreira, and L. Pinto. H^1-second order convergent estimates for non-Fickian models. *Applied Numerical Mathematics*, 61:201–215, 2011.

[18] T. Barth. Numerical methods for conservation laws on structured and unstructured meshes. *VKI Lecture Series*, 5, 2003.

[19] T. Barth and D. Jespersen. The design and application of upwind schemes on unstructured meshes. *AIAA Report 89-0366*, 1989.

[20] T. Barth and M. Larson. A posteriori error estimates for higher order Godunov finite volume methods on unstructured meshes. *NASA Technical Report NAS-02-001*, 2002.

[21] T. Barth and M. Ohlberger. Finite volume methods: foundation and analysis. *Encyclopedia of Computational Mechanics*, 1:439–474, 2004.

[22] P. Bastian. Higher order discontinuous Galerkin methods for flow and transport in porous media. In *Challenges in Scientific Computing*, 2002.

[23] J. Bear. *Hydraulics of groundwater*. McGraw-Hill, 1979.

[24] N. Bellomo, B. Firmani, and L. Guerri. Bifurcation analysis for a nonlinear system of integro-differential equations modelling tumor-immune cells competition. *Applied Mathematical Letters*, 12:39–44, 1999.

[25] M. Benzi. Preconditioning techniques for large linear systems: a survey. *Journal of Computational Physics*, 182:418–477, 2002.

[26] M. Benzi, G. Golub, and J. Liesen. Numerical solution of saddle point problems. *Acta Numerica*, pages 1–137, 2005.

[27] L. Bergamaschi, S. Mantica, and G. Manzini. A mixed finite element–finite volume formulation of the black-oil model. *SIAM Journal on Scientific Computing*, 20:970–997, 1998.

[28] L. Bergamaschi, S. Mantica, and F. Saleri. Mixed finite element approximation of Darcy's law in porous media. *Technical Report CRS4-AppMath-94-17, CRS4*, 1994.

[29] B. Berkowitz, A. Cortis, M. Dentz, and H. Scher. Modeling non-Fickian transport in geological formations as a continuous time random walk. *Reviews of Geophysics*, 44:1–49, 2006.

[30] J. Bramble, J. Pasciak, and A. Vassilev. Analysis of the inexact Uzawa algorithm for saddle point problems. *SIAM Journal on Numerical Analysis*, 34:1072–1092, 1997.

[31] J. Brandts. Superconvergence and a posteriori error estimation for triangular mixed finite elements. *Numerische Mathematik*, 68:311–324, 1994.

[32] J. Brandts and M. Křížek. Superconvergence of tetrahedral quadratic finite elements. *Journal of Computational Mathematics*, 23:27–36, 2005.

[33] S. Brenner. A multigrid algorithm for the lowest-order Raviart-Thomas mixed triangular finite element method. *SIAM Journal on Numerical Analysis*, 29:647–678, 1992.

[34] F. Brezzi, A. Buffa, and K. Lipnikov. Mimetic finite differences for elliptic problems. *ESAIM: Mathematical Modelling and Numerical Analysis*, 43:277–295, 2009.

[35] F. Brezzi and M. Fortin. *Mixed and hybrid finite element methods*. Springer, 1991.

[36] M. Bromly and C. Hinz. Non-fickian transport in homogeneous unsaturated repacked sand. *Water Resources Research*, 40:W07402, 2004.

[37] T. Buffard and S. Clain. Monoslope and multislope MUSCL methods for unstructured meshes. *Journal of Computational Physics*, 229:3745–3776, 2010.

[38] J. Cannon and Y. Lin. Non-classical H^1 projection and Galerkin methods for non-linear parabolic integro-differential equations. *Calcolo*, 25:187–201, 1988.

[39] J. Cannon and Y. Lin. A priori L^2 error estimates for finite element methods for nonlinear diffusion equations with memory. *SIAM Journal on Numerical Analysis*, 27:595–607, 1990.

[40] C. Cattaneo. Sulla condizione del calore. *Atti del Seminario Matematico e Fisico della Università di Modena*, 3:83–101, 1948.

[41] P. Chatzipantelidis, R. Lazarov, and V. Thomée. Error estimates for a finite volume element method for parabolic equations in convex polygonal domains. *Numerical Methods for Partial Differential Equations*, 20:650–674, 2004.

[42] P. Chatzipantelidis, R. Lazarov, V. Thomée, and L. Wahlbin. Parabolic finite element equations in nonconvex polygonal domains. *Numerical Methods for Partial Differential Equations*, 25:507–525, 2009.

[43] H. Chen, R. Ewing, and R. Lazarov. Superconvergence of mixed finite element methods for parabolic problems with nonsmooth initial data. *Numerische Mathematik*, 78:495–521, 1998.

[44] L. Chen. Superconvergence of tetrahedral linear finite elements. *International Jounal of Numerical Analysis and Modeling*, 3:273–282, 2006.

[45] Z. Chen and R. Ewing. Mathematical analysis for reservoir models. *SIAM Journal on Mathematical Analysis*, 30:431–453, 1999.

[46] C. Chuanmiao and S. Tsimin. *Finite element methods for integrodifferential equations*. World Scientific Publishing, 1998.

[47] P. Ciarlet. *The finite element method for elliptic problems*. North-Holland Publishing Company, 1978.

[48] K. Cliffea, I. Grahamb, R. Scheichlb, and L. Stalsc. Parallel computation of flow in heterogeneous media modelled by mixed finite elements. *Journal of Computational Physics*, 164:258–282, 2000.

[49] A. Cortis and B. Berkowitz. Anomalous transport in "classical" soil and sand columns. *Soil Science Society of America Journal*, 68:1539–1548, 2004.

[50] A. Cortis and B. Berkowitz. Computing "anomalous" contaminant transport in porous media: the CTRW MATLAB toolbox. *Ground Water*, 43:947–950, 2005.

[51] M. Crouzeix. Une méthode multipas implicite-explicite pour l'approximation des équations d'évolution paraboliques. *Numerische Mathematik*, 35:257–276, 1980.

[52] J. Cushman and T. Ginn. Nonlocal dispersion in media with continuously evolving scales of heterogeneity. *Transport in Porous Media*, 13:123–138, 1993.

[53] C. Dawson. Godunov mixed methods for immiscible displacement. *International Journal for Numerical Methods in Fluids*, 11:835–847, 1990.

[54] C. Dawson. Godunov-mixed methods for advection-diffusion equations in multidimensions. *SIAM Journal on Numerical Analysis*, 30:1345–1332, 1993.

[55] C. Dawson. High resolution upwind-mixed finite element methods for advection diffusion equations with variable time-stepping. *Numerical Methods for Partial Differential Equations*, 11:525–538, 1995.

[56] M. Dentz, A. Cortis, H. Scher, and B. Berkowitz. Time behavior of solute transport in heterogeneous media: transition from anomalous to normal transport. *Advances in Water Resources*, 27:155–173, 2004.

[57] M. Dentz and D. Tartakovsky. Delay mechanisms of non-Fickian transport in heterogeneous media. *Geophysical Research Letters*, 33:L16406, 2006.

[58] V. Dolejší and M. Vlasák. Analysis of a BDF-DGFE scheme for nonlinear convection-diffusion problems. *Numerische Mathematik*, 110:405–447, 2008.

[59] J. Douglas. Superconvergence in the pressure in the simulation of miscible displacement. *SIAM Journal on Numerical Analysis*, 22:962–969, 1985.

[60] J. Douglas, R. Ewing, and M. Wheeler. The approximation of the pressure by a mixed method in the simulation of miscible displacement. *RAIRO - Analyse numérique*, 17:17–33, 1983.

[61] J. Douglas and B. Jones. Numerical methods for integro-differential equations of parabolic and hyperbolic types. *Numerische Mathematik*, 4:96–102, 1962.

[62] J. Douglas, F. Pereira, and L. Yeh. A locally conservative Eulerian-Lagrangian numerical method and its application to nonlinear transport in porous media. *Computational Geosciences*, 5:1–40, 2000.

[63] J. Douglas and J. Roberts. Global estimates for mixed methods for second order elliptic equations. *Mathematics of Computation*, 44:39–52, 1985.

[64] J. Douglas and T. Russell. Numerical methods for convection-dominated diffusion problems based on combining the method of characteristics with finite element or finite difference procedures. *SIAM Journal on Numerical Analysis*, 19:871–885, 1982.

[65] C.-P. El-Soueidy, A. Younes, and P. Ackerer. Solving the advection-diffusion equation on unstructured meshes with discontinuous/mixed finite elements and a local time stepping procedure. *International Journal for Numerical Methods in Engineering*, 79:1068–1093, 2009.

[66] L. Evans. *Partial differential equations*. American Mathematical Society, 1998.

[67] R. Ewing. *The mathematics of reservoir simulation*. SIAM, 1984.

[68] R. Ewing. Upscaling issues in parameter estimation of models for flow in porous media. In *Proceedings of Inverse Problems, Control, and Shape Optimization*, 1998.

[69] R. Ewing and R. Lazarov. Superconvergence of the mixed finite element approximations of parabolic problems using rectangular finite elements. *East-West Journal of Numerical Mathematics*, 1:199–212, 1993.

[70] R. Ewing, R. Lazarov, and Y. Lin. Finite volume element approximations of nonlocal in time one-dimensional flows in porous media. *Computing*, 64:157–182, 2000.

[71] R. Ewing, R. Lazarov, and Y. Lin. Finite volume element approximations of nonlocal reactive flows in porous media. *Numerical Methods for Partial Differential Equations*, 16:285–311, 2000.

[72] R. Ewing, R. Lazarov, P. Lu, and P. Vassilevski. Preconditioning indefinite systems arising from mixed finite element discretization of second-order elliptic problems. *Lecture Notes in Mathematics*, 1457:28–43, 1990.

[73] R. Ewing, R. Lazarov, J. Pasciak, and A. Vassilev. Mathematical modeling, numerical techniques, and computer simulation of flows and transport in porous media. In *Proceedings of Computational Techniques and Applications*, 1995.

[74] R. Ewing, T. Lin, and Y. Lin. On the accuracy of the finite volume element method based on piecewise linear polynomials. *SIAM Journal on Numerical Analysis*, 39:1865–1888, 2002.

[75] R. Ewing, Y. Lin, T. Sun, J. Wang, and S. Zhang. Sharp L^2-error estimates and superconvergence of mixed finite element methods for non-Fickian flows in porous media. *SIAM Journal on Numerical Analysis*, 40:1538–1560, 2002.

[76] R. Ewing, Y. Lin, and J. Wang. A numerical approximation of nonFickian flows with mixing length growth in porous media. *Acta Mathematica Universitatis Comenianae*, LXX:75–84, 2001.

[77] R. Ewing, Y. Lin, J. Wang, and S. Zhang. L^∞-error estimates and superconvergence in maximum norm of mixed finite element methods for nonfickian flows in porous media. *International Jounal of Numerical Analysis and Modeling*, 2:301–328, 2005.

[78] R. Ewing, M. Liu, and J. Wang. A new superconvergence for mixed finite element approximations. *SIAM Journal on Numerical Analysis*, 40:2133–2150, 2003.

[79] R. Ewing, T. Russell, and M. Wheeler. Convergence analysis of an approximation of miscible displacement in porous media by mixed finite elements and a modified method of characteristics. *Computer Methods in Applied Mechanics and Engineering*, 47:73–92, 1984.

[80] R. Ewing, J. Shen, and J. Wang. Application of superconvergence to problems in the simulation of miscible displacement. *Computer Methods in Applied Mechanics and Engineering*, 89:73–84, 1991.

[81] R. Ewing and M. Wheeler. Galerkin method for miscible displacement problems in porous media. *SIAM Journal on Numerical Analysis*, 17:351–365, 1980.

[82] J. Ferreira and R. Grigorieff. Supraconvergence and supercloseness of a scheme for elliptic equations on nonuniform grids. *Numerical Functional Analysis and Optimization*, 27:539–564, 2006.

[83] J. Ferreira and L. Pinto. A non-Fickian single phase flow model. In *Proceedings of Computational and Mathematical Methods in Science and Engineering*, 2011.

[84] J. Ferreira and L. Pinto. An unexpected convergence behaviour in diffusion phenomena in porous media. In *Proceedings of Computational and Mathematical Methods in Science and Engineering*, 2012.

[85] J. Ferreira and L. Pinto. Supraconvergence and supercloseness in quasilinear coupled problems. *Journal of Computational and Applied Mathematics*, 252:120–131, 2013.

[86] J. Ferreira, L. Pinto, and G. Romanazzi. Supraconvergence and supercloseness in Volterra equations. *Applied Numerical Mathematics*, 62:1718–1739, 2012.

[87] L. Franca, G. Hauke, and A. Masud. Revisiting stabilized finite element methods for the advective-diffusive equation. *Computer Methods in Applied Mechanics and Engineering*, 195:1560–1572, 2006.

[88] G. Gao, H. Zhan, S. Feng, G. Huang, and X. Mao. Comparison of alternative models for simulating anomalous solute transport in a large heterogeneous soil column. *Journal of Hydrology*, 377:391–404, 2009.

[89] L. Gastaldi and R. Nochetto. Optimal L^∞-error estimates for nonconforming and mixed finite element methods of lowest order. *Numerische Mathematik*, 50:587–611, 1987.

[90] L. Gelhar, C. Welty, and K. Rehfeldt. A critical review of data on field-scale dispersion in aquifers. *Water Resources Research*, 28:1955–1974, 1992.

[91] W. Hackbusch. *Elliptic differential equations: theory and numerical treatment.* Springer, 2003.

[92] R. Haggerty and S. Gorelick. Multiple-rate mass transfer for modeling diffusion and surface reactions in media with pore-scale heterogeneity. *Water Resources Research*, 31:2383–2400, 1995.

[93] S. Hassanizadeh. On the transient non-Fickian dispersion theory. *Transport in Porous Media*, 23:107–124, 1996.

[94] H. Hoteit, J. Erhel, R. Mosé, B. Philippe, and P. Ackerer. Numerical reliability for mixed methods applied to flow problems in porous media. *Computational Geosciences*, 6:161–194, 2002.

[95] G. Huang, Q. Huang, and H. Zhan. Evidence of one-dimensional scale-dependent fractional advection-dispersion. *Journal of Contaminant Hydrology*, 85:53–71, 2006.

[96] K. Huang, N. Toride, and M. van Genuchten. Experimental investigation of solute transport in large, homogeneous and heterogeneous, saturated soil columns. *Transport in Porous Media*, 18:283–302, 1995.

[97] M. Hubbard. Multidimensional slope limiters for MUSCL-type finite volume schemes on unstructured grids. *Journal of Computational Physics*, 155:54–74, 1999.

[98] T. Hughes, A. Masud, and J. Wan. A stabilized mixed discontinuous Galerkin method for Darcy flow. *Computer Methods in Applied Mechanics and Engineering*, 195:3347–3381, 2006.

[99] W. Hundsdorfer. Partially implicit BDF2 blends for convection dominated flows. *SIAM Journal on Numerical Analysis*, 38:1763–1783, 2001.

[100] W. Hundsdorfer and J. Jaffré. Implicit-explicit time stepping with spatial discontinuous finite elements. *Applied Numerical Mathematics*, 45:231–254, 2003.

[101] W. Hundsdorfer and S. Ruuth. IMEX extensions of linear multistep methods with general monotonicity and boundedness properties. *Journal of Computational Physics*, 225:2016–2042, 2007.

[102] W. Hundsdorfer, S. Ruuth, and R. Spiteri. Monotonicity-preserving linear multistep methods. *SIAM Journal on Numerical Analysis*, 41:605–623, 2003.

[103] P. Jiránek and M. Rozložník. Maximum attainable accuracy of inexact saddle point solvers. *SIAM Journal on Matrix Analysis and Applications*, 29:1279–1321, 2008.

[104] C. Johnson and V. Thomée. Error estimates for some mixed finite element methods for parabolic type problems. *RAIRO - Analyse numérique*, 15:41–78, 1981.

[105] D. Joseph and L. Preziosi. Heat waves. *Reviews of Modern Physics*, 61:41–73, 1989.

[106] A. Kreft and A. Zuber. On the physical meaning of the dispersion equation and its solutions for different initial and boundary conditions. *Chemical Engineering Science*, 33:1471–1480, 1978.

[107] H.-O. Kreiss, T. Manteuffel, B. Swartz, B. Wendroff, and A. White. Supra-convergent schemes on irregular grids. *Mathematics of Computation*, 47:537–554, 1986.

[108] M. Křížek, P. Neittanmäki, and R. Sternberg, editors. *Finite element methods: superconvergence, post-processing and a posteriori estimates*. Marcel Dekker, 1998.

[109] M. Levy and B. Berkowitz. Measurement and analysis of non-Fickian dispersion in heterogeneous porous media. *Journal of Contaminant Hydrology*, 64:203–206, 2003.

[110] Q. Lin and S. Zhang. An immediate analysis for global superconvergence for integrodifferential equations. *Applications of Mathematics*, 42:1–21, 1997.

[111] Y. Lin. Semi-discrete finite element approximations for linear parabolic integro-differential equations with integrable kernels. *Journal of Integral Equations and Applications*, 10:51–83, 1998.

[112] Y. Lin, V. Thomée, and L. Wahlbin. Ritz-Volterra projections to finite element spaces and applications to integro-differential and related equations. *SIAM Journal on Numerical Analysis*, 28:1047–1070, 1991.

[113] K. Lipnikov, M. Shashkov, and I. Yotov. Local flux mimetic finite difference methods. *Numerische Mathematik*, 112:115–152, 2009.

[114] J. Liu, L. Mu, and X. Ye. A comparative study of locally conservative numerical methods for Darcy's flows. *Procedia Computer Science*, 4:974–983, 2011.

[115] J. Logan. Solute transport in porous media with scale-dependent dispersion and periodic boundary conditions. *Journal of Hydrology*, 184:261–276, 1996.

[116] A. Lunardi and E. Sinestrati. Fully nonlinear integrodifferential equations in general Banach space. *Mathematische Zeitschrift*, 190:225–248, 1985.

[117] S. Malta and A. Loula. Numerical analysis of finite element methods for miscible displacements in porous media. *Numerical Methods for Partial Differential Equations*, 14:519–548, 1998.

[118] S. Malta, A. Loula, and E. Garcia. Numerical analysis of stabilized finite element method for tracer injection simulations. *Computer Methods in Applied Mechanics and Engineering*, 187:119–136, 2000.

[119] A.-M. Matache, C. Schwab, and T. Wihler. Fast numerical solution of parabolic integrodifferential equations with applications in finance. *SIAM Journal on Scientific Computing*, 27:369–393, 2005.

[120] D. Mavriplis. Revisiting the least-squares procedure for gradient reconstruction on unstructured meshes. *NASA/CR*, 212683, 2003.

[121] A. Mazzia and M. Putti. High order Godunov mixed methods on tetrahedral meshes for density driven flow simulations in porous media. *Journal of Computational Physics*, 208:154–174, 2005.

[122] W. McLean, I. Sloan, and V. Thomée. Time discretization via Laplace transformation of an integro-differential equation of parabolic type. *IMA Journal of Numerical Analysis*, 24:439–463, 2004.

[123] M. Meerschaert, D. Benson, and B. Bäumer. Multidimensional advection and fractional dispersion. *Physical Review E - Statistical Physics, Plasmas, Fluids, and Related Interdisciplinary Topics*, 59:5026–5028, 1999.

[124] S. Mishra and J. Parker. Analysis of solute transport with a hyperbolic scale-dependent dispersion model. *Hydrological Processes*, 4:45–57, 1990.

[125] S. Neuman and D. Tartakovsky. Perspective on theories of non-Fickian transport in heterogeneous media. *Advances in Water Resources*, 32:670–680, 2009.

[126] L. Oganesjan and L. Rukhovets. Study of the rate of convergence of variational difference schemes for second-order elliptic equations in a two-dimensional field with a smooth boundary. *USSR Computational Mathematics and Mathematical Physics*, 9:158–183, 1969.

[127] M. Ohlberger. Mixed finite element-finite volume methods for two phase flow in porous media. *East-West Journal of Numerical Mathematics*, 5:183–210, 1999.

[128] A. Pani. An H^1-Galerkin mixed finite element method for parabolic partial differential equations. *SIAM Journal on Numerical Analysis*, 35:712–727, 1998.

[129] A. Pani and G. Fairweather. H^1-Galerkin mixed finite element methods for parabolic partial integro-differential equations. *IMA Journal of Numerical Analysis*, 22:231–252, 2002.

[130] A. Pani, G. Fairweather, and I. Fernandes. ADI orthogonal spline collocation methods for parabolic partial integro-differential equations. *IMA Journal of Numerical Analysis*, 30:248–276, 2010.

[131] A. Pani and E. Peterson. Finite element methods with numerical quadrature for parabolic integrodifferential equations. *SIAM Journal on Numerical Analysis*, 33:1084–1105, 1996.

[132] A. Pani and R. Sinha. Finite element approximation with quadrature to a time dependent parabolic integro-differential equation with nonsmooth initial data. *Journal of Integral Equations and Applications*, 13:35–72, 2001.

[133] A. Pani, V. Thomée, and L. Wahlbin. Numerical methods for hyperbolic and parabolic integro-differential equations. *Journal of Integral Equations and Applications*, 4:533–584, 1992.

[134] J. Park, S.-H. Yoon, and C. Kim. Multi-dimensional limiting process for hyperbolic conservation laws on unstructured grids. *Journal of Computational Physics*, 229:788–812, 2010.

[135] J. Parker and M. van Genuchten. Flux-averaged and volume-averaged concentrations in continuum approaches to solute transport. *Water Resources Research*, 20:866–872, 1984.

[136] M. Putti and F. Sartoretto. Linear Galerkin vs mixed finite element 2D flow fields. *International Journal for Numerical Methods in Fluids*, 60:1011–1031, 2009.

[137] P. Raviart and J. Thomas. A mixed finite element method for 2-nd order elliptic problems. *Mathematical Aspects of Finite Element Methods, Lecture Notes in Mathematics*, 606:292–315, 1977.

[138] B. Rivière. *Discontinuous Galerkin methods for solving elliptic and parabolic equations: theory and implementation*. SIAM, 2008.

[139] B. Rivière and S. Shaw. Discontinuous Galerkin finite element approximation of nonlinear non-Fickian diffusion in viscoelastic polymers. *SIAM Journal on Numerical Analysis*, 44:2650–2670, 2006.

[140] B. Rivière and S. Shaw. Discontinuous Galerkin finite element approximation of nonlinear non-Fickian diffusion in viscoelastic polymers. *SIAM Journal on Numerical Analysis*, 44:2650–2670, 2007.

[141] B. Rivière and M. Wheeler. Discontinuous Galerkin methods for flow and transport problems in porous media. *Communications in Numerical Methods in Engineering*, 18:63–68, 2002.

[142] R. Scheichl. *Iterative solution of saddle point problems using divergence-free finite elements with applications to groundwater flow*. PhD thesis, University of Bath, 2000.

[143] R. Scheichl. Decoupling three-dimensional mixed problems using divergence-free finite elements. *SIAM Journal on Scientific Computing*, 23:1752–1776, 2002.

[144] A. Scheidegger. An evaluation of the accuracy of the diffusivity equation for describing miscible displacement in porous media. In *Proceedings of Theory of Fluid Flow in Porous Media*, 1959.

[145] R. Schwartz, K. McInnes, A. Juo, and L. Wilding. Boundary effects on solute transport in finite soil columns. *Water Resources*, 35:671–681, 1999.

[146] M. Shafto, M. Conroy, R. Doyle, E. Glaessgen, C. Kemp, J. LeMoigne, and L. Wang. Modeling, simulation, information technology and processing. *NASA, Space Technology Roadmaps*, 2010.

[147] P. Siegel, R. Mosé, P. Ackerer, and J. Jaffre. Solution of the advection-diffusion equation using a combination of discontinuous and mixed finite elements. *International Journal for Numerical Methods in Fluids*, 24:595–613, 1997.

[148] R. Sinha, R. Ewing, and R. Lazarov. Some new error estimates of a semidiscrete finite volume element method for a parabolic integro-differential equation with nonsmooth initial data. *SIAM Journal on Numerical Analysis*, 43:2320–2344, 2006.

[149] I. Sloan and V. Thomée. Time discretization of an integro-differential equation of parabolic type. *SIAM Journal on Numerical Analysis*, 23:1052–1061, 1986.

[150] S. Sternberg, J. Cushman, and R. Greenkorn. Laboratory observation of nonlocal dispersion. *Transport in Porous Media*, 23:135–51, 1996.

[151] S. Sun, B. Rivière, and M. Wheeler. A combined mixed finite element and discontinuous Galerkin method for miscible displacement problems in porous media. In *Recent Progress in Computational and Applied PDEs*, 2001.

[152] S. Sun and M. Wheeler. A dynamic, adaptive, locally conservative, and nonconforming solution strategy for transport phenomena in chemical engineering. *Chemical Engineering Communications*, 193:1527–1545, 2006.

[153] V. Thomé and L. Wahlbin. Long-time numerical solution of a parabolic equation with memory. *Mathematics of Computation*, 62:477–496, 1994.

[154] V. Thomée and N.-Y. Zhang. Error estimates for semidiscrete finite element methods for parabolic integro-differential equations. *Mathematics of Computation*, 53:121–139, 1989.

[155] A. Tompson. On a new functional form for the dispersive flux in porous media. *Water Resources Research*, 24:1939–1947, 1988.

[156] J. Verwer, W. Hundsdorfer, and J. Blom. Numerical time integration for air pollution models. *Modelling, Analysis and Simulation*, R9825, 1998.

[157] L. Wahlbin. *Superconvergence in Galerkin finite element methods.* Springer, 1995.

[158] D. Wang and S. Ruuth. Variable step-size implicit-explicit linear multistep methods for time-dependent partial differential equations. *Journal of Computational Mathematics*, 26:838–855, 2008.

[159] H. Wang, D. Liang, R. Ewing, S. Lyons, and G. Qin. An improved numerical simulator for different types of flows in porous media. *Numerical Methods for Partial Differential Equations*, 19:343–362, 2003.

[160] M. Wheeler. A priori L_2 error estimates for Galerkin approximations to parabolic partial differential equations. *SIAM Journal on Numerical Analysis*, 10:723–759, 1973.

[161] M. Wheeler, G. Xue, and I. Yotov. A multipoint flux mixed finite element method on distorted quadrilaterals and hexahedra. *Numerische Mathematik*, 121:165–204, 2012.

[162] M. Wheeler and I. Yotov. A multipoint flux mixed finite element method. *SIAM Journal on Numerical Analysis*, 44:2082–2106, 2006.

[163] E. Yanik and G. Fairweather. Finite element methods for parabolic and hyperbolic partial integro-differential equations. *Nonlinear Analysis*, 12:785–809, 1988.

[164] S. Yates. An analytical solution for one-dimensional transport in porous media with an exponential dispersion function. *Water Resources Research*, 28:2149–2154, 1992.

[165] A. Younes and P. Ackerer. Solving the advection-diffusion equation with the eulerian-lagrangian localized adjoint method on unstructured meshes and non uniform time stepping. *Journal of Computational Physics*, 208:384–402, 2005.

[166] C. Zhang and S. Vandewalle. Stability analysis of Runge-Kutta methods for nonlinear Volterra delay-integro-differential equations. *IMA Journal of Numerical Analysis*, 24:193–214, 2004.

[167] C. Zhang and S. Vandewalle. Stability analysis of Volterra delay-integro-differential equations and their backward differentiation time discretization. *Journal of Computational and Applied Mathematics*, 164-165:797–814, 2004.

[168] C. Zhang and S. Vandewalle. General linear methods for Volterra integro-differential equations with memory. *SIAM Journal on Scientific Computing*, 27:2010–2031, 2006.

[169] N. Zhang. On fully discrete Galerkin approximations for partial integro-differential equations of parabolic type. *Mathematics of Computation*, 60:133–166, 1993.

[170] S. Zou, J. Xia, and A. Koussis. Analytical solutions to non-Fickian subsurface dispersion in uniform groundwater flow. *Journal of Hydrology*, 179:237–258, 1996.